

Development of Ni-Al intermetallic compounds
with cellular structure by combustion synthesis
reaction and space holder method

January, 2020

Kobashi & Takata Laboratory

Department of Materials Science and Engineering
Graduate School of Engineering, Nagoya University

SHU Yunmao

Catalog

Chapter 1. Preface	4
1.1 Introduction	4
1.2 Applications of porous metals	5
1.3 Fabrications of open-cell porous metals	9
1.4 Comparison of several fabricating methods	13
1.5 Strategy of this study	18
1.6 Purpose of this study	20
Reference	22
Chapter2. Development of fabrication of bi-porous Ni-Al	25
2.1, Introduction	25
2.2 Experimental method	27
2.2.1 Fabricating and analyzing methods	27
2.3 Results	33
2.3.1 Ignition temperature of combustion synthesis reaction	33
2.3.2 Combination of spacer method and combustion synthesis reaction	34
2.3.3 Effects of sintering parameters	37
2.4 Discussion	42
2.5 Summary	46
Reference	47
Chapter 3. Investigation of effects on porous structure and constituting phases	49
3.1 Introduction	49
3.2 Experimental method	50
3.2.1 Fabrication and evaluation	50
3.2.2 Volume fraction of constituting phases	51
3.3 Results	51
3.3.1 The effects of space-holder addition	51
3.3.2 The effects of Ni:Al molar ratio	55
3.4 Discussion	66
3.5 Summary	75
Reference	76
Chapter 4. Investigation of mechanical properties	77
4.1 Introduction	77
4.2 Experimental method	79
4.3 Results	81
4.31 Comparison with porous Al	81
4.32 Comparison between single-phase and multiple-phase products	82
4.4 Discussion	85
4.41 Comparison with porous Al	85
4.42 Comparison between single-phase and multiple-phase products	85
4.5 Summary	86
Reference	87

Chapter.5 Investigation of fluid permeability	88
5.1 Introduction.....	88
5.2 Experimental method	89
5.3 Results.....	93
5.3.1 Size distribution of pores contributing to permeability.....	93
5.3.2 Optimization on permeability	96
5.4 Discussion	97
5.4.1 Size distribution of pores contributing to permeability.....	97
5.4.2 Optimization on permeability	99
5.5 Summary	100
Reference	101
Chapter 6. Summary	102
Acknowledgements.....	105
Published Thesis	106

Chapter 1. Preface

1.1 Introduction

Since ancient times, the progress of human civilization has been accompanied with the development of material science, which is the basic of material civilization. Also, material science is a symbol of era development. For example, the Stone Age, Bronze Age, and Iron Age which are defined by different kinds of representative materials are well known. Up to this day, with the progress of materials science and technology, many new categories of materials like metallic materials, inorganic nonmetallic materials, polymer materials are developed and applied in various fields. For structural uses, these materials are mostly fabricated into dense materials and voids inside the structural materials are considered as flaws which result in low strength and fracture. However, natural materials like animal bones and woods which have cellular structure inside also exist as structural materials [1-1]. Thus, the concept of “Porous Material” was proposed formally decades ago, and materials with cellular structure are defined as porous materials normally. Because of the cellular structure, many unique characteristics which could not be found in dense materials have been created, and then bring us many advantages and a variety of emerging applications.

Among various porous materials, the ones made of metals are defined as Porous Metals, Metallic Foams, or Metal Sponges [1-2]. Comparing with dense metals, the strengths of porous metals is lower but more lightweight. The apparent density of porous metals can be fabricated lower than pure water (density of porous aluminum with porosities higher than 96% is below 1.0 Mg/m^3) so that porous metals are able to be applied as ultra-light materials. Due to these unique properties, porous metals can be applied to automobile industry to realize lightweight, and then realize energy conservation and emission reduction. Also, porous metals could be applied in electrochemical field and thermal management because of the ideal electrical conductivity and thermal conductivity, which are superior to those of other categories of porous materials. Moreover, porous metals also possess a number of other physical properties such as high specific stiffness, capillarity, impact energy absorption and flow permeability, which indicate a broader range of applications in future [1-3-1.5]. For example, porous metals have been utilized as the anode wicks of Direct Methanol Fuel Cell for increasing the working performance because of the strong capillary force, good permeability, and the superior electrical conductivity comparing to other porous materials [1-30].

Fig.1-1 shows image of the typical porous metal of porous aluminum. As aforementioned, metallic metals with cellular structure are defined as porous metals, which have a number of unique properties that dense metallic materials don't possess. Because of metallic matrix, porous metals also possess higher strength, better resistance to thermal shock than other categories of porous material.



Fig.1-1 Image of typical porous Al [1-44].

1.2 Applications of porous metals

The applications of porous metals are involved in a variety of fields, including filtration and separation, energy absorption, electrochemistry, distribution and control of fluid, catalysts, heat exchange, constructions, biomedicine, electromagnetic shielding and so on [1-27]. As known, metallic materials are usually utilized as structural materials because of the good mechanical properties such as high specific stiffness, thermal-shock resistance. On the other hand, porous materials are generally utilized as functional materials because of the high specific surface area and good permeability derived from the cell structures. Due to the combination of metallic material and porous material, commonly porous metals are both functional and structural, which is considered as the reason of widespread application prospects of porous metals. In particular, the applications depend not only on the material properties of matrix materials but more on the porous structures. For example, porous metals can be applied to the filters or loop heat pipe (LHP) wicks because of the excellent permeability, which is highly affected by porous structure of interconnectivity and porosity.

In foamed and sintered materials, the shape of pores is usually nearly isotropic and spherical, while the shape in lotus and Gasar-type porous materials is anisotropic and long cylindrical [1-6]. Lotus and Gassar-type porous metals are usually prepared by

the mold casting method, which is based on the difference of gas solubility between molten and solidified metals. Gas solubility in both molten and solidified metals varies depending on the temperature, and it commonly decreases with lowering the temperature. Typically, gas solubility has an abrupt decrease when temperature drops down to the melting point, which indicates that anisotropic pores derived from insoluble gas can be easily generated through the unidirectional solidification. However, the pores generated by mold casting method are usually isolated and disconnected. It is suggested that the porous metals with Lotus and Gassar-type pores are not appropriate for functional uses in fields of catalytic, thermal management or electrochemical because of the low permeability.

Pores inside materials have a variety of shapes and can be divided into open-cell structure and closed-cell structure according to the shape of the pores. Closed pores are surrounded by the walls of solid material, and they are separated from each other. On the other hand, open pores are connected to each other by the support from matrix materials [1-41]. The structure with pores which are not connected to the external is defined as closed-cell structure (Fig.1-2(a)), and structure with connecting pores to the external is defined as open-cell structure (Fig.1-2(b)) [1-42]. The porous structures highly affect the characteristics of porous metals and determine the applications of porous metals. For example, porous metals with closed-cell structure exhibit good mechanical properties like impact energy absorption and specific stiffness, and can be used as vibration-absorptive materials, sound insulation materials, shock absorbing materials (Fig.1-3(a)) and so on. On the other hand, the ones with open-cell structure exhibit great gas/ liquid permeability, and can be used as wicks of Loop Heat Pipe (LHP), catalysts or anode materials of fuel cells (Fig. 1-3(b)-(d)).

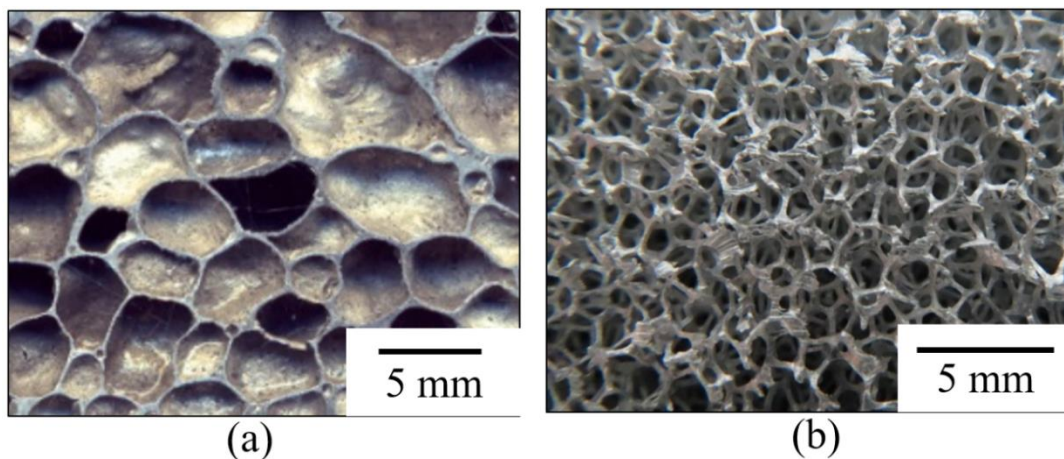


Fig.1-2 Images of (a) closed-cell structure and (b) open-cell structure [1-45].

As for the Loop Heat Pipe, it is considered as a prominent cooling device which has

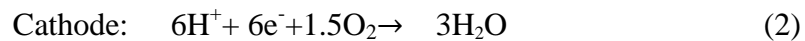
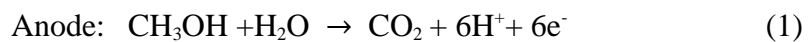
a high effective and efficient thermal transport capability [1-7, 1.8]. On the other hand, thermal management has been a popular subject over recent decades due to the extensive applications of semiconductor apparatus like power amplifier, MPU (microprocessor unit), and LED (light-emitting diode) [1-9]. Not surprisingly, intense researches on optimization of Loop Heat Pipe for superior thermal management have begun. In the Loop Heat Pipe, the porous wick inside evaporator provides the circulation of working fluid with the necessary fluid channels and driving force. Therefore, the heat transport capability of Loop heat pipe depends heavily on the porous wicks. Sintered metal wicks have been used for rising thermal performance successfully [1-9], but the flow permeability of the sintered metal wicks is still low because of the small size of pores which may cause pressure drop or non-ideal interconnectivity of pores inside the sintered metal wicks [1-10]. Hence, the technique of fabricating open-cell porous metal with controllable pore shape and good interconnectivity is the key to facilitate the development of Loop Heat Pipe.

In addition to LHP, applications on filter/ catalytic and anode materials have also attracted intense research over recent years.

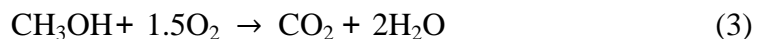
With proposing higher and higher request on environmental quality, people started to attach more and more importance to environment protection. Especially, the emission standard of motors has been constantly raised all over the world. In motor vehicle exhaust, serious environmental pollutants such as Hydrocarbon (HC), Carbon Monoxide (CO), Nitrogen oxides (NO_x) and particulate matters (PM) abound, which seriously affect human health. Hence, a high-performance tail gas treating units attached on motor vehicles are necessary for purifying exhaust gas. As known, the core components of tail gas treating unit are the catalysts (for oxidizing HC, CO, NO_x and so on) and filtering materials (for collecting PMs). Due to the unique sieve-like cell structures, porous materials have been investigated and applied as high-performance filters extensively [1-34-36]. On the other hand, by combining the porous framework with catalytic active material, the porous filter could also be made into a catalytic carrier which can significantly enhance the catalytic performance. The Tanaka Co., LTD developed the innovative oxidation catalysts for volatile organic compounds (VOCs) with a honeycomb porous metal (Fig.1-3(c)). As shown in the section schematic diagram of Fig.1-3(c), the matrix material of framework is Fe-Cr-Al alloy and catalytic active material is attached on the metal matrix by the wash-coat layer, which indicates the reactivating and recycling of this filter. Comparing with ceramic honeycomb porous materials, the wash layer supporting the catalytic materials is thinner which indicates a higher catalytic activity. Hence, we can infer that porous material is playing a more and more crucial role in tail gas treating units. It is also noted that permeability and pore morphologies are two keys for filtering & catalytic applications, so permeability and optimal pore morphologies need to be investigated.

Besides the environmental issues, energy issues have attracted the most attention and concerned us all today. With the depletion of traditional energy sources and request of environmental quality, clean energy will gradually replace the traditional energy like petroleum and coal. As an emerging energy, electric energy has been

utilized in various fields including home appliances, motor vehicles and so on. As a means of power supply, fuel cell possesses a high efficiency of power supply and environmental protection property because of the high capacity density and zero discharge of pollutants. Direct Methanol Fuel Cell (DMFC) has a high capacity density for supporting a wide range of low power and portable applications. In particular, DMFC has easier storage and transport, lower manufacturing cost, more stable in contact with acidic membranes, higher energy density, lower theoretical electro-oxidation potential (E^\ominus) than those of hydrogen cell [1-29-32]. Hence, as a representative, we are going to introduce the semi-passive DMFC here (Fig.1-3(d)). It is noted that methanol delivery in semi-passive DMFC is performed by the capillary force derived from porous wick inside anode site. The reactions on anode and cathode are:



Then we obtain the overall reaction:



In semi-passive DMFC, electrons are released in the anode and then transferred to the cathode via an external circuit, while the released hydrogen ions penetrate through the membrane directly to the cathode. And, only CO_2 and $2\text{H}_2\text{O}$ are produced during the entire process. However, it is reported that CO_2 gas might gather in the catalyst layer to hinder the reaction process, which decrease the performance of DMFC seriously [1-33]. Therefore, an anode that CO_2 gas can easily penetrate through towards outside is expected simultaneously. Porous metals possess not only electrical conductivity but also flow permeability of work liquid and gas, so the generated CO_2 in anode might be released to the external environment by utilizing porous-metal anodes in the future. However, we need to optimize the permeability and control porous structure before realize this application.

From what have been introduced above, we confirmed one thing that permeability and porous structure control play the most crucial roles in functional applications of porous metals.

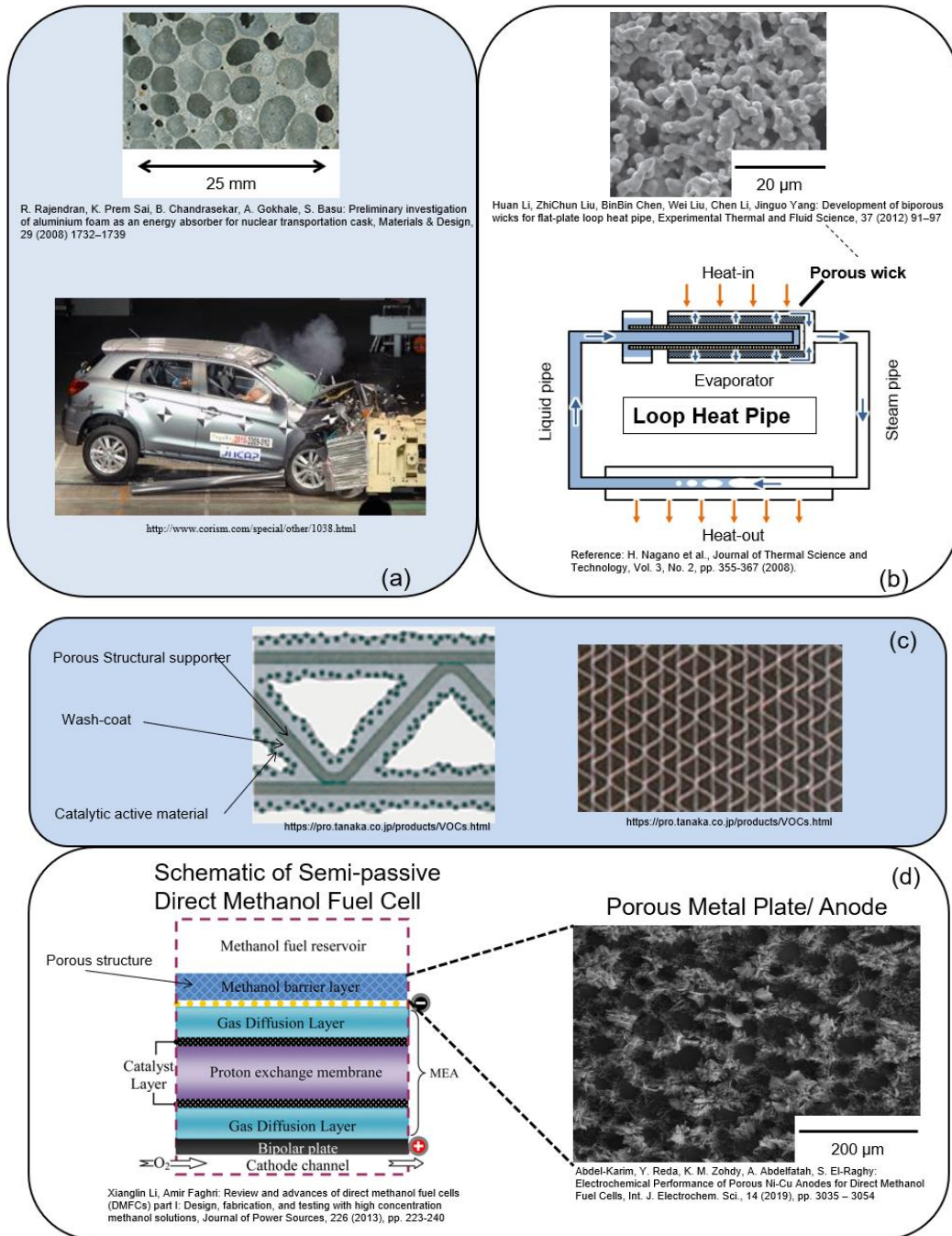


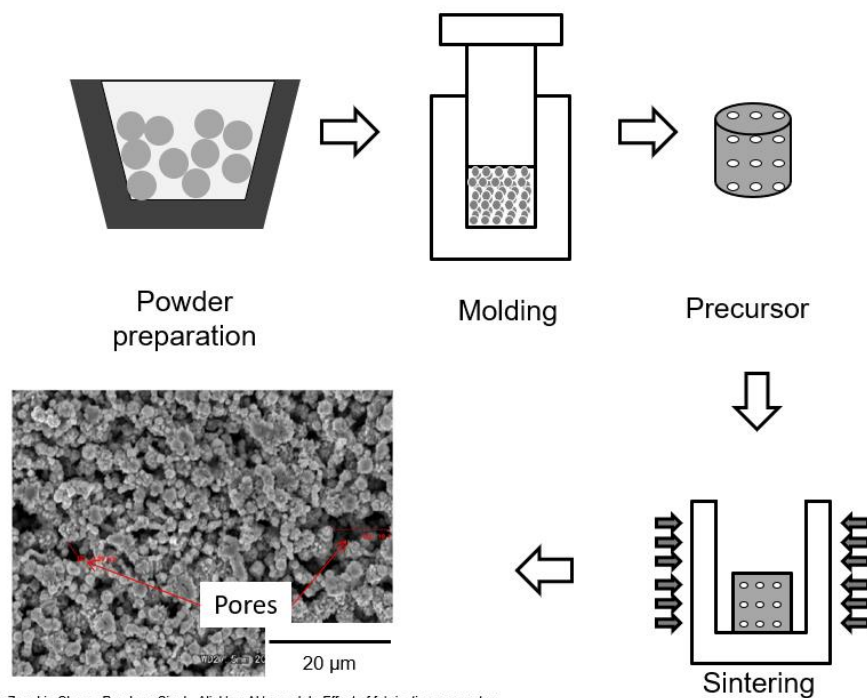
Fig.1-3 Images of applications on (a) shock absorption, (b) heat transport, (c) catalytic carrier, and (d) parts of fuel cell electrode.

1.3 Fabrications of open-cell porous metals

The most apparent distinction between closed-cell and open-cell porous structure is the flow permeability which only open-cell porous metals possess. Because of this characteristic, open-cell porous metals are capable for a number of functional uses,

such as filtration, catalysis and heat transport. It is suggested that the performance of open porous metals on functional applications could be enhanced by increasing flow permeability. In addition, the uniformity within the pore size, shape and porosity can lead to superior applications properties [1-11], so techniques of fabricating highly ordered open-cell porous metal have also become crucial over recent years. In other word, methods of fabricating open-cell porous metals with high flow permeability and uniform porous structure are expected. In this section, several common methods for fabricating open-cell porous metals are introduced.

In the beginning of fabricating porous metal, sintering method like powder sintering method (Fig. 1-4) and fiber sintering method (Fig. 1-5) was mainly used. The procedures of powder sintering and fiber sintering are nearly identical. First, raw metallic powder or metallic fiber is prepared. Next, prepared metallic fiber or metallic powder is felted or molded. Depending on the requirements of porosity and strength, the process of molding or felting could be pressurized or pressureless. The precursor with desired aspect is heat treated by sintering in the last step. The pores generated by powder sintering method or fiber sintering method are derived from the voids inside precursors, so the applied pressure during the process could affect the porosity. Multiple types of material migration are involved during sintering process, including the initial combination (caused by bonding), growth of sintering neck (caused by mass transfer) and shrinkage of pores/ coarsening of cell walls (caused by mass transfer) from the perspective of pores variation. Moreover, in order to obtain highly porous metals with powder sintering method, some researchers attempted to add the pore-forming materials which could be decomposed during sintering process and successfully obtained the porous metals with porosity over 80%.



Jinwang Li, Yong Zou, Lin Cheng, Randeep Singh, Aliakbar Akbarzadeh: Effect of fabricating parameters on properties of sintered porous wicks for loop heat pipe, Powder Technology, 204 (2010), pp. 241–248

Fig. 1-4 Schematic of powder sintering procedure.

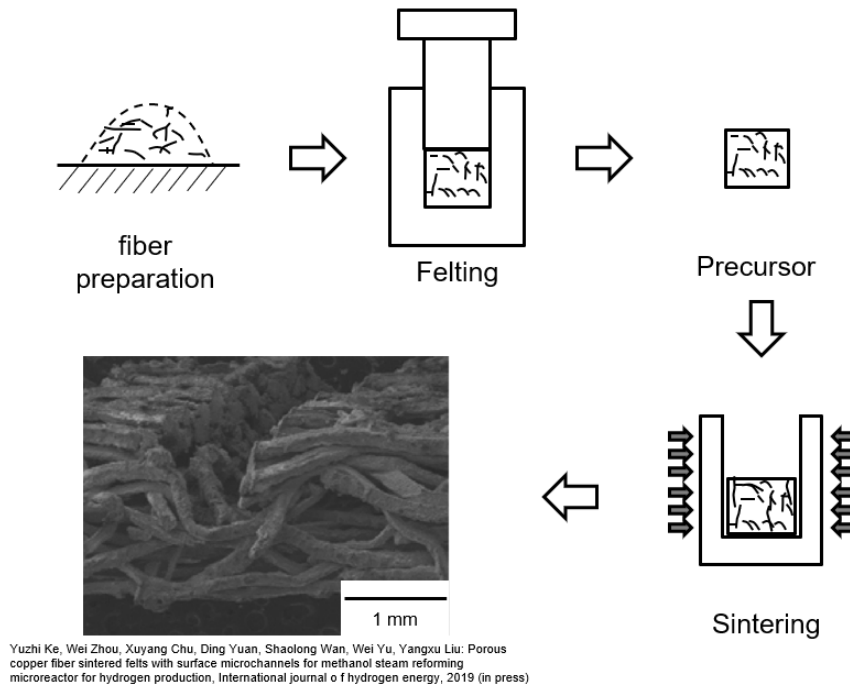


Fig. 1-5 Schematic of fiber sintering procedure.

Figure 1-6 shows the schematic of slurry method procedure. Slurry of foaming agent and metallic powder is made first, then foaming process is carried out which consumes the foaming agent. Subsequently, solidify and intensify the foaming slurry by drying or freezing. The last step is heat treatment of sintering precursor to intensify the bonding strength between metallic particles [1-12]. Foaming agents like Liquefied Petroleum Gas (LPG), Pentane or Hexane are commonly used. Also, mechanical foaming can be used instead of using foaming agent in the foaming process. Due to the surface tension of slurry, metallic particles shift from cell face to cell edge when bubbles evolve during foaming process, which results in an open-cell porous structure. Commonly, we can obtain highly porous metals (over 90%) with good interconnectivity by the slurry method.

Figure 1-7 illustrates the schematic of investment cast method procedure. First, a polyurethane foam with reticulated structure is selected, and then embedding of the plaster mold is carried out by infusing plaster slurry into polyurethane foam. It is noted that the used plaster is water-soluble and able to withstand the high temperature of molten metal under tapping and vibrating [1-13]. Subsequently, dry and bake the mold to decompose the polyurethane foam so that we could obtain the plaster mold for casting molten metal. Solidification of the molten metal is conducted by cooling after filling into the plaster mold with molten metal. The last step is removal of the plaster framework by water, and then the metal foam which replicates the cell structure of polyurethane foam is left. Comparing with slurry method, investment cast method is relatively easier to control cell structure roughly through selecting a polyurethane foam with desired cell structure.

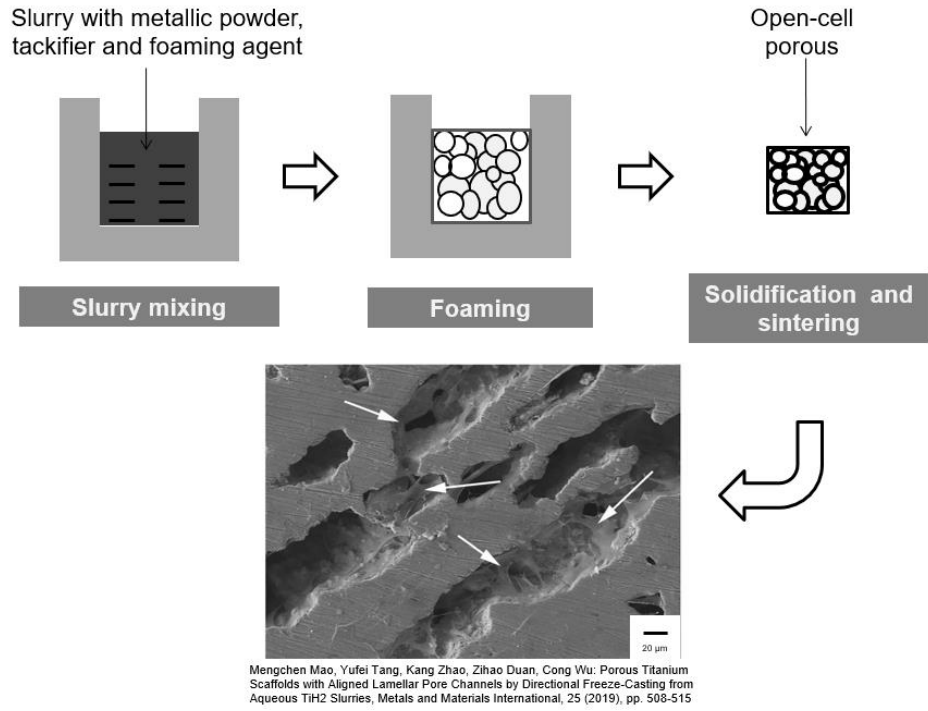


Fig.1-6 Schematic of slurry method procedure.

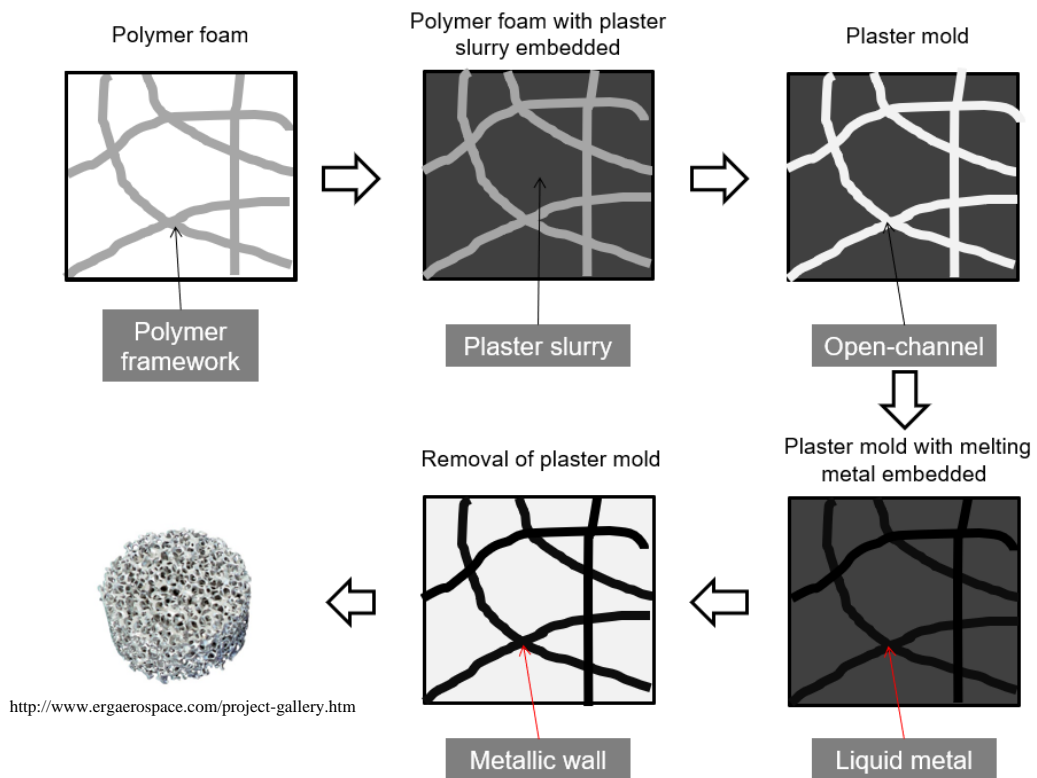


Fig.1-7 Schematic of investment cast procedure.

Nevertheless, the procedures of above two methods are not simple and efficient enough to meet the need of today's mass production. Therefore, the spacer method which possesses not only simple and efficient procedure but also precise controllability has attracted much attention recently. The process of spacer method is illustrated schematically in Fig. 1-8. First step is the selection of space-holder materials, which can be decomposed during sintering or removed by water after sintering. Then powder mixture of metallic powder and space holder is prepared to be followed by molding the precursor. After that, heat treatment is carried out to obtain an as-sintered sample. The last step is removal of space-holder if it has not been decomposed during heat treatment. The shape and volume of the pores are in accordance with the added space holder, so that porous structures like size, shape or porosity could be controlled precisely and simply by spacer method [1-14-1.15].

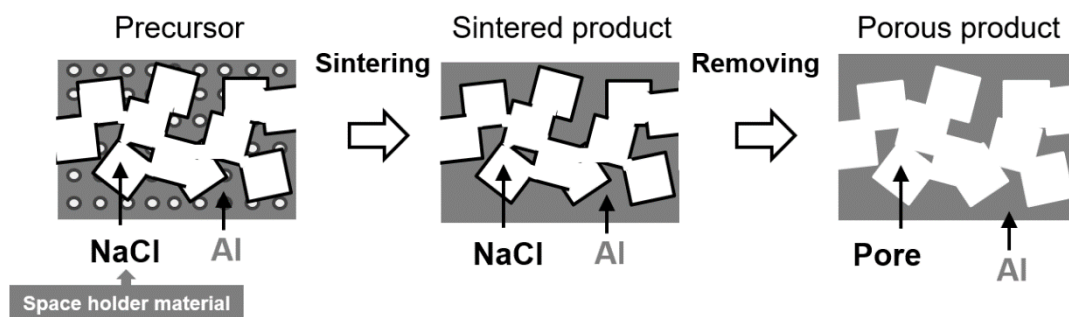


Fig.1-8 Schematic of spacer method procedure.

1.4 Comparison of several fabricating methods

The relative density and pore size of various fabricating methods is shown in Fig. 1-9, and the comparison of several methods of fabricating open-cell porous metals is shown in Table 1-1. Many limitations on pore size and porosity exist in each method of fabricating open-porous metals (Fig. 1-9), which also indicates the limitations on practical applications. Open-cell porous structure could be achieved in all the five methods of powder sintering, fiber sintering, slurry method, investment cast and spacer method. Both of powder sintering and fiber sintering possess simple procedures which are appropriate for mass productions, and both slurry method and investment cast provide us a highly porous structure ($\geq 80\%$) which contributes to flow permeability. In stark contrast, porosity could be adjusted by the addition of space holder in the case of spacer method, which can make a precise control on porosity or pore size to acquire highly porous structure. Also, simple and efficient fabrication procedure which powder sintering and fiber sintering possess, could be

achieved in the case of spacer method.

Comparing with spacer method, slurry method and investment cast exhibit more complicated fabrication process and the difficulty on controlling porous structure precisely. Moreover, products produced by investment cast usually show a low strength and low thermostability due to extremely high porosity and low melting point of embedded metal. As for conventional powder sintering and fiber sintering, the control of porous structure is still limited. Therefore, spacer method has become the more ideal and suitable candidate for manufacturing open-cell porous metal than other aforementioned methods.

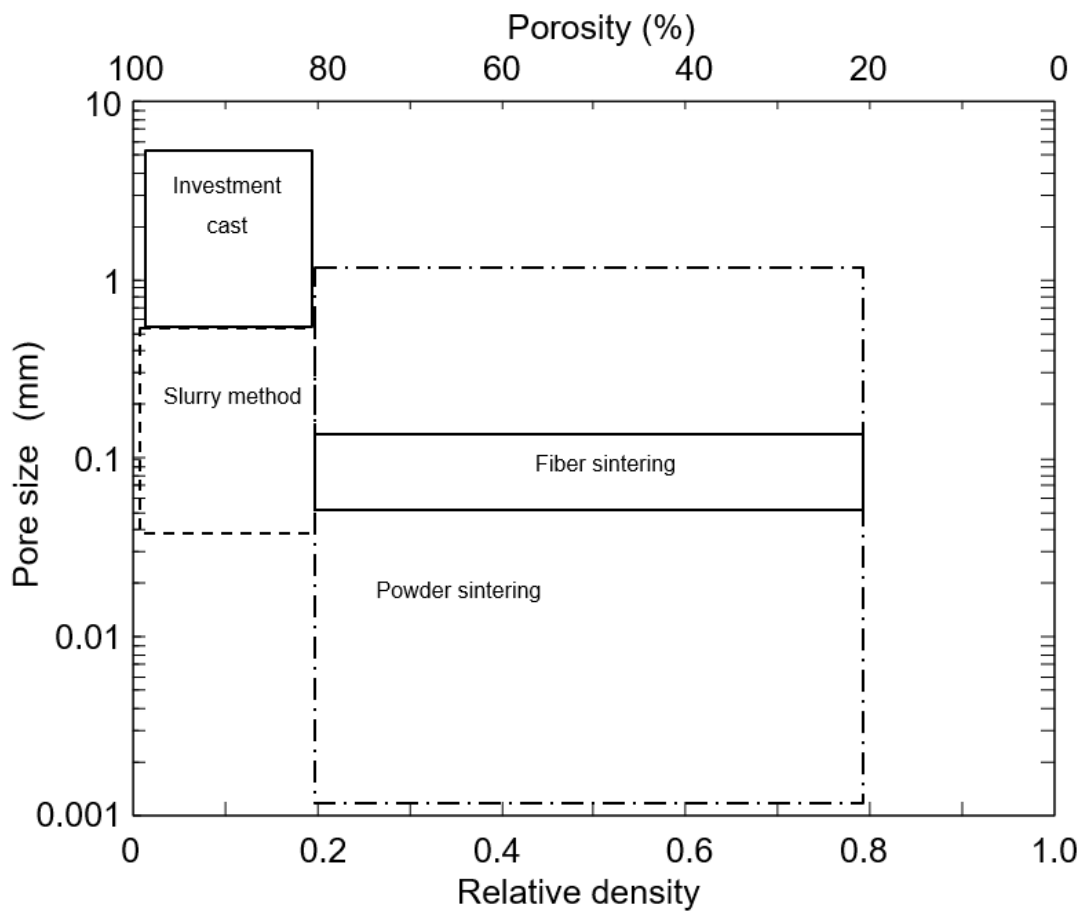


Fig.1-9 Relative densities and pore size of various fabricating methods [1-3, 1-12, 1-13, 1-26, 1-43].

Table 1-1. Comparison of several methods of fabricating open-cell porous metals [1- 12, 1.13, 1. 26, 1.27].

	Porous structure	Merit	Demerit
Powder sintering	Open-cell	Procedure is simple and could achieve mass production	Porous structure (size, morphology, porosity)is difficult to be controlled.
Fiber sintering	Open-cell	Procedure is simple and could achieve mass production. Higher strength than powder sintering	Porous structure (size, morphology, porosity)is difficult to be controlled.
Slurry method	Open-cell	High porosity could be achieved	Strength is low and procedure is complex, and flow permeability is not ideal.
Investment cast	Open-cell	High porosity and permeability could be achieved	Procedure is complex as well. And thermostability of product is not ideal, because the melt point of metal must be lower than that of plaster.
Spacer method	Open-cell/ Intermediate structure between open-cell and closed-cell structure	Highly controllable porosity and pore size	Flow permeability is lower

However, there is also a demerit in spacer method which needs to be improved. That is the distinctly lower flow permeability of products fabricated by spacer method. Figure 1-10 shows the flow permeability of porous metals as a function of relative density. The flow permeability K in Fig. 1-10 was normalized by the square of mean equivalent circle diameter d of pores. The data of porous metal fabricated by spacer method and general open-cell metal foams are respectively from the previous researches of Hakamada et al. [1-16] and Despois et al. [1-17]. From this figure we mainly obtained the following two pieces of information: the flow permeability decreases with increasing relative density of porous metal, and permeability of spacer method is distinctly lower than that of other general methods in the same relative density.

The first information we got from Fig. 1-10 could be explained by the correlation between porosity and relative density. In the case of single-phase material, porosity decreases with increasing relative density. Pores inside porous metal provide the flow passages which promote higher flow permeability, indicating that high porosity may generate more flow passages. Taken together, relative density increases with decreasing of flow passages, thereby decreasing the flow permeability. In addition, the pressure loss ($\Delta P/L$) of laminar flow flowing through solid particle packed bed with L in thickness is expressed by the following Kozeny-Carman's equation [1-38-40].

$$\frac{\Delta P}{L} = \frac{180V_0\mu}{\Phi_s^2 D_p^2} \frac{(1-\varepsilon)^2}{\varepsilon^3}, \quad (4)$$

where μ is the viscosity, V_0 is the superficial velocity, D_p is the equivalent sphere diameter of the particles, Φ_s is the sphericity of the particles in the packed bed and ε is the porosity. From the Kozeny-Carman's equation, we can infer that porous structures such as pore size and porosity highly affect the permeability as well.

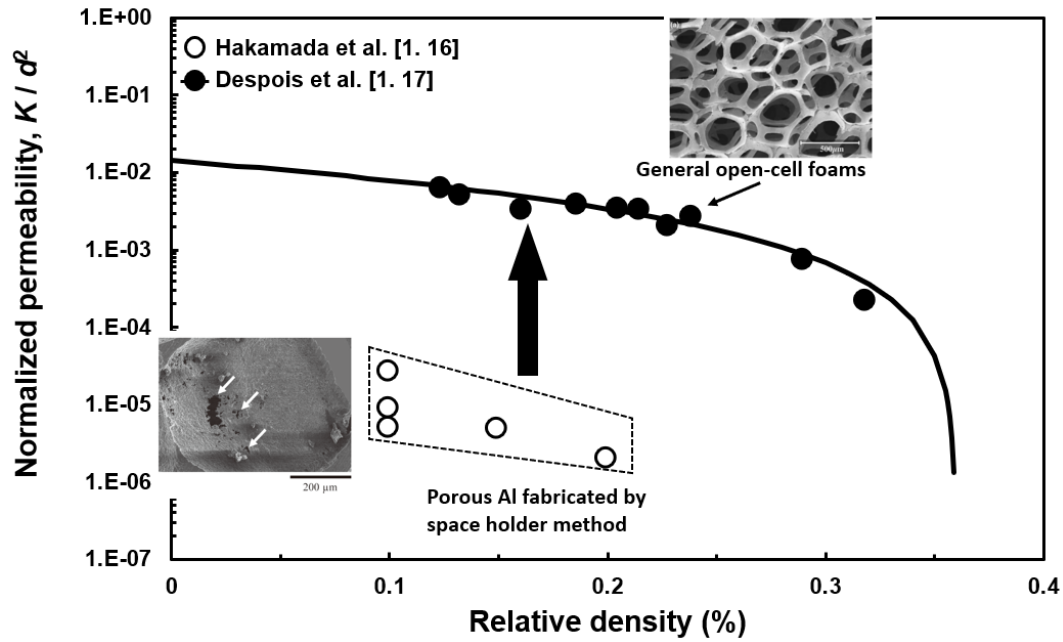


Fig. 1-10 Permeability of general open-cell foams and porous metals fabricated by space holder method.

The second information we obtained from Fig. 1-10 is correlated with the spacer method. Reason for the low permeability of porous metal fabricated by spacer method is considered as the poor contact and connection between pores. Typical morphologies of pores derived from space holder method are shown in Fig.1-11. The dark gray area and light gray area represent the pores derived from space holders and the metallic cell walls respectively, and the positions marked by red arrows indicate the size of actual contact areas between pores. The contacts between the pores replicated from space holders are random and uncontrollable, suggesting that contact areas between pores are usually lower than the sectional areas of pores (Fig.1-11). In other word, the effective flow passages are relatively narrow than pores, and not able to penetrate through materials ideally. As a result, the output flow decreases comparing to input flow. Especially, due to the characteristic of forming pores by spacer method, flow passages are not able to penetrate through materials to improve flow permeability only by increasing porosity. Hence, improving the flow permeability of porous metal prepared by spacer method became our subject in this research, in turn, facilitating the capabilities on various functional applications significantly.

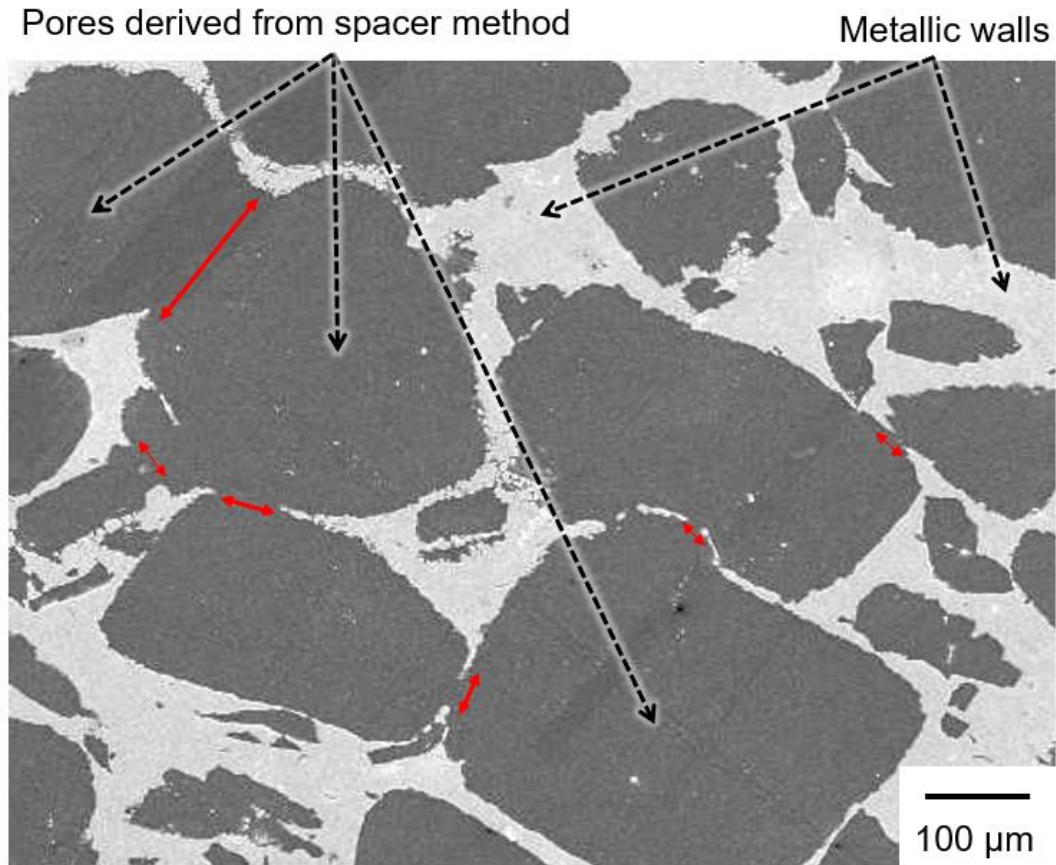


Fig.1-11 Morphologies of the pores inside typical porous Al fabricated by spacer method.

1.5 Strategy of this study

The lack of effective flow passages is considered as the reason of low permeability of porous metal, which is fabricated by spacer method. Therefore, increasing effective flow passages to improve flow permeability became the basic strategy of this study.

T.Kimata et. al enhanced densification of combustion synthesized Ni–Al intermetallic compound by addition of Si [1-18]. That is because voids usually exist in the Ni-Al intermetallic compounds prepared by combustion synthesis reaction. The typical sectional images of scanning electron microscope (SEM) of Ni-Al as-sintered samples are shown in Fig. 1-12. There were a number of gaps (dark contrasted area) generated by combustion synthesis remaining in the microstructures of the Ni-Al intermetallic compound. And also the gaps are interconnected both in images (a) and (b). It is suggested that open-cell pores are generated during the process of combustion synthesis reaction. Because of this, many researchers fabricated porous metal with utilizing combustion synthesis reaction successfully [1-19- 1.21].

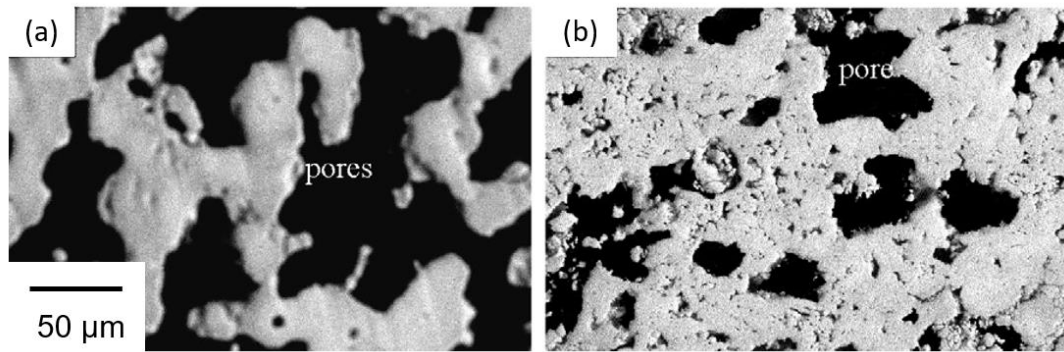


Fig.1-12 SEM images of the Ni -Al powder compacts heated at (a) 670 °C, Ni–30 wt% Al, (b) 670 °C, Ni–14wt% Al [1- 28].

Moreover, Intermetallic compounds exhibit excellent properties such as high melt point, high specific strength, corrosion and oxidation resistance at high temperature compared with ceramic and metal materials, so porous intermetallic compounds can be used as high impact energy absorption materials in many fields such as auto industry, aerospace industry and so on [1-22-1.24]. Due to these great properties, intermetallic compounds have been considered as innovation materials which attract much more attention among various structural and functional materials currently. Thus, fabrication methods of intermetallic compounds have been very important and also become a focus. Among various fabrication methods, combustion synthesis is the most popular one because of low cost, simple procedure and high production efficiency. In combustion synthesis, the exothermal character of redox chemical reaction is actively utilized to synthesize useful materials [1-25], and over 500 categories of composite materials composed of ceramics and intermetallic compounds can be obtained.

Taken together, our strategy for improving permeability could be described as a combination of spacer method and combustion synthesis reaction. Figure 1-13 illustrates our strategy schematically. Spacer method is utilized to generate highly controllable pores. On the other hand, combustion synthesis reaction is utilized to generate pores in the cell walls of the pores derived from space holders so that pores derived from space holders could be connected by the pores generated by combustion synthesis reaction. Thereby, contact among the pores derived from space method could be increased and more effective flow passages could be generated.

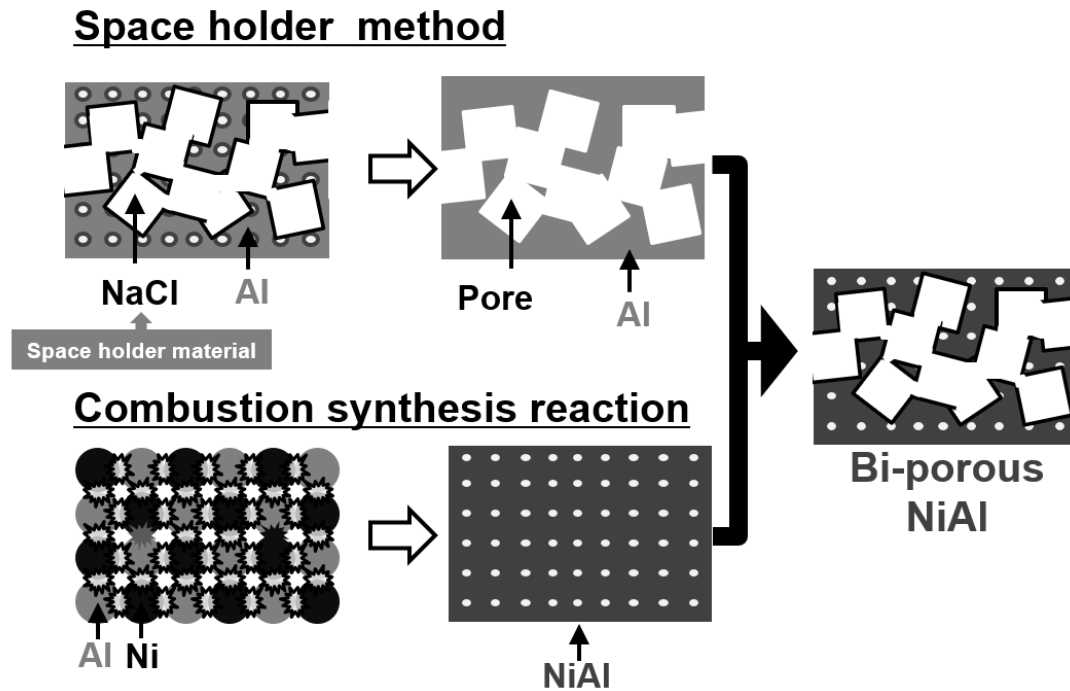


Fig.1-13 Strategy of obtaining bi-modal open-cell pore structure in this research.

1.6 Purpose of this study

In order to achieve a precise control of porous structure to meet the needs of various functional uses, simple and efficient spacer method is selected in this research. Also, there is still a demerit of low flow permeability in spacer method, which has been the biggest barrier of coming into use for spacer method. Therefore, we attempted to combine the spacer method and combustion synthesis reaction for improving the flow permeability of products fabricated by spacer method.

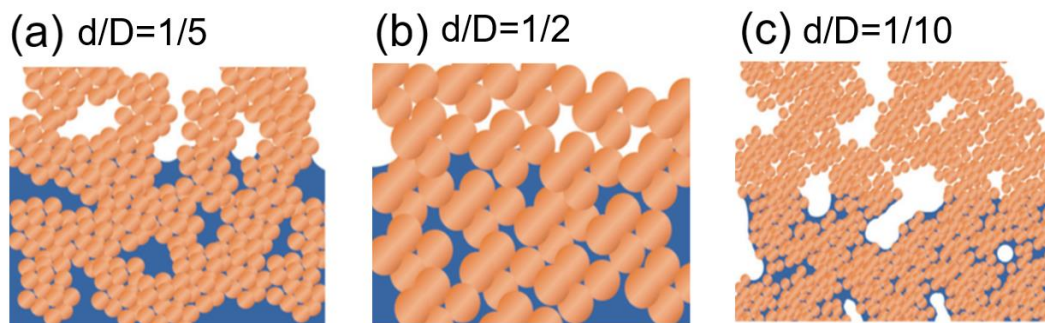
As aforementioned in previous section, combustion synthesis reaction could generate interconnected gaps inside metallic walls, which may contribute to increase the contact between pores derived from spacer method. The gaps inside the metallic walls by combustion synthesis reaction would promote the permeability of the walls to increase the real contact area between pores derived by space holders, thereby increasing the flow passages to improve the overall flow permeability of porous metals. Figure 1-14 shows the phantom drawings of the bi-modal porous materials, and ratios between small pore (in cell walls) and large pore (between cell walls) sizes (d/D) are 1/5 (a), 1/2 (b), 1/10 (c) [1-10]. The permeability of these above three porous structures were also investigated, pore size ratio of 1/5 (a) exhibited the highest flow permeability. It is suggesting that the ratio of small pore (derived from synthesis reaction) and large pore (derived from spacer) sizes also affect the flow

permeability distinctly. Therefore, for increasing the flow permeability, not only fabricating porous metal by combination of combustion synthesis reaction and spacer method but also investigating the optimal porous structure (size, porosity) pores derived from reaction is crucial. As known, before we figure out the optimal porous structure of pores derived from combustion synthesis reaction we have to investigate the effects of porous structure first, thereby controlling the porous structure. The previous studies on formation mechanism of pores derived from combustion synthesis reaction were still limited, so it is also going to be investigated in this study. Hence, our purpose of this study is summarized as follow:

We want to develop an innovative porous metal with preconceived hierarchical porous structure by the method of combination of spacer method and combustion synthesis reaction. The significantly higher flow permeability and high mechanical property of the innovative porous metal are expected in this research. Finally, by investigating the effects on porous structure we can achieve the control of porous structure of pores derived from combustion synthesis reaction, so that the optimal porous structure for functional applications like Loop Heat Pipe could be found in the future.

And, we have the following four specific steps to achieve the purpose:

- (1) Developing the porous intermetallic compounds with two kind of pores derived from spacer method and combustion synthesis reaction respectively;
- (2) Investigating the effects on porous structures of pores derived from combustion synthesis reaction;
- (3) Investigating the mechanical properties of the products, making sure the capability of practical applications;
- (4) Investigating the flow permeability of our products, making sure the significant increasing of flow permeability is achieved.



Chan Byon, Sung Jin Kim: Capillary performance of bi-porous sintered metal wicks, International Journal of Heat and Mass Transfer, 55 (2012), 4096-4103

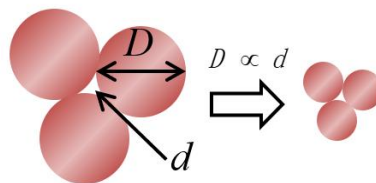


Fig.1-14 Schematic of the bi-modal porous structure with large-scale and small-scale pores [1-10].

Reference

- [1-1] 小橋眞: ポーラスメタルの現状と展望, 軽金属, 第 55 巻, 第 7 号 (2005), pp. 327-332.
- [1-2] 金武直幸, 小橋眞: ポーラスアルミニウム材料, 軽金属, 第 62 巻, (2012.3), pp. 122-134.
- [1-3] J. Banhart: Manufacture, characterisation and application of cellular metals and metal foams, *Prog. Mater. Sci.*, 46 (2001), pp. 559-632.
- [1-4] J. Banhart: Light - Metal Foams—History of Innovation and Technological Challenges, *Adv. Eng. Mater.*, 15 (2013), pp. 82-111.
- [1-5] L.-P. Lefebvre, J. Banhart, D. Dunand: Porous Metals and Metallic Foams: Current Status and Recent Developments, *Adv. Eng. Mater.*, 10 (2008), pp. 775-786.
- [1-6] Hideo Nakajima: Fabrication, properties and application of porous metals with directional pores, *Progress in Materials Science*, 52 (2007), pp. 1091-1173.
- [1-7] S.C. Wong, J.H. Liou, C.W. Chang: Evaporation resistance measurement with visualization for sintered copper-powder evaporator in operating flat-plate heat pipes, *International Journal of Heat and Mass Transfer*, 53 (2010), pp. 3792–3798.
- [1-8] C.B. Sobhan, R.L. Rag, G.P. Peterson: A review and comparative study of the investigations on micro heat pipes, *International Journal of Energy Research*, 31 (2007), pp. 664–688.
- [1-9] S.P. Jang, S.J. Kim: Fluid flow and thermal characteristics of a microscale heat sink subject to an impinging air jet, *Journal of Heat Transfer*, 127 (2005), pp. 770-779.
- [1-10] Chan Byon, Sung Jin Kim: Capillary performance of bi-porous sintered metal wicks, *International Journal of Heat and Mass Transfer*, 55 (2012), pp. 4096-4103.
- [1-11] Mark E. Davis: Ordered Porous Materials for Emerging Applications, *Nature*, 417(2002), pp.813-821.
- [1-12] 和田正弘: スラリー発泡法による発泡金属, 化学と工業, 54-7(2001), pp. 811-813.
- [1-13] Lucai WANG, Haijuan LI, Fang WANG, Jianfu REN: Preparation of open-cell metal foams by investment cast, *CHINA FOUNDRY*, 2-1(2005), pp. 56-59.
- [1-14] C.E.Wen, M.Mabuchi, Y.Yamada, K.Shimojima, Y.Chino and T.Asahina: Processing of biocompatible porous Ti and Mg, *Scripta Mater.*, 45 (2001), pp. 1147-1153.
- [1-15] C.E.Wen, Y.Yamada, K.Shimojima, Y.Chino, H.Hosokawa and M.Mabuchi: Novel titanium foam for bone tissue engineering, *J. Mater. Res.*, 17 (2002), pp. 2633-2639.
- [1-16] M. Hakamada, M. Mabuchi: Fabrication by spacer method and evaluation of porous metals, *Journal of The Japan Institute of Light Metals*, Vol. 62, No.8 (2012), pp.313-321.
- [1-17] J. F. Despois, A. Marmottant, L. Salvo and A. Mortensen: Influence of the infiltration pressure on the structure and properties of replicated aluminium foams, *Mater. Sci. Eng. A*, 462 (2007), pp. 68-75.
- [1-18] Tetsuro Kimataa, Keisuke Uenishia, Akira Ikenagab, Kojiro F. Kobayashia:

Enhanced densification of combustion synthesized Ni–Al intermetallic compound by Si addition, *Intermetallics*, 11(2003), pp. 947-952.

[1-19] Emily M. Hunt, Michelle L. Pantoya, R. Jason Jouet: Combustion synthesis of metallic foams from nanocomposite reactants, 14 (2006), pp. 620-629.

[1-20] M. Kobashi, N. Kanetake: Processing of Intermetallic Foam by Combustion Reaction, 2002.

[1-21] Makoto Kobashi, Norio Inoguchi, Naoyuki Kanetake: Effect of elemental powder blending ratio on combustion foaming behavior of porous Al–Ti intermetallics and Al₃Ti/Al composites, *Intermetallics*, 18 (2010), pp. 1039-1045.

[1-22] F. Wang, Y. Liang, S. Shang: Phase transformation in Ti–48Al–6Nb porous alloys and its influence on pore properties, *Mater. Des.*, 83 (2015), pp. 508-513.

[1-23] Y. Jiang, C. Deng, Y. He: Reactive synthesis of microporous titanium-aluminide membranes, *Mater. Lett.*, 63 (2009), pp. 22-24.

[1-24] H. Sina, S. Iyengar: Reactive synthesis and characterization of titanium aluminides produced from elemental powder mixtures, *J. Therm. Anal. Calorim.*, 122 (2015), pp. 1-10.

[1-25] Patil KC, Aruna ST. In: Borisov AA, De Luca LT, Merzhanov AG, Scheck YN: Redox methods in SHS practice in self-propagating high temperature synthesis of materials, New York: Taylor & Francis; (2002).

[1-26] Peisheng Liu : Introduction to Porous Materials (Second Edition), Tsinghua University Press; (2012).

[1-27] LIU Pei-sheng, YU Bing, HU An-Min, LIANG Kai-ming, GU Shou-Ren: Development in applications of porous metals, *Trans. Nonferrous Met.Soc. China*, 11 (2001), pp. 629-638.

[1-28] H.X.Dong, Y.Jiang, Y.H.He, M.Song, J.Zou, N.P.Xu, B.Y.Huang, C.T.Liu, P.K.Liaw: Formation of porous Ni–Al intermetallics through pressureless reaction synthesis, *Journal of Alloys and Compounds*, 484 (2009), pp. 907-913.

[1-29] Xianglin Li, Amir Faghri: Review and advances of direct methanol fuel cells (DMFCs) part I: Design, fabrication, and testing with high concentration methanol solutions, *Journal of Power Sources*, 226 (2013), pp. 223-240.

[1-30] S. Arisetty, A. K. Prasad, S.G. Advani: Metal foams as flow field and gas diffusion layer in direct methanol fuel cells, *J. Power Sources*, 165 (2007), pp. 49-57.

[1-31] R. Abdel-Karim, Y. Reda, K. M. Zohdy, A. Abdelfatah, S. El-Raghy: Electrochemical Performance of Porous Ni-Cu Anodes for Direct Methanol Fuel Cells, *Int. J. Electrochem. Sci.*, 14 (2019), pp. 3035 – 3054.

[1-32] P. Joghee, J. N. Malik, S. Pylypenko, R. O’Hayre: A review on direct methanol fuel cells – In the perspective of energy and sustainability, *MRS Ener. Sustain. A Review*, 2 (2015).

[1-33] Mohammad Ali Abdelkareem, Nobuto Morohashi, Nobuyoshi Nakagawa: Factors affecting methanol transport in a passive DMFC employing a porous carbon plate, *Journal of Power Sources*, 172 (2007), pp. 659–665.

[1-34] Printz Ringbæk T, Simeonov Y, Witt M, Engenhardt-Cabillic R, Kraft G, Zink K, Weber U: Modulation power of porous materials and usage as ripple filter in particle therapy, *Physics in Medicine and Biology*, 62 (2017), pp. 2892-2909.

- [1-35] Yu. Yu. Belous: Methods of investigating porous filter materials by scanning electron beam, Soviet Powder Metallurgy and Metal Ceramics, 28 (1989), pp. 121-124.
- [1-36] Li Yong-jin, Liu Xiao-cui, Ding Ying-jie: Theoretical Study on Fluid Resistance in Pores of Gasar Metal Porous Filter Material, Electrical and Control Engineering (ICECE), 2010.
- [1-37] Yunmao Shu, Asuka Suzuki, Naoki Takata, Makoto Kobashi: Fabrication of porous NiAl intermetallic compounds with a hierarchical open-cell structure by combustion synthesis reaction and space holder method, Journal of Materials Processing Tech., 264 (2019), pp. 182–189.
- [1-38] PC. Carman: Fluid flow through granular beds. Trans. Inst. Chem. Eng., 15 (1937), pp. 150-167.
- [1-39] PC. Carman: Permeability of saturated sands, soils and clays. J. Agric. Sci., 29 (1939), pp. 263–273.
- [1-40] PC. Carman: Flow of gases through porous media. London: Butterworth; 1956.
- [1-41] Hideo Nakajima: Porous metals with directional pores. Springer Japan; 2013.
- [1-42] BaiduBaiké, <https://baike.baidu.com/>
- [1-43] M.F. Ashby, A.G. Evans, N.A. Fleck, L.J. Gibson, J.W. Hutchinson, H.N.G. Wadley: Metal Foams, A Design Guide, Butterworth-Heinemann; 2000.
- [1-44] 岡 優斗: 気孔構造とセル壁材料を制御した高衝撃吸収能ポーラス金属の開発, 名古屋大学大学院 工学研究科修士論文, (2017).
- [1-45] 上松 敬右: スペーサーを用いたポーラス Ti-Al 合金の反応合成と高強度化, 名古屋大学大学院 工学研究科修士論文, (2016).

Chapter2. Development of fabrication of bi-porous

Ni-Al

2.1, Introduction

In several fields such as filtration and separation, energy absorption, electrochemistry, distribution and control of fluid, catalysts, heat exchange, constructions, biomedicine, electromagnetic shielding, porous materials are playing more and more important roles over these years. Especially, porous metals also possess the unique characteristics of high thermal conductivity, high electrical conductivity, high thermal-shock resistance, and high mechanical properties.

Intense researches of porous metals on various applications such as Loop Heat Pipe [2-1, 2-2, 2-3], catalytic/ filter [2-4, 2-5], anode materials of direct methanol fuel cell (DMFC) [2-6, 2-7, 2-8] have been conducted. In the case of LHP, porous materials are used as the wicks inside evaporators, which are considered as the core components of LHP. And porous metals are attracting more and more attention due to the ideal mechanical properties and relatively high melting point. In the case of particulate filter, porous materials not only work as particulate filters but also can work as catalyst carriers, which is able to enhance the performance of filters such as tail gas treating unit or factory emission treating plant. Moreover, because of high thermal conductivity and good mechanical properties at high temperatures, porous metals have been the most attractive options for filters. As for the DMFC, porous material is also playing an important role because of the capillary force which can supply the liquid methanol without extra device. Besides, porous metals possessing high electronic conductivity and high mechanical strength also might be used as current collectors in anodes in the future. It is noted that all the functional applications of porous metals introduced above have a common request on flow permeability which decides the performance of the porous component, because higher flow permeability results in a higher working performance commonly.

Several common fabricating methods of open-cell porous metals have been introduced in previous chapter. By powder sintering and fiber sintering method, open-cell porous metals could be fabricated in simple and efficient procedures, which indicate a capability in mass productions. But the porosity of porous metals made by powder sintering is relatively low and precise control of porous structure is hard to achieve by these two methods. By slurry method and investment cast method, highly porous metals (over 90%) with good interconnectivity could be obtained [2-9, 2-10]. But the permeability of porous metals made by slurry method and the control of porous structure of the two methods are not ideal. As for spacer method, the most striking difference between other methods is that precise and simple control of porous structure like pore size or porosity can be achieved only by spacer method [2-11, 2-12]. Structure controllability indicates the scope of applications objectively because

optimal porous structures vary with changing applications or applying conditions. However, spacer method also has a demerit of low permeability, which is considered as one of the biggest barriers to functional applications like wicks of LHP, filters or anode materials of DMFC. Therefore, there is no fabricating method which enables both high permeability and high porous-structure controllability by far. In order to enable both high permeability and high porous-structure controllability, we expect to improve the fabricating technique of spacer method to endow a higher permeability.

On the other hand, previous study revealed that Ni-Al intermetallic compounds made by combustion synthesis reaction possess a number of open pores in cell walls [2-13]. Inspired by this result, we plan to increase the interconnectivity of pores derived from spacer holders by generating open pores in cell walls of the pores, thereby enhance the permeability of materials. Moreover, due to a higher melting point and stiffness than other pure metallic materials, intermetallic compounds have become the extremely attractive matrix materials of porous metals these years [2-14, 2-15, 2-16]. Therefore, combustion synthesis reaction between Ni and Al is adopted in this study.

In order to meet the request of more widespread applications, we combined spacer method with combustion synthesis reaction to develop an innovative fabrication technique for improving porous-structure controllability and permeability of porous metals concurrently. In this study, we selected the Ni-Al intermetallic compounds as the matrix materials. All the possible constituting phases of sintered products during the combustion synthesis reaction between Ni and Al can be inferred from the following possible reaction equations in the case of Al/Ni=1/1 [2-17]:



From above equations, we can infer that NiAl (B2), NiAl₃ (D0₂₀), Ni₂Al₃ (D5₁₃), Ni₃Al (L1₂) as well as Ni and Al are the possible constituting phases in final products. Though NiAl is the most possible and easy Ni-Al intermetallic compound to obtain by combustion synthesis due to the lowest Gibbs free energy of formation [2-17], single-phase NiAl without other impurities is still difficult to prepare. Since single-phase structure might contribute to enhancing strength and decreasing brittleness of products, preparing single-phase Ni-Al intermetallic compound has become one of the goals in this study. Therefore, we tried to fabricate the porous

Ni-Al intermetallic compound with single phase, by controlling the sintering parameter of sintering temperature.

2.2 Experimental method

2.2.1 Fabricating and analyzing methods

In this process, Al powders (purity of 99.99%, size under 2 μm), Ni powders (purity of 99%, size under 1 μm), and NaCl space-holder powders (purity of 99.99%, size within 30–50 μm) were utilized as the raw powders. The space-holder powders (NaCl) were blended with the Al powders and Ni powders using an automatic mixer, so that the volume fractions of NaCl (V_{NaCl}) in raw mixture were 0% and 60%. In view of the equilibrium phase diagram of the Ni-Al binary system presented by Okamoto [2-18], the Al and Ni powders were blended in an atomic ratio of 1:1 to turn NiAl with a B2 crystal structure into the final product of Ni-Al combustion synthesis reaction (Fig. 2-1). Then filled the mixed raw mixture of Ni, Al and NaCl in a graphite mold (inner diameter of 10 mm, outer diameter of 20 mm, and height of 50 mm) and pre-compressed by a pressure of 100 MPa at an ambient temperature to prepare a cylindrical precursor with a diameter of 10 mm and height of 5 mm. The precursor was heated by electric current sintering in vacuum (lower than 20 Pa) at a constant compressive pressure (5 MPa). And the temperature was measured by a thermocouple inserted into the wall of graphite mold at a depth of 2 mm (Fig. 2-2). The temperature was raised at a rate of 0.5 $^{\circ}\text{C}/\text{s}$ and held at 450 $^{\circ}\text{C}$, 550 $^{\circ}\text{C}$, 600 $^{\circ}\text{C}$, and 650 $^{\circ}\text{C}$ respectively. The sintering time was set in 300 s, 1800 s, and 10800 s respectively. After sintering, the samples were cooled in furnace to the ambient temperature. The specimens were soaked in pure water for 24 h to remove the NaCl space holder for the formation of pores, which were replicated from space-holder Na

In order to prove the necessity of combustion synthesis reaction, porous pure Al which was considered as a control sample was also prepared by the same process in this study. The V_{NaCl} was set at 60%. The electric current sintering with a constant pressure of 5 MPa was performed with a setting temperature of 550 $^{\circ}\text{C}$ for 300 s, followed by furnace cooling and removal of the space-holder NaCl by pure water as described above.

At last the removal rate of space-holder NaCl was estimated to make sure that the NaCl was totally removed. Removal rate of space-holder NaCl (Z) can be calculated by a follow equation:

$$Z = \frac{M' - M}{M_{NaCl}} \quad (5)$$

where M' , M , M_{NaCl} are the mass before NaCl removal, after NaCl removal, and the mass of NaCl in the precursor respectively.

Subsequently, the constituting phase was observed by scanning electron microscope (SEM) and measured by X-ray diffraction (XRD) and electron back-scattered diffraction (EBSD). The crystal structure of each intermetallic compound is shown in Fig. 2-3, and utilized for the EBSD measurement. At last, the sectional image analysis was performed to estimate porosity and size of small pores derived from combustion synthesis reaction between Ni and Al.

Moreover, the temperature history of samples during sintering was also investigated, so that we can acquire the relationship between temperatures of graphite mold and sample in this research.

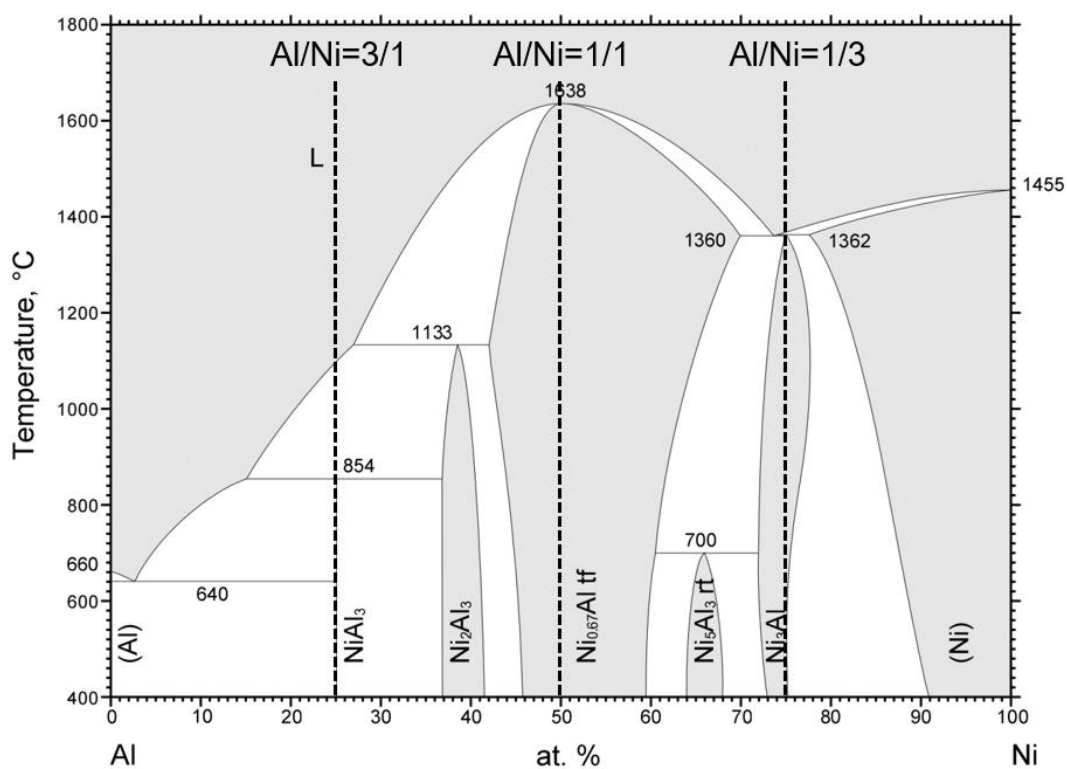


Fig. 2-1. Equilibrium phase diagram of the Ni-Al binary system.

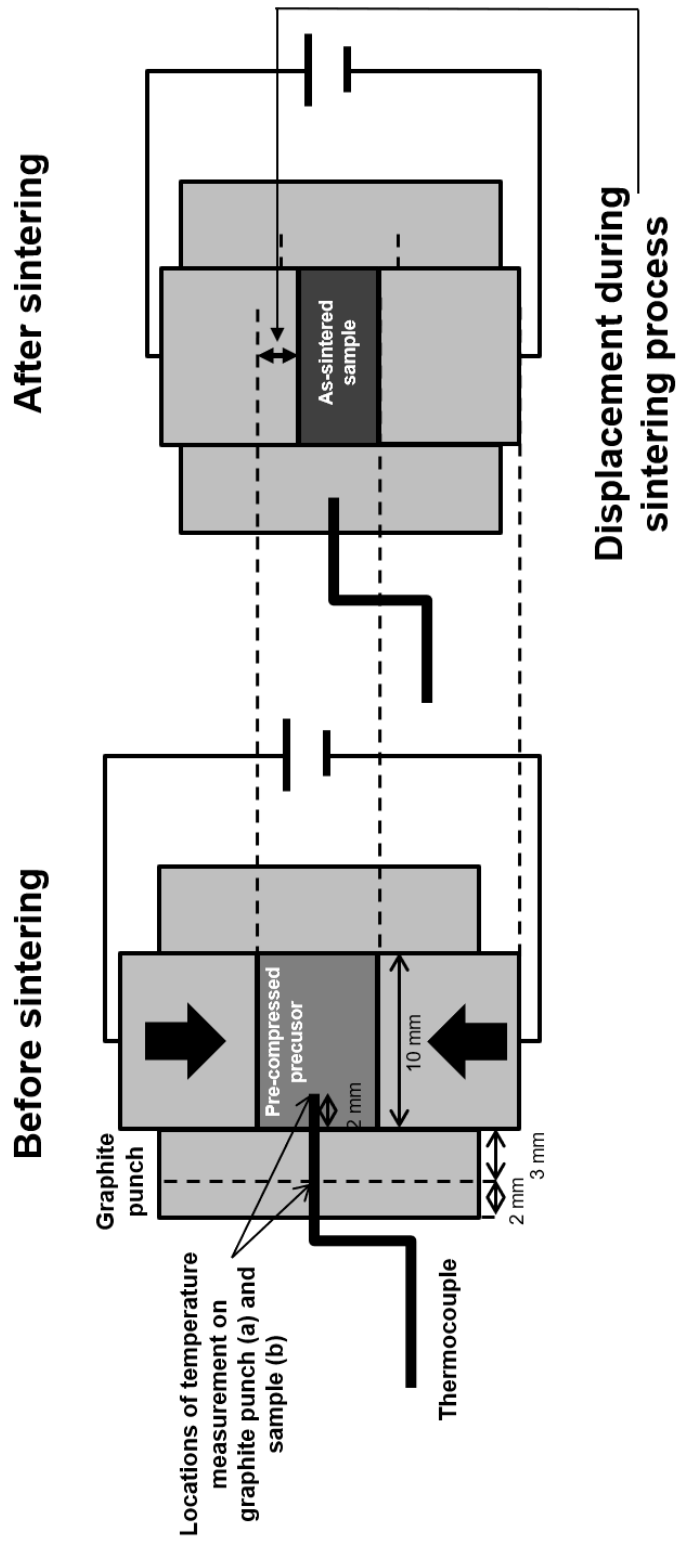


Fig. 2-2 Schematic of pressure sintering process.

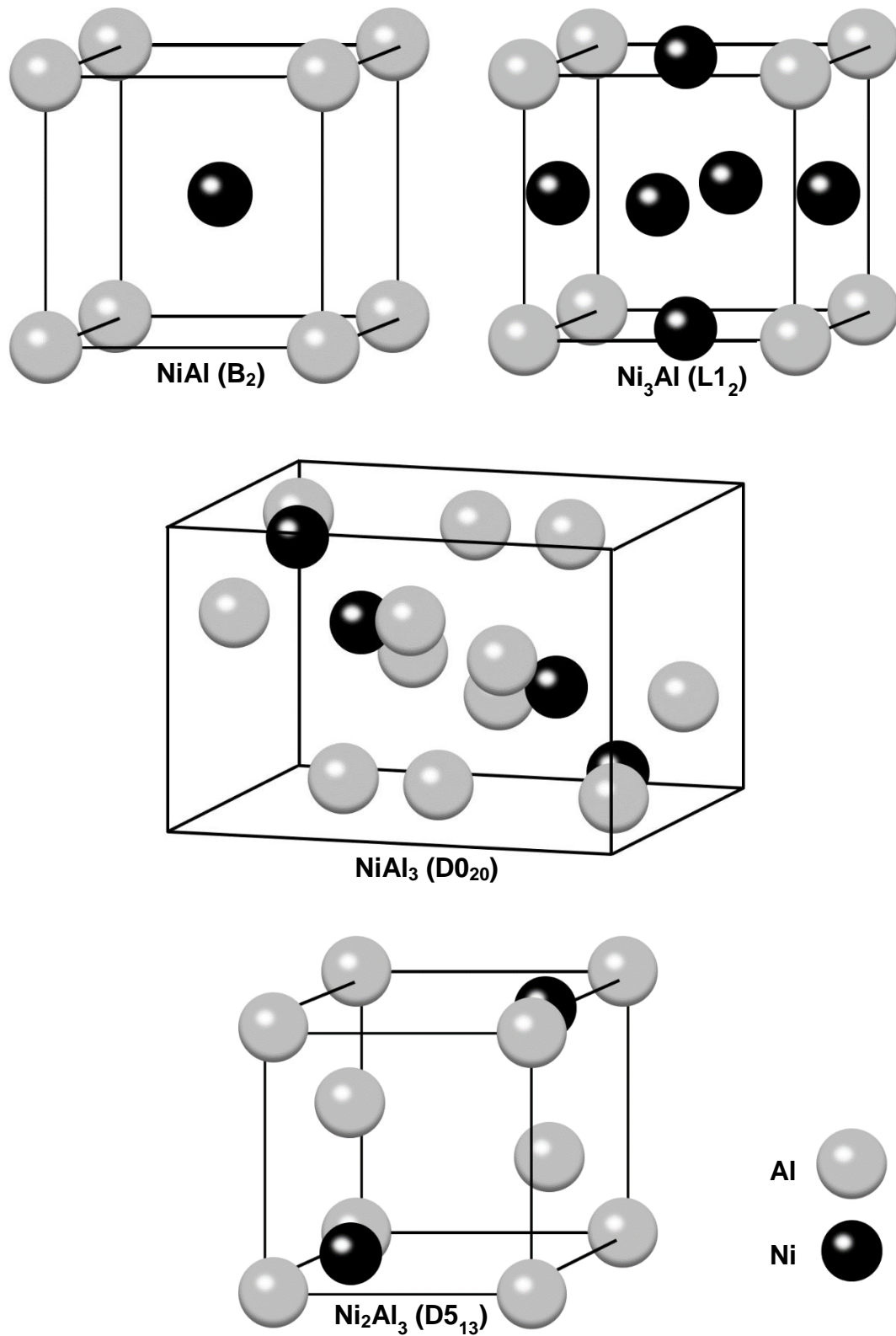


Fig. 2-3 Crystal structures of NiAl, Ni₃Al, NiAl₃, Ni₂Al₃ [2-26].

2.2.2 Surface treatments

Before analyzing the microstructure and constituting phases of samples, necessary surface treatments were carried out. First, we soaked samples in an uncured epoxy resin and then cured the epoxy resin for 24 h. After curing the resin, the samples were polished by SiC abrasive papers (#320, 800, 1200, and 2400) and diamond slurries (9 μm and 3 μm), using an automatic polisher. The polished samples possessed a light-reflecting smooth plane on the surface. Subsequently, final polishing with 0.02 μm alumina particles was performed. Then JSM-6610A scanning electron microscope (SEM) and X-ray diffraction (XRD) were used to analyze the morphologies of pores and constituting phases. In the case of electron back-scattered diffraction (EBSD), an extra polishing procedure of argon polishing (24 h) is essential for obtaining a finer plane of grain boundary.

2.2.3 Evaluation of pore size and porosity

Porosity and pore size of small pores derived from combustion synthesis reaction were estimated by sectional image analysis as mentioned in Chapter 1. By this method, porosity in the cell walls, mean pore size (mean equivalent circle diameter) and size distribution (distribution of mean equivalent circle diameter) can be obtained.

On the other hand, porosity and pore size of large pores replicated from space-holder NaCl virtually inherit the volume fraction and size of NaCl. Therefore, the porosity of large pores can be estimated by the follow equation:

$$\varepsilon_{\text{NaCl}} = \frac{m_{\text{NaCl}}}{V_{\text{sample}} \rho_{\text{NaCl}}} \quad (6)$$

where $\varepsilon_{\text{NaCl}}$ is the porosity of large pores derived from NaCl, ρ_{NaCl} is the true density of NaCl, V_{sample} is the bulk volume of the sample, and m_{NaCl} is the mass of NaCl powder used. Combining with the porosity of NaCl, the porosity of small pores can be expressed as follow:

$$\varepsilon_c = \varepsilon_{cs} (1 - \varepsilon_{\text{NaCl}}) \quad (7)$$

where ε_c is the porosity of small pores derived from reaction, and ε_{cs} is the porosity in cell walls of small pores derived from reaction which is measured by image analysis.

The total porosity of fabricated porous Ni-Al intermetallic compound can be estimated as follow:

$$\varepsilon_{\text{total}} = \varepsilon_c + \varepsilon_{\text{NaCl}} \quad (8)$$

Where $\varepsilon_{\text{total}}$ and is the total porosity. Method of measuring the porosity in cell walls and pore size of small pores derived by reaction were carried out by utilizing sectional image analysis as mentioned before, with image processing software. Figure 2-4

shows the mechanism of measuring the pore size and porosity by using image processing software. Black area and gray area represent soaked resin and metallic cell wall respectively, and green area represent image analyzed area. The resin penetrated into the pores inside porous materials, so the black area and gray area could be considered as the “pore zone” and “cell wall zone”. The green area includes “pore zone” and “cell wall zone”, and then porosity can be estimated by combining the follow equation:

$$\varepsilon = \frac{S_p}{S_p + S_c} \quad (9)$$

Where S_c represents the sectional area of cell wall zone, and S_p is the sectional area of pore zone. On this basis, Image J (image processing software) was utilized for the measurement of pore size like mean equivalent circle diameter and the size distribution by the calculation and statistics of spacing. The porosity of large pores and small pores and total porosity could be calculated by equations aforementioned.

Thus, calculation method and sectional image analysis were combined to estimate the porosity and pore size in this study.

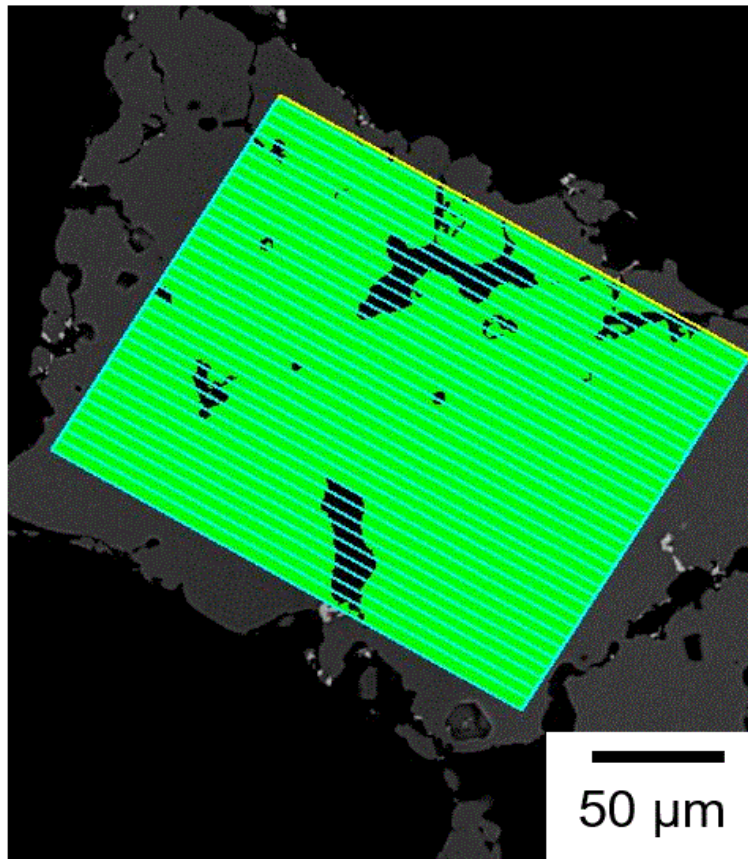


Fig. 2-4 Method of measuring pore size and porosity by using image processing software.

2.3 Results

2.3.1 Ignition temperature of combustion synthesis reaction

During sintering process, temperature of graphite mold and samples were measured by the inserted thermocouple and the shrinkage condition of samples was also monitored by measuring the displacement of graphite punch (Fig. 2-2). Typical changes of temperature and displacement of the graphite punch (a) and Ni-Al sample (b) during sintering process are shown in Fig. 2-5. In this graph, positive displacement was defined as the direction which the graphite mold compressed towards. A small peak was presented at 500°C, where the displacement rose sharply to form a clear peak both in Fig. 2-5 (a) and (b). It is suggesting that temperatures of graphite mold and sample are extremely close, and can be considered as approximately the same. As a result, the temperature measured in the graphite mold wall could represent the true temperature of sample during sintering process. The temperature rose and sharp shrinkage of sample indicated that the combustion synthesis reaction between Al and Ni occurred at around 500°C [2-20]. And the XRD profiles of the Ni-Al samples sintered at 450°C, 500°C, 550°C, 600°C shown in Fig. 2-6 also reveal the ignition temperature of 500°C, because the products of intermetallic compounds were formed from the temperature of 500°C.

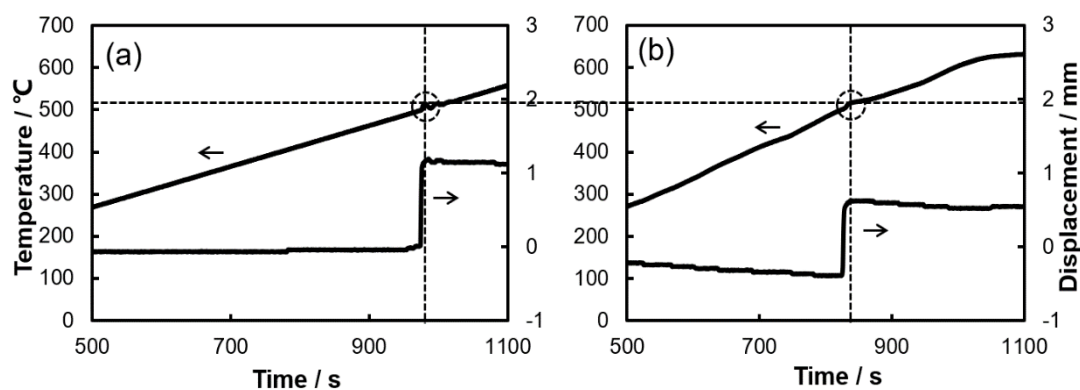


Fig. 2-5 Typical changes of temperature and displacements of (a) graphite punch and (b) Ni-Al sample during sintering process.

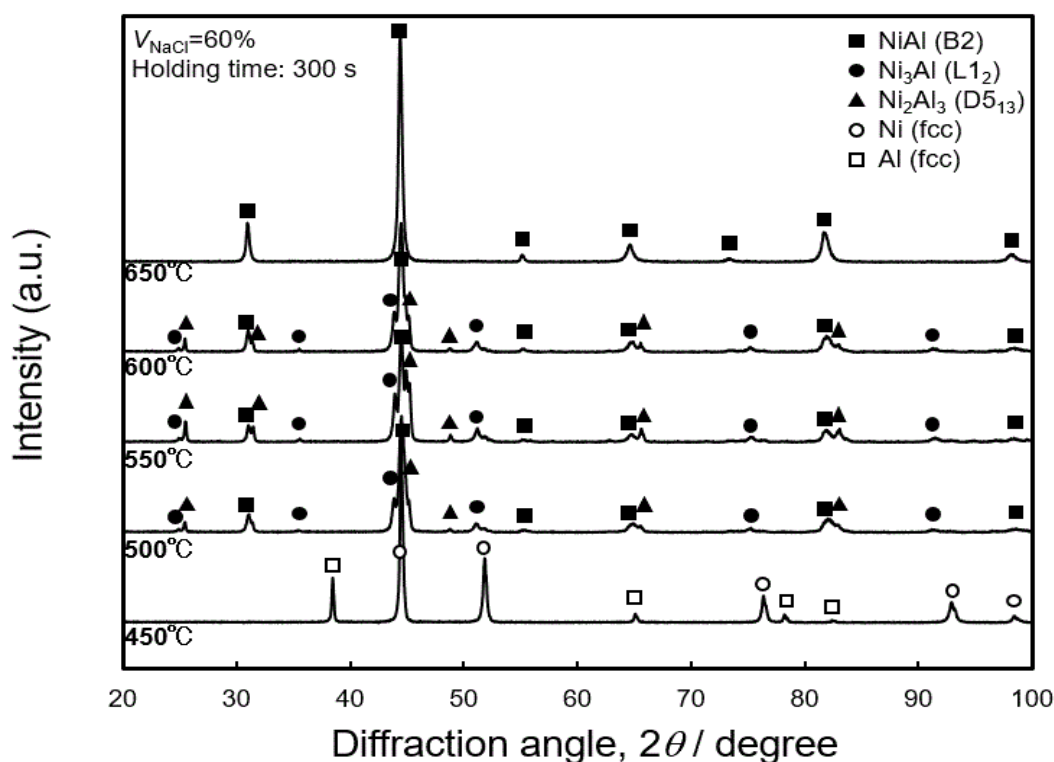


Fig. 2-6 XRD profiles of the Ni-Al samples sintered at 450°C, 500°C, 550°C, 600°C and 650°C for 300 s ($V_{\text{NaCl}} = 60\%$).

2.3.2 Combination of spacer method and combustion synthesis reaction

Fig. 2-7 shows the morphologies of these raw powders and the appearance of representative sintered specimen heated at 650°C for 300 s. Al particles presented a spherical shape and Ni powders presented a cubic shape as well as NaCl particles. The sintered sample shows a cylindrical aspect which is replicated from the shape of graphite mold.

SEM images of the microstructures of the Ni-Al samples ($V_{\text{NaCl}} = 60\%$ and 0%, sintering at 650°C for 300 s) and contrast material of porous Al are presented in Fig. 2-8. The regions of light contrast represent the metallic walls and the regions of dark contrast represent the cured epoxy resin which infiltrated the pores. Large pores derived from NaCl were observed in both pure Al and Ni-Al sample ($V_{\text{NaCl}} = 60\%$) from the low-magnification SEIs. The shape of these large pores inherited the shape of the NaCl particles virtually. The cell wall of the porous Al was dense and small pores were not observed. And, in the cell wall of the Ni-Al sample, small pores in the

scale of several micrometers existed. However, Ni-Al sample ($V_{\text{NaCl}} = 0\%$) shows neither large pores derived from NaCl particles nor small pores derived from combustion synthesis reaction between Ni and Al. Therefore, the combination of spacer method and combustion synthesis reaction was essential to form small pores in cell walls. Moreover, it is noted here that the pure Ni sample were not able to be prepared by spacer method because Ni has a high melting point (1455°C) and the sintering could not proceed at the temperature below the melting point of NaCl (801°C).

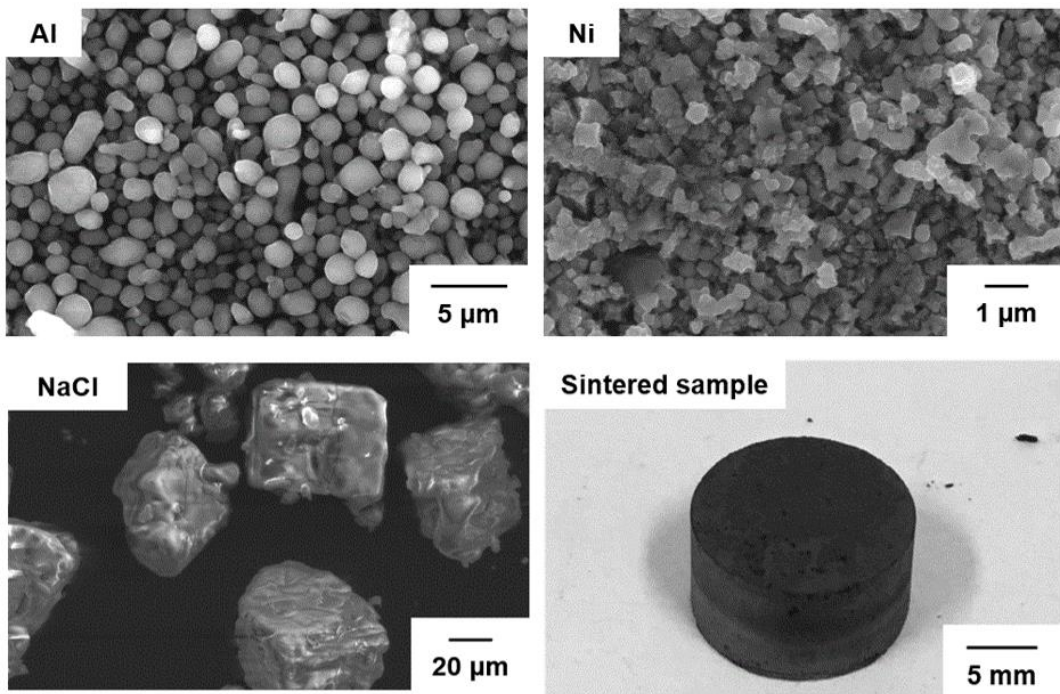


Fig. 2-7 Morphologies of raw powders (Al, Ni, NaCl), and the appearance of representative sintered specimen.

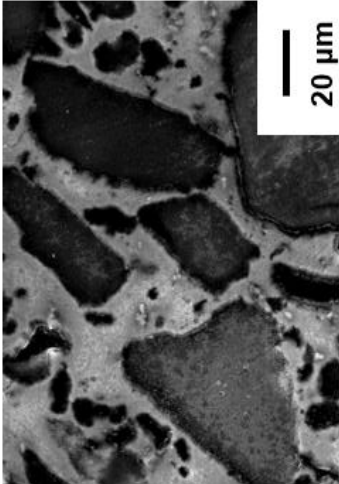
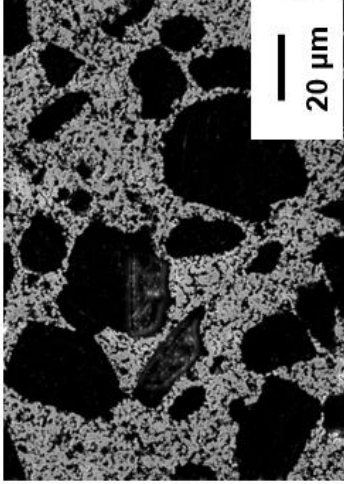
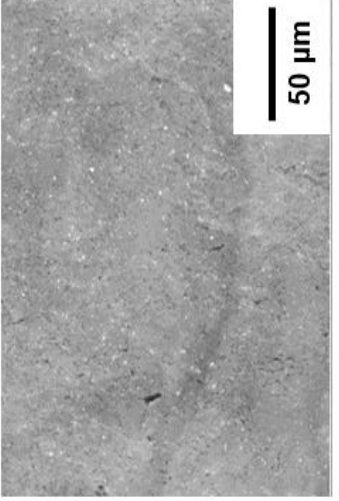
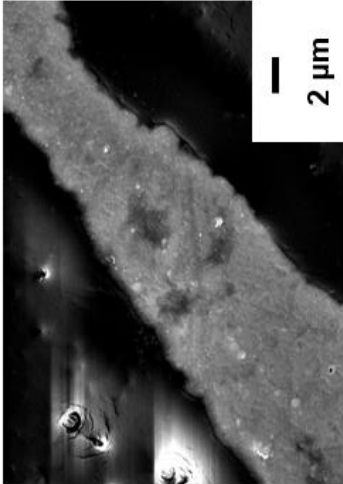
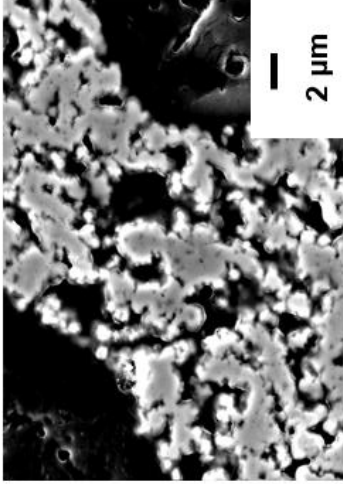
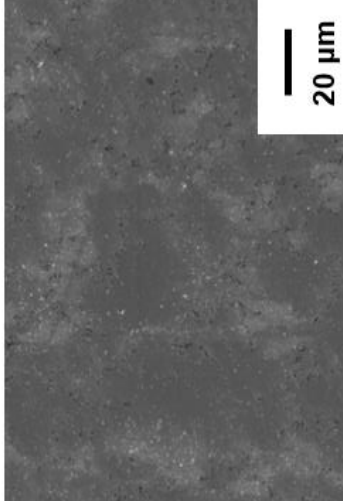
	Pure Al	Ni-Al (NaCl 60 vol%)	Ni-Al (NaCl 0 vol%)
Large pore structure			
Cell wall of large pore			

Fig. 2-8 SEM images of porous pure Al and porous Ni-Al samples with NaCl of 60 vol% and 0 vol%. The Ni-Al sample was sintered at 650°C for 300 s.

2.3.3 Effects of sintering parameters

Figure 2-9 shows the size distribution of large pores derived from NaCl particles (a) and pores formed by combustion synthesis reaction (b). From this result, we understood the pore size distribution of large pores is almost the same with the particle size distribution of NaCl, and the pore size was mostly distributed below 50 μm . And the pore size distribution of small pores derived from combustion synthesis reaction was mostly distributed below 2.5 μm . In the case that NaCl volume fraction is 60%, the parameters of porous structure are shown in Table 2-1. The volume fraction of small pores in cell wall and total porosity reach 32% and 68.56% respectively. The mean size of small pores is 0.42 μm and the mean size of large pores is 42.18 μm , which is distributed in the range of used NaCl particle size.

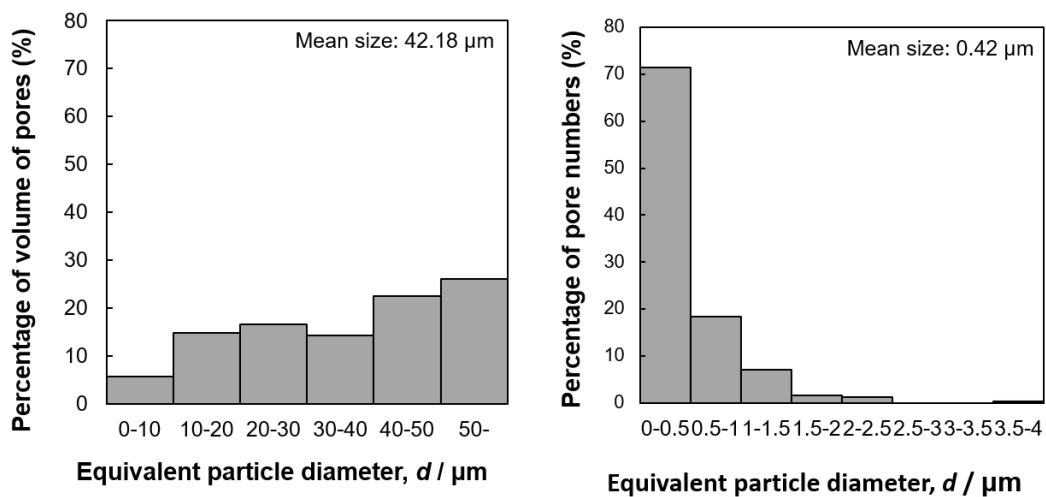


Fig. 2-9 Size distributions of large pores derived from NaCl particles (a) and pores formed by combustion synthesis reaction (b).

Table 2-1. Parameters of porous Ni-Al compound with NaCl volume fraction of 60% (Ni:Al=1:1).

NaCl (vol %)	Volume fraction of small pores in cell wall (%)	Porosity of small pores (%)	Porosity of large pores (%)	Total porosity of porous Ni- Al (%)	Mean size of small poes (μm)	Mean size of large pores (μm)
60	32	14.67	53.89	68.56	0.42	42.18

Fig. 2-10 shows the SEM images of the cell wall of the porous Ni-Al sample ($V_{NaCl} = 60\%$) held at various sintering temperatures for 300 s. At 450°C, which is below the ignition temperature (around 500°C), only the unreacted Ni particles with light contrast and unreacted Al particles with dark contrast were observed. At the temperature from 500°C to 600°C, due to the occurrence of reaction, unreacted Ni was not observed. In particular, different contrasts of multiple phases including various Ni-Al intermetallic compounds were observed. At the temperature of 650°C, only one contrast were observed in the metallic cell wall. The constituting phases of porous Ni-Al samples were also detected by X-ray diffraction (XRD) and shown in Fig. 2-6. The diffraction peaks of Al (fcc) and Ni (fcc) were detected at 450°C, and diffraction peaks of 1 Ni-Al intermetallic compounds including NiAl (B_2), Ni₃Al ($L1_2$), and Ni₂Al₃ ($D5_{13}$) were detected at the range of 500°C - 600°C. However, at 650°C, only the diffraction peaks of NiAl (B_2) were detected. The superlattice lines corresponding to the ordered B2 crystal structure of NiAl are clearly observed in this XRD profile. From results of Fig 2-10 and Fig 2-6, we understood that the sintering temperature have to be raised up above 650°C to promote sintering process for obtaining single-phase porous NiAl with an ordered B2 crystal structure. However, from the EBSD analysis of Ni-Al sample (Fig. 2-11), we found that there were still a small amount of other phases remain, which indicated that absolute single-phase samples are difficult to prepare in practice.

Variations of mean small pore size and porosity of small pores in cell walls with increasing sintering temperatures are shown in Fig. 2-12. Basically, small pores generated from 500°C, which is considered as the ignition temperature of combustion synthesis reaction. Therefore, the porosity of small pores at 450 °C was nearly 0%. On the other hand, both the porosity and mean size of small pores in cell walls drastically increased when sintering temperature reached 500 °C, which also indicated the start of combustion synthesis reaction between Ni and Al. From 500 °C

to 650 °C, both the porosity in cell walls and the pore size kept generally consistent with only a minor decreasing. We also investigated the effects of sintering time on porosity in cell walls and mean circle equivalent pore diameter (Fig. 2-13). There were no obvious changes both in porosity and mean size when we extended the sintering time from 300s to 10800s.

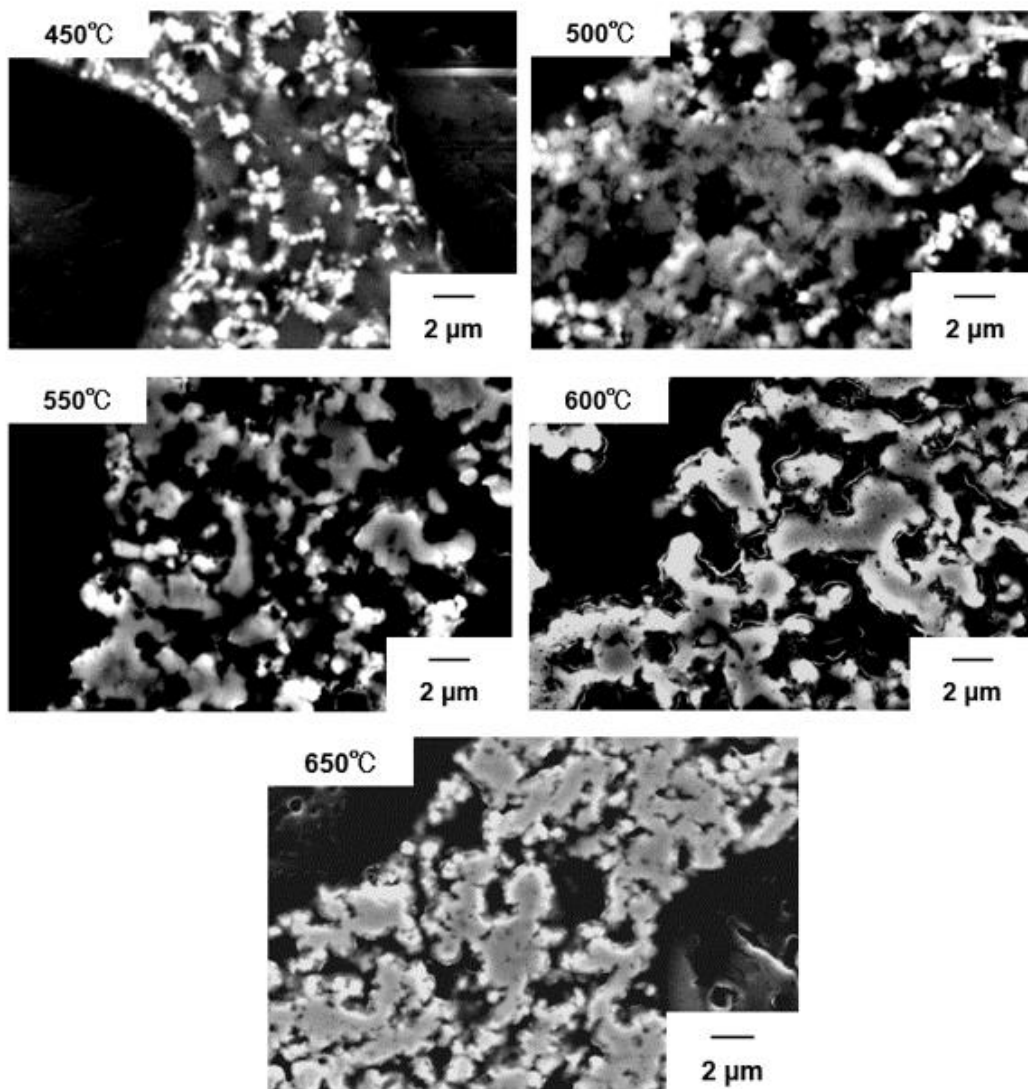


Fig. 2-10 The metallic cell walls of the Ni-Al samples sintered at 450°C, 500°C, 550°C, 600°C, and 650°C for 300 s ($V_{\text{NaCl}} = 60\%$).

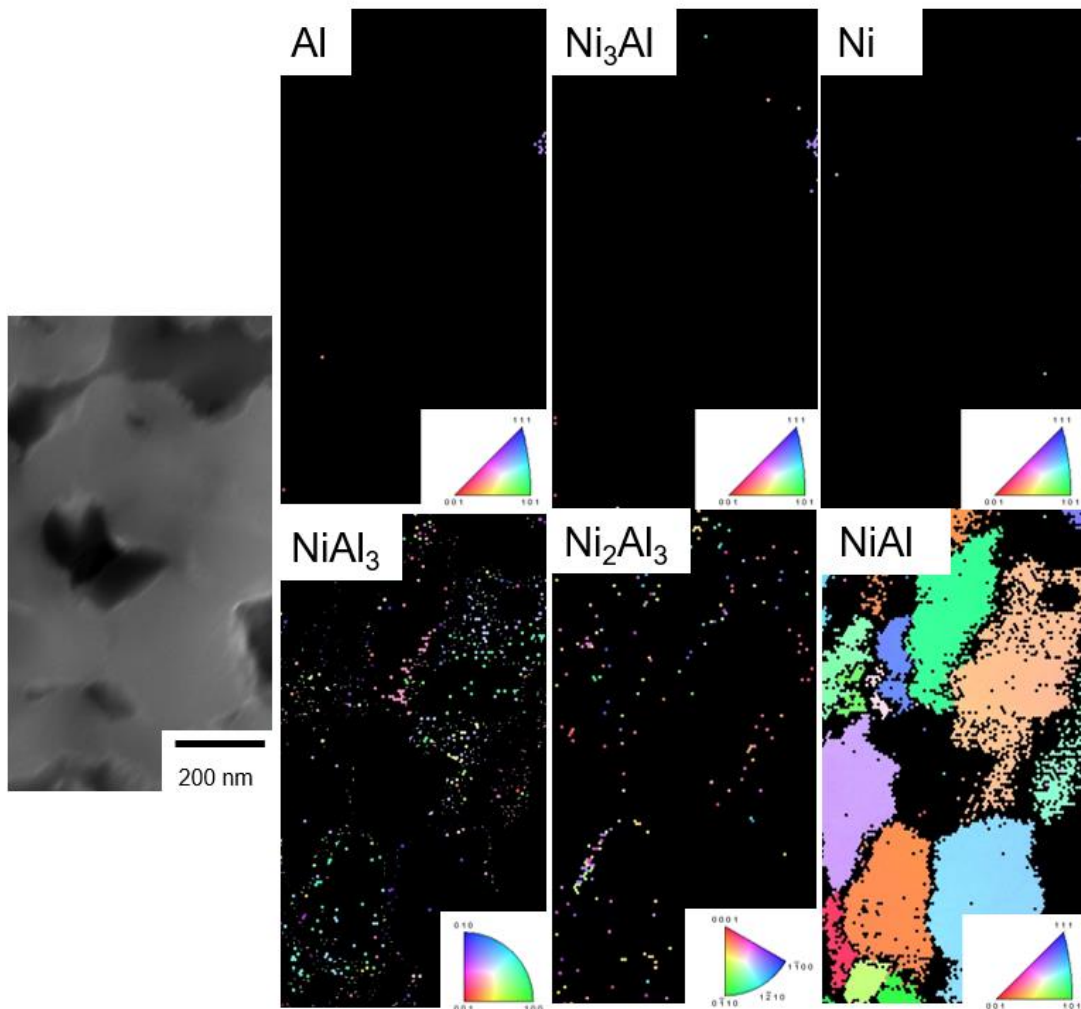


Fig. 2-11 EBSD analysis of Ni-Al samples sintered at 650°C for 300 s ($V_{\text{NaCl}} = 60\%$).

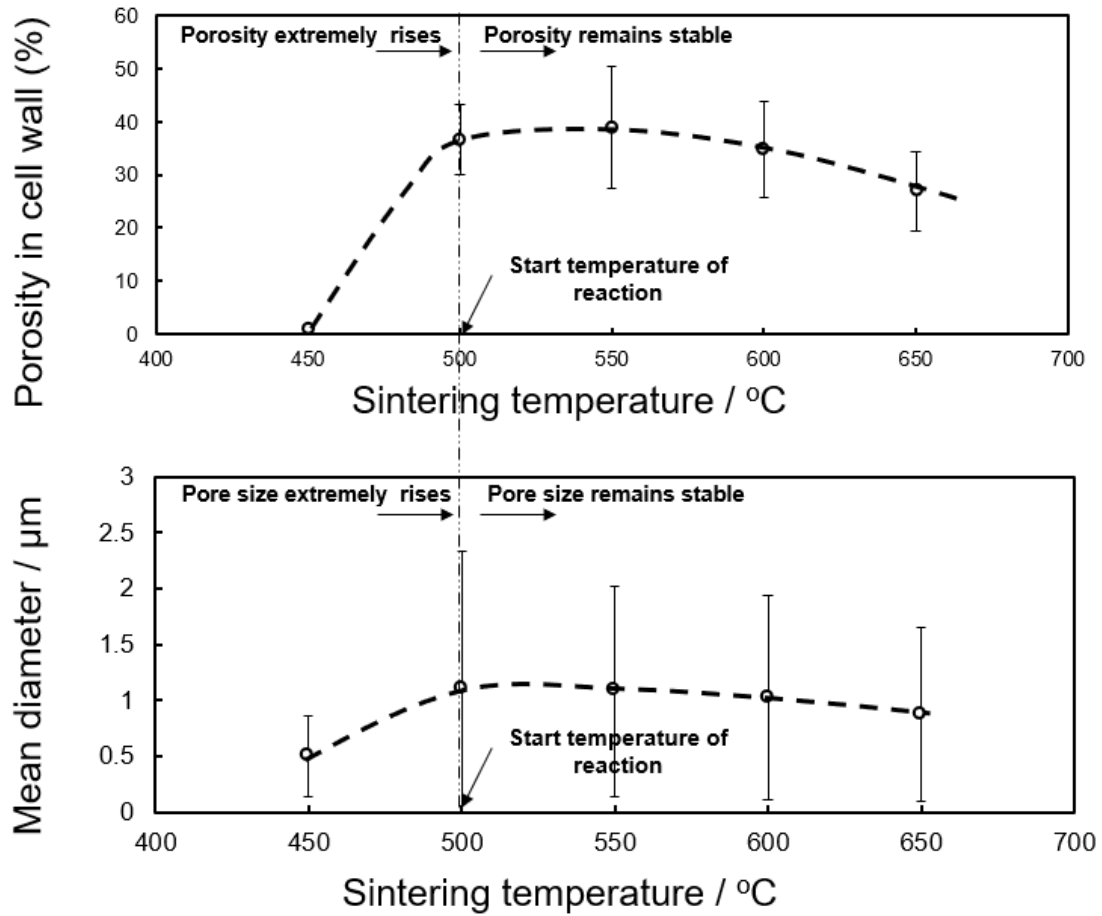


Fig. 2-12 Changes of the pore size and porosity in metallic cell wall at various sintering temperatures with NaCl volume fraction of 60% when Ni:Al=1:1.

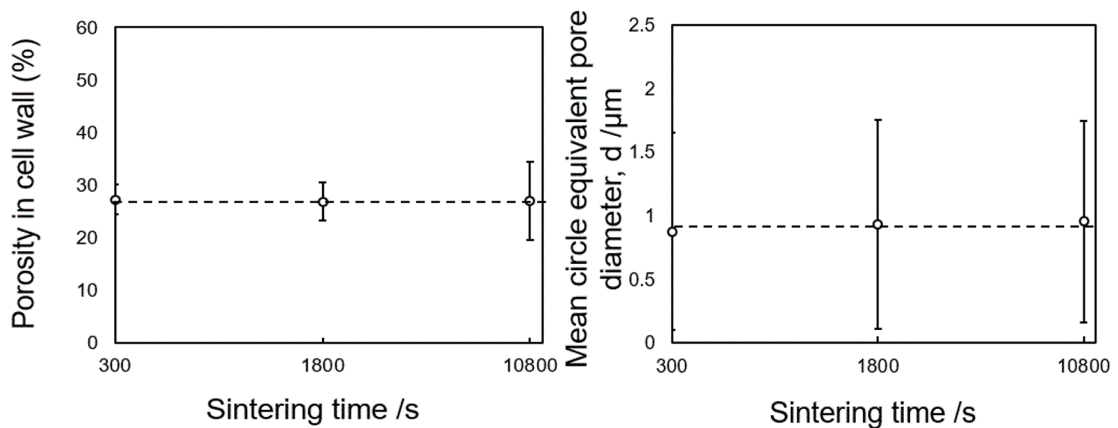


Fig. 2-13 Effects of sintering time on porosity in cell walls and mean circle equivalent pore diameter in the case of Ni:Al=1:1, $V_{\text{NaCl}}=60\%$.

2.4 Discussion

Dr. Hibino claimed that the combustion synthesis reaction of a Ni-Al system begins from the melting of Al or eutectic melting between Al and Ni [2-19]. Thus, one of the hypotheses is that the temperature of sample reached the eutectic melting temperature (640°C) or the melting point of Al (660°C) when the temperature measured by the thermocouple was 500°C. Another viewpoint is that the combustion synthesis reaction between Ni and Al can be induced below 600 °C by the solid diffusion of solid Ni and Al powders [2-21, 2-22]. The mechanism of the combustion synthesis reaction between Al and Ti to synthesize TiAl was investigated in previous study [2-23]. At the beginning of the reaction between Al and Ti, melting of Al is involved. Subsequently, the molten Al infiltrates into the gaps among the Ti particles, and then the Al atoms diffuse into the Ti particles to start the reaction. The generated reaction heat ignites the further reaction between Al and Ti to form intermetallic compounds such as TiAl₃ and TiAl. Finally, the liquid Al phase is exhausted to form Ti-Al intermetallic compounds. In the case of the Ni-Al system, a similar process is also reported [2-24].

However, in this present study we realized the low-temperature fabrication of Ni-Al intermetallic compounds by pressurized electric current sintering. The occurrence of combustion synthesis was measured at approximately 500°C, which is much lower than the melting point of Al (660°C). Therefore, the viewpoint that the combustion synthesis reaction between Ni and Al can be induced below 600°C by the solid diffusion of solid Ni and Al powders [2-21, 2-22] was considered as the mechanism of the Ni-Al combustion synthesis reaction in this study. This is because the constant pressure during sintering promoted the diffusion of Al and Ni particles, so that the reaction was ignited at a relatively lower temperature than the melting point of Al (660°C) or the eutectic melting temperature (640°C). Also, the low ignition temperature of Ni-Al combustion synthesis reaction could be explained from the perspective of melting point. The equilibrium phase diagram (Fig. 2-14) and metastable phase diagrams (Fig. 2-15) of Ni-Al binary system were calculated by CALPHAD method for further discussion on the ignition temperature. The eutectic melting temperature of Al is about 640°C in equilibrium (Fig. 2-14), but this value decreases significantly in metastable state (Fig. 2-15). As shown in Fig. 2-15, the eutectic melting temperature of Al phase (Al) drops to about 550°C in the case of three-phase equilibrium (Liquid, B2 And Al), and the melting temperature of Al phase (Al) could even drop below 100°C in the case of two-phase equilibrium (Liquid And Al). It is suggesting that the melting of Al might happen below 600°C in practice of this study, resulting in a lower ignition temperature (below 600°C) of Ni-Al combustion synthesis reaction.

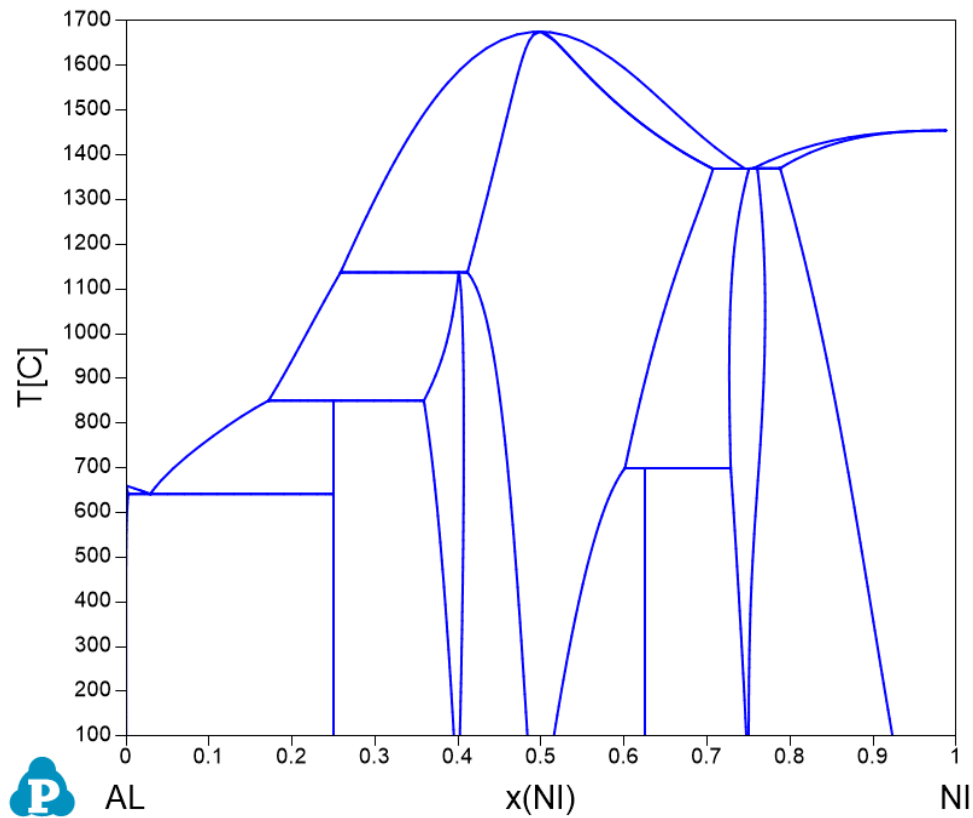


Fig. 2-14 Equilibrium phase diagram of Ni-Al binary system. (The thermodynamic Gibbs energy parameters are available from [I. Ansara, N. Dupin, H. L. Lukas and B. Sundman, 'Thermodynamic assessment of the Al-Ni system', J. alloys and compounds, 247 (1997), 20-30.]

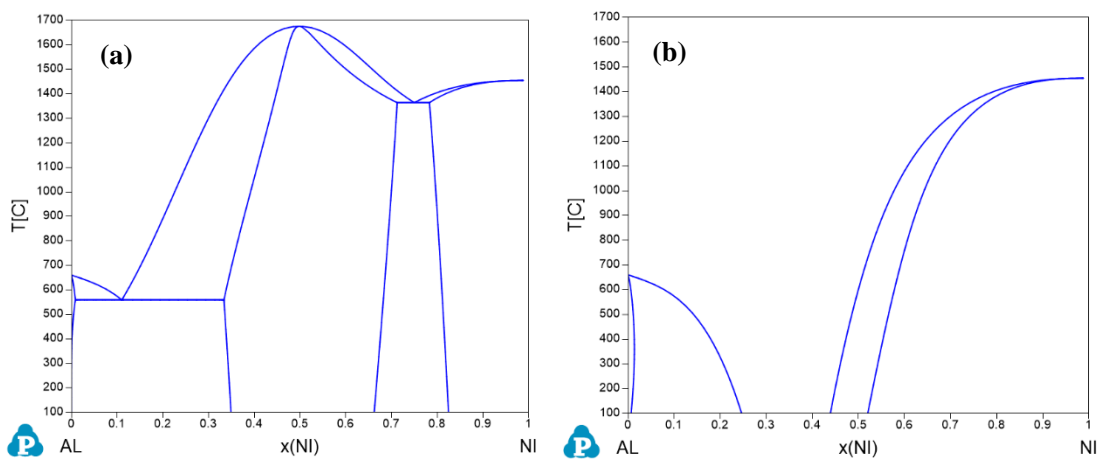


Fig. 2-15 Metastable phase diagrams of Ni-Al binary system: (a) Phase equilibria among three phases (Liquid, B2 and A1); (b) Phase equilibria between two phases (Liquid and A1).

When the sintering temperature was 650 °C, the reaction was completed and the single-phase NiAl was obtained by sintering for 300 s. However, the reaction did not finish when the sintering temperature was below 650 °C. This is because higher temperature provides the energy to overcome the barrier, so that promote the progress of the reaction between Ni and Al. As a result, the combustion synthesis reaction between Ni and Al did not propagate and finish in low temperature. Moreover, sintering time has no effects on the morphologies of small pores derived from reaction. That is because the formed Ni-Al intermetallic compounds have much higher melting points (Ni₃Al: 1395 °C, NiAl: 1639 °C, NiAl₃: 854 °C) than 650 °C, so pores surrounded by Ni-Al intermetallic compounds can be maintained well to the end.

In this research, the temperature of reaction was considered to be influenced by three factors: adiabatic temperature (T_{ad} , assuming that 100% conversion of final products), actual percent conversion of final products, and heat dissipation to outside. In the process of combustion synthesis reaction, temperature of sample rises from initial temperature to ignition temperature to start reaction, and the temperature of sample rises from ignition temperature to highest combustion temperature because of the exothermal energy derived from combustion synthesis. The highest combustion temperature is equal to adiabatic temperature by assuming that the released heat from combustion synthesis reaction is used only for raising sample temperature without heat dissipation. Adiabatic temperature has important significance on exothermal reaction, especially on combustion synthesis reaction. That's because adiabatic temperature highly affects the status of products if it's higher than the melting point of products. We calculated adiabatic temperature, we assume that enthalpy change does not exist ($\Delta H = 0$), which means all the released heat including actual heat loss is used for raising temperature of products. The adiabatic temperature (T_{ad}) of Ni-Al combustion synthesis reaction and the theoretical liquidus molar fraction were calculated in Fig. 2-16. The thermodynamic parameters used for the calculation have been described by Bari [2-25]. In a strict sense, during the reaction progress various Ni-Al compounds like NiAl, Ni₃Al and Ni₂Al₃ were formed, although only formation of final product is considered in each Ni:Al molar ratio here for simplicity. The molar fraction of the liquidus phase decreases curvilinearly within the V_{NaCl} range from 0 to 46.7% as shown in Fig 2-16 (a). This is because the volume fraction is used instead of the molar fraction of NaCl on the horizontal axis. As shown in Fig 2-16 (b), T_{ad} decreased with increasing V_{NaCl} because the reaction heat is absorbed by space-holder NaCl. When V_{NaCl} is in the range of 0-46.7%, T_{ad} becomes constant due to the latent heat derived from the melting of NiAl. Most of the NiAl phase formed by the combustion synthesis reaction melts to form Ni-Al liquid in the case of no NaCl addition ($V_{NaCl} = 0\%$). Thus, the small pores disappear during the pressurized sintering. When V_{NaCl} is above 46.7%, the entire NiAl phase does not melt, and the size of small pores tended to be constant when V_{NaCl} was larger than 46.7%. Figure 2-17 shows the XRD profiles of the Ni-Al samples with NaCl of 60 vol% and 0 vol% sintered around 500 °C (right after reaction). The combustion synthesis reaction was adequately promoted in the case of $V_{NaCl} = 0\%$ and only the peaks of NiAl were observed, which indicated that the true temperature in the case of $V_{NaCl} = 0\%$ was higher than that in

the case of $V_{\text{NaCl}} = 60\%$. Thus, in order to form small pores in cell walls, it is essential to add NaCl into raw mixture for avoiding melting the products.

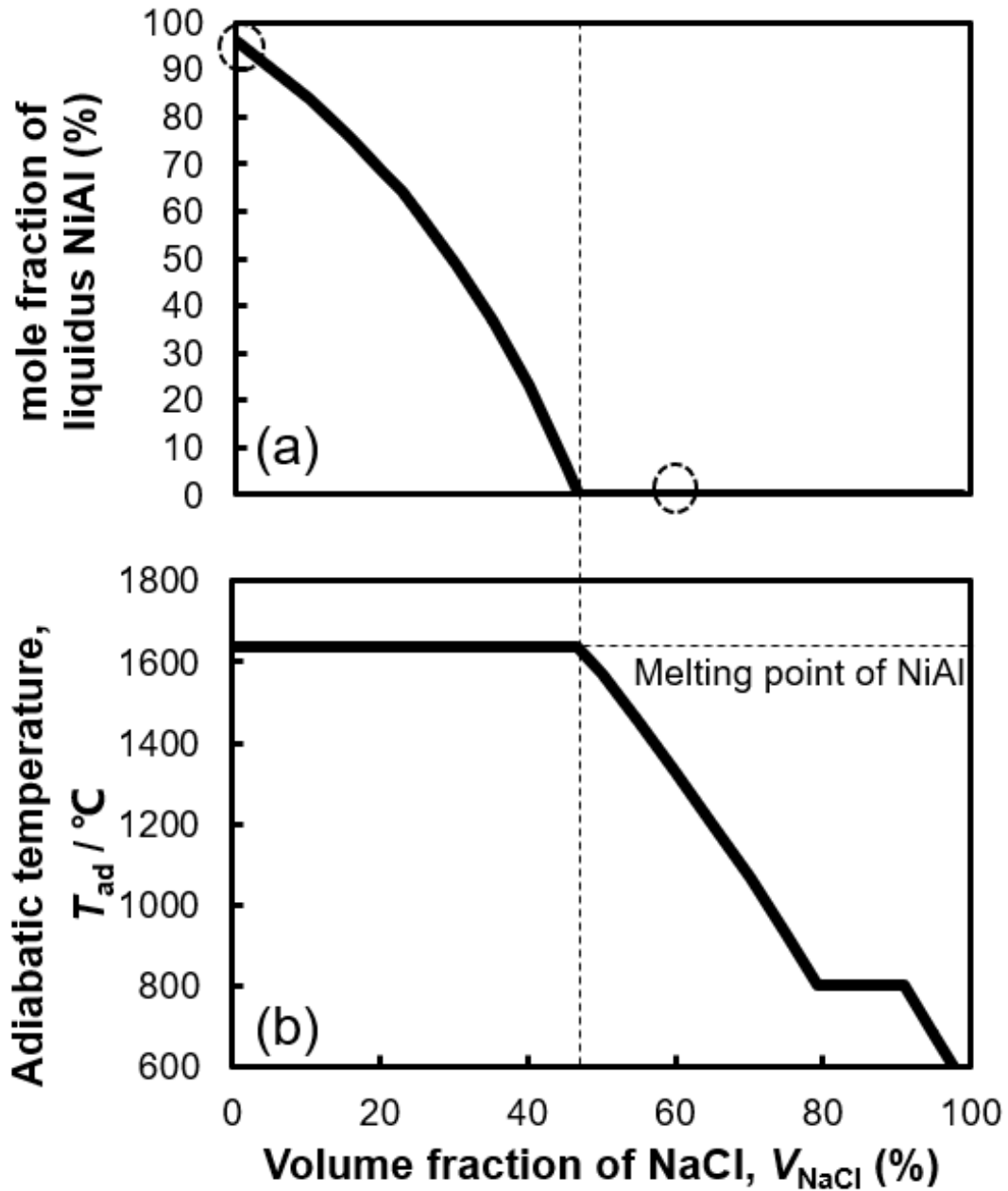


Fig. 2-16 Changes in the (a) mole fraction of liquidus NiAl and (b) adiabatic combustion temperature as a function of the volume fraction of NaCl.

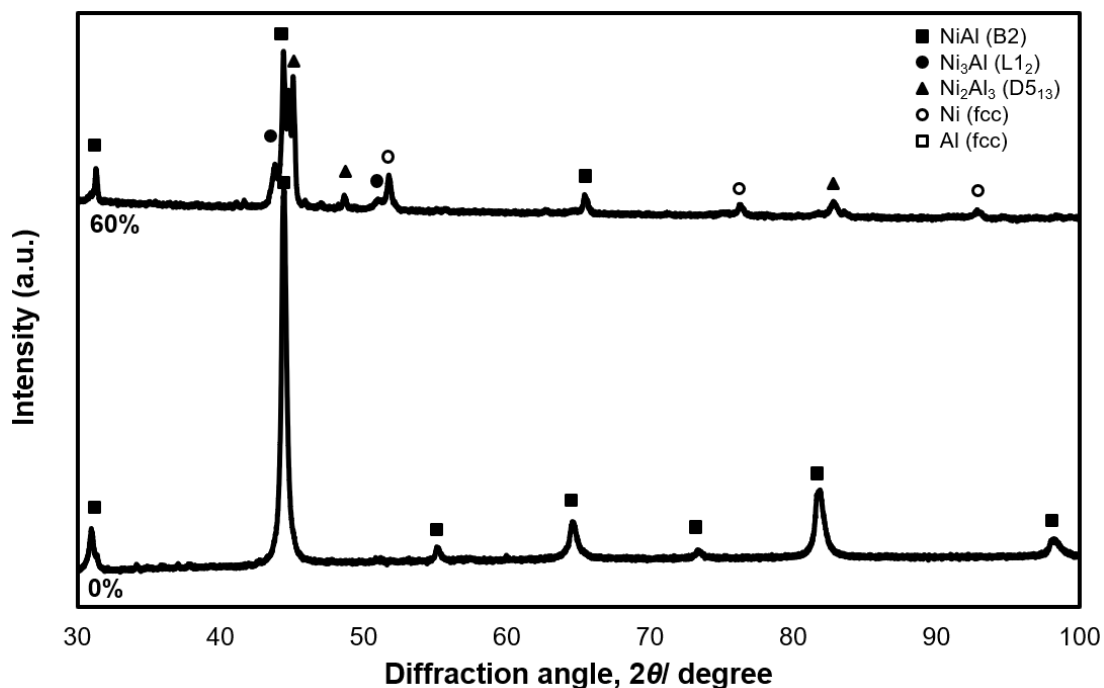


Fig. 2-17 XRD profiles of the Ni-Al samples with NaCl of 60 vol% and 0 vol% sintered around 500°C (right after reaction).

2.5 Summary

We successfully developed a simple and rapid process of fabricating porous Ni-Al intermetallic compounds with hierarchical porous structures by combining the combustion synthesis reaction and the space holder method. We also revealed that space-holder NaCl is not only used for forming large pores derived from NaCl, but also essential for forming small pores derived from reaction. Fabricated NiAl had large pores replicated from space-holder NaCl particles, and small pores derived from combustion synthesis reaction between Ni and Al in the range of 2.5 micrometers and below. The control of the sintering temperature and time (650 °C, holding for 300 s) permits the formation of dominate-phase NiAl in the case of $V_{\text{NaCl}} = 60\%$.

Reference

- [2-1] S.C. Wong, J.H. Liou, C.W. Chang: Evaporation resistance measurement with visualization for sintered copper-powder evaporator in operating flat-plate heat pipes, *International Journal of Heat and Mass Transfer*, 53 (2010), pp. 3792–3798.
- [2-2] C.B. Sobhan, R.L. Rag, G.P. Peterson: A review and comparative study of the investigations on micro heat pipes, *International Journal of Energy Research*, 31 (2007), pp. 664–688.
- [2-3] Chan Byon, Sung Jin Kim: Capillary performance of bi-porous sintered metal wicks, *International Journal of Heat and Mass Transfer*, 55 (2012), pp. 4096-4103.
- [2-4] J. M. Lee, N. W. Sun, G. B. Cho, K. O. Oh: Performance of radial-type metal foam diesel particulate filters, *International Journal of Automotive Technology*, 11 (2010), pp. 307-316.
- [2-5] Kwanhee Choi, Juwon Kim, Ahyun Ko, Cha-Lee Myung, Simsoo Park, Jeongmin Lee: Size-resolved engine exhaust aerosol characteristics in a metal foam particulate filter for GDI light-duty vehicle, *Journal of Aerosol Science*, 57 (2013), pp. 1-13.
- [2-6] S. Arisetty, A. K. Prasad, S.G. Advani: Metal foams as flow field and gas diffusion layer in direct methanol fuel cells, *J. Power Sources*, 165 (2007), pp. 49-57.
- [2-7] R. Abdel-Karim, Y. Reda, K. M. Zohdy, A. Abdelfatah, S. El-Raghy: Electrochemical Performance of Porous Ni-Cu Anodes for Direct Methanol Fuel Cells, *Int. J. Electrochem. Sci.*, 14 (2019), pp. 3035 – 3054.
- [2-8] P. Joghee, J. N. Malik, S. Pylypenko, R. O’Hayre: A review on direct methanol fuel cells – In the perspective of energy and sustainability, *MRS Ener. Sustain. A Review*, 2 (2015).
- [2-9] 和田正弘: スラリー発泡法による発泡金属, *化学と工業*, 54-7(2001), pp. 811-813.
- [2-10] Lucai WANG, Haijuan LI, Fang WANG, Jianfu REN: Preparation of open-cell metal foams by investment cast, *CHINA FOUNDRY*, 2-1(2005), pp. 56-59.
- [2-11] C.E.Wen, M.Mabuchi, Y.Yamada, K.Shimajima, Y.Chino and T.Asahina: Processing of biocompatible porous Ti and Mg, *Scripta Mater.*, 45 (2001), pp. 1147-1153.
- [2-12] C.E.Wen, Y.Yamada, K.Shimajima, Y.Chino, H.Hosokawa and M.Mabuchi: Novel titanium foam for bone tissue engineering, *J. Mater. Res.*, 17 (2002), pp. 2633-2639.
- [2-13] H.X.Dong, Y.Jiang, Y.H.He, M.Song, J.Zou, N.P.Xu, B.Y.Huang, C.T.Liu, P.K.Liaw: Formation of porous Ni–Al intermetallics through pressureless reaction synthesis, *Journal of Alloys and Compounds*, 484 (2009), pp. 907-913.
- [2-14] Naoki Takata, Keisuke Uematsu, Makoto Kobashi: Compressive properties of porous Ti–Al alloys fabricated by reaction synthesis using a space holder powder, *Materials Science and Engineering: A*, 697 (2017), pp. 66-70.
- [2-15] ZHENG Zhi, JIANG Yao, DONG Hong-xing, TANG Lie-min, HE Yue-hui, HUANG Bai-yun: Environmental corrosion resistance of porous TiAl intermetallic

compounds, Transactions of Nonferrous Metals Society of China, 19 (2009), pp. 581-585.

[2-16] Nakajima, Hideo: Fabrication of Lotus-Type Porous Metals, Intermetallic Compounds and Semiconductors, Materials Science Forum, 502 (2005), pp. 367-372.

[2-17] Guo Jian-ting: Ordering Ni-Al intermetallics, Beijing: Science Press, 2003, pp. 3-5. (in Chinese)

[2-18] Okamoto, H.: Al-Ni (Aluminum-Nickel), J. Ph. Equilib. 14 (1993), pp. 257–259.

[2-19] Hibino, A.: Reaction Process and Model Simulation of Combustion Synthesis of Ni₃Al Intermetallic Compounds, J. Japan Inst. Metals 56 (1992), pp. 1435 – 1443.

[2-20] Yunmao Shu, Asuka Suzuki, Naoki Takata, Makoto Kobashi: Fabrication of porous NiAl intermetallic compounds with a hierarchical open-cell structure by combustion synthesis reaction and space holder method, Journal of Materials Processing Tech., 264 (2019), pp. 182–189.

[2-21] H.X.Dong, Y.Jiang, Y.H.He, M.Song, J.Zou, N.P.Xu, B.Y.Huang, C.T.Liu, P.K.Liaw: Formation of porous Ni–Al intermetallics through pressureless reaction synthesis, Journal of Alloys and Compounds, 484 (2009), pp. 907-913.

[2-22] X.Qiu, J.Wang: Experimental evidence of two-stage formation of Al₃Ni in reactive Ni:Al multilayer foils, Scripta Materialia, 56 (2007), pp. 1055-1058.

[2-23] Hibino, A., Watanabe, R.: Reaction Mechanism of Combustion Synthesis of TiAl Intermetallic Compound, J. Japan Inst. Metals, 55 (1991), pp. 1256–1262.

[2-24] Inoue, M., Suganuma, K.: Reactive sintering behavior of intermetallic compounds in Ni-Al system, J. Japan Inst. Light Metals 44 (1994.), pp. 658–662.

[2-25] Bari, I., Sauert, F., Schultze-Rhonhof, E., Sheng, W.S.: Thermochemical Data of Pure Substances. VCH Verlagsgesellschaft mbH. 1993.

[2-26] The Materials Project, <https://www.materialsproject.org/>

Chapter 3. Investigation of effects on porous structure and constituting phases

3.1 Introduction

Porous structures have a range of effects on various properties and applications of porous materials. For example, Chan Byon et al. [3-1] reported that utilizing a hierarchical porous structure could enhance the capillary performance of porous media, and Christopher M. A. Parlett et al. [3-2] optimized the catalytic applications of porous materials by utilizing hierarchical porous structure on catalytic applications. Also, remarkable effects of porous structure on compressive properties are reported [3-3, 3-4].

Porous structures include a number of aspects such as porosity, size distribution and pore morphologies, which affect the mechanical properties, specific surface area, flow permeability and so on. In the application of LHP, high permeability and capillary force of porous wicks are achieved by suitable porous structure. In the case of filter application, people filter impurities by fabricating porous materials with required pore size. In terms of catalysis, we enhance the catalytic efficiency by increasing the specific surface area for more contact area with catalyst. Therefore, control of porous structures is the key factor for practical applications of porous materials.

In previous chapter, we combined spacer method and combustion synthesis reaction to fabricate porous metals. As known, in the case of spacer method, porous structure such as porosity, pore size distribution and pore morphologies could be precisely controlled by adjusting the addition of space-holder material. Hence, controlling the porous structure of small pores generated by combustion synthesis reaction has become our main subject in this study. Parameters of mixing powder including Ni:Al molar ratio and NaCl volume fraction were mainly investigated. Ni:Al molar ratio in raw powders were set in 3:1, 1:1 and 1:3 for representing Ni-rich state, equilibrium state, Al-rich state respectively. Moreover, recording to the equilibrium phase diagram of the Ni-Al binary system shown in Chapter 2, the final products are inferred to be Ni_3Al , NiAl and NiAl_3 respectively corresponding to the Ni:Al molar ratios of 3:1, 1:1 and 1:3 [3-5]. Effects of volume fraction of space holder (NaCl) in raw powders which absorb reaction heat were also investigated. We expect to acquire the strategy of controlling porous structure by investigating the effects on porous structure of pores derived from combustion synthesis reaction in this study.

3.2 Experimental method

3.2.1 Fabrication and evaluation

Porous Ni-Al intermetallic compounds were fabricated by the process introduced in last chapter, and the flowchart of this process is shown in Fig.3-1. First, the volume fractions of NaCl (V_{NaCl}) in raw mixture were prepared in 20%, 40%, 60% and 80% respectively for investigating the effects of NaCl on porous structure of small pores derived by reaction. Then, the Ni and Al powders were blended in an atomic ratio of 3:1, 1:1 and 1:3 for further investigating the effects of Ni:Al molar ratio on porous structure of small pores derived by reaction. After sintering, the samples were cooled in furnace to ambient temperature. Then, the specimens were soaked in static pure water for 24 h to remove the NaCl space holder for the formation of large pores, which were replicated from space-holder NaCl. After removing the NaCl particles, surface treatment was performed for microstructure evaluation. Subsequently, the porous structure was observed by scanning electron microscope (SEM) and the constituting phase was evaluated and measured by X-ray diffraction (XRD) operating at 40 kV and 40 mA with a Cu-K α radiation source. Also, the sectional image analysis introduced in last chapter was performed to estimate porosity in cell walls, mean pore size, and size distribution.

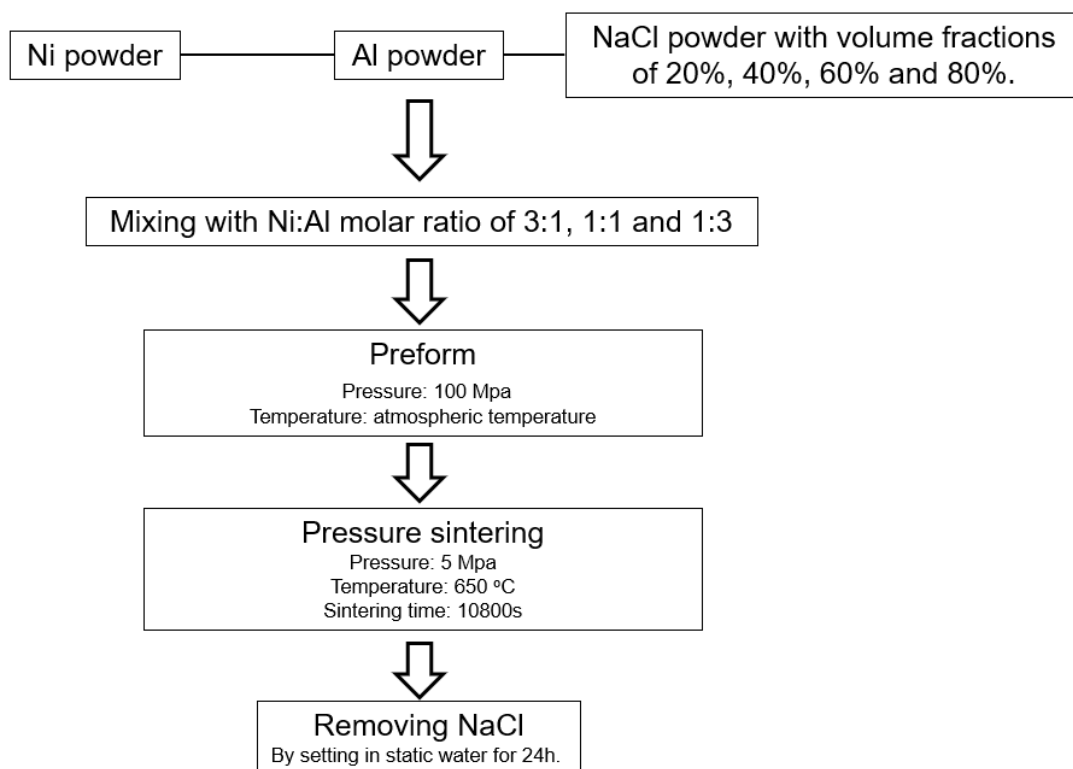


Fig. 3-1 Process of fabricating porous Ni-Al intermetallic compounds.

3.2.2 Volume fraction of constituting phases

In order to evaluate the volume fraction of constituting phases right after the combustion synthesis reaction occurred, the XRD profiles of the samples sintered at 500 °C were analyzed by the Reference Intensity Ratio (RIR) method. It is noted that the mass fraction of constituting phases could be estimated directly by RIR method, and then the volume fraction could be calculated according to the density of various phases.

Here we utilize the parameter K to represent the reference intensity ratio of materials, and the K can be expressed by follow equation:

$$K = I/I_c \quad (1)$$

Where I is the intensity of the diffraction of the specified phase, and I_c is the intensity of the diffraction of contrast phase, which has the equal mass to that of specified phase. Usually, the K value is known and able to be queried from references. If multiple phases exist in some material, the correlation of diffraction intensity between any two phases (phase 1 and phase 2) could be expressed below:

$$\frac{I_1}{I_2} = \frac{K_1}{K_2} \times W_{12} \quad (2)$$

Where w_{12} is the mass ratio of phase 1 and phase 2. By this equation, mass ratio of each component inside material could be calculated directly, thereby mass fractions of each phases could be estimated. In this study, we aimed at estimating the overall volume change of materials by the RIR method.

3.3 Results

3.3.1 The effects of space-holder addition

From the results of previous chapter, we understood that NaCl has effects on combustion synthesis reaction because of the heat absorption. Thus, the small pores derived from the combustion synthesis reaction are certainly thought to be affected by space-holder NaCl. In this part, effects of NaCl on small pores were concretely investigated from the additive amount of NaCl.

Porous Ni-Al samples with NaCl volume fractions of 20%, 40%, 60%, and 80% were prepared in Ni:Al molar ratio of 1:1 first. Figure 3-2 presents the

micromorphologies of porous Ni-Al intermetallic compound with Ni:Al molar ratio of 1:1 in various NaCl volume fractions (20%, 40%, 60%, and 80%), and shows the small pores in the metallic wall derived from reaction surrounding large pores derived from NaCl space holder. Darkest contrast shows epoxy resin infiltrated into pores. Epoxy resin was perfectly infiltrated into small pores derived from combustion synthesis reaction between Ni and Al, which indicates that all the small pores connected each other. From the SEM images, it is obvious that amount of large pores (porosity) was increasing with increasing NaCl volume fraction. Also, small pores had a changing tendency on size with changing NaCl volume fraction. Small pores on the cell wall decreased on size with increasing the NaCl volume fraction in the case of Ni:Al=1:1. The XRD profiles are presented in Fig. 3-3. When NaCl volume fraction (V_{NaCl}) was ranging from 0% to 60%, single-phase porous NiAl samples were formed. However, the phases of the Ni_3Al and Ni_2Al_3 were also detected, which indicated that reaction could not be completed by sintering at 650°C for 300 s when NaCl volume fraction was 80%. In other words, heat absorption by space-holder NaCl actually affects the combustion synthesis reaction, and large amount of space-holder NaCl ($V_{\text{NaCl}} = 80\%$) might result in the reaction insufficiency. The results of chapter 2 is suggesting that porous structure of small pores derived from combustion synthesis reaction is not changed by extending sintering time to obtain single-phase product. However, the constituting phases was affected by sintering time when we used the same way to investigate the formation of single-phase porous Ni-Al sample in the case of $V_{\text{NaCl}}=80\%$. Ni-Al samples (Ni:Al=1:1) with NaCl volume fraction of 80% were prepared by sintering at 650°C for 300 s, 1800 s and 10800 s respectively. And the XRD profiles are presented in Fig. 3-4. From Fig. 3-4, we understood that extents of combustion synthesis reaction can be promoted effectively by extending sintering time to 10800 s to obtain single-phase final products. Therefore, conditions of heat treatment were set in 650°C for 10800 s in the research.

Moreover, the removal rate of NaCl space holder was investigated. Figure 3-5 presents change in removal ratio of NaCl as a function of the volume fraction of NaCl in Ni+Al+NaCl powder mixture when Ni:Al molar ratio was 1:1. When the volume fraction of NaCl was in the range of 40% and above, NaCl space holder could be completely removed, which indicates that large pores derived from NaCl connected each other. On the other hand, When the volume fraction of NaCl was 20%, NaCl could not be completely removed because NaCl particles was partially isolated and could not contact with water. In order to obtain open-cell structure, NaCl needs to be added over 40%.

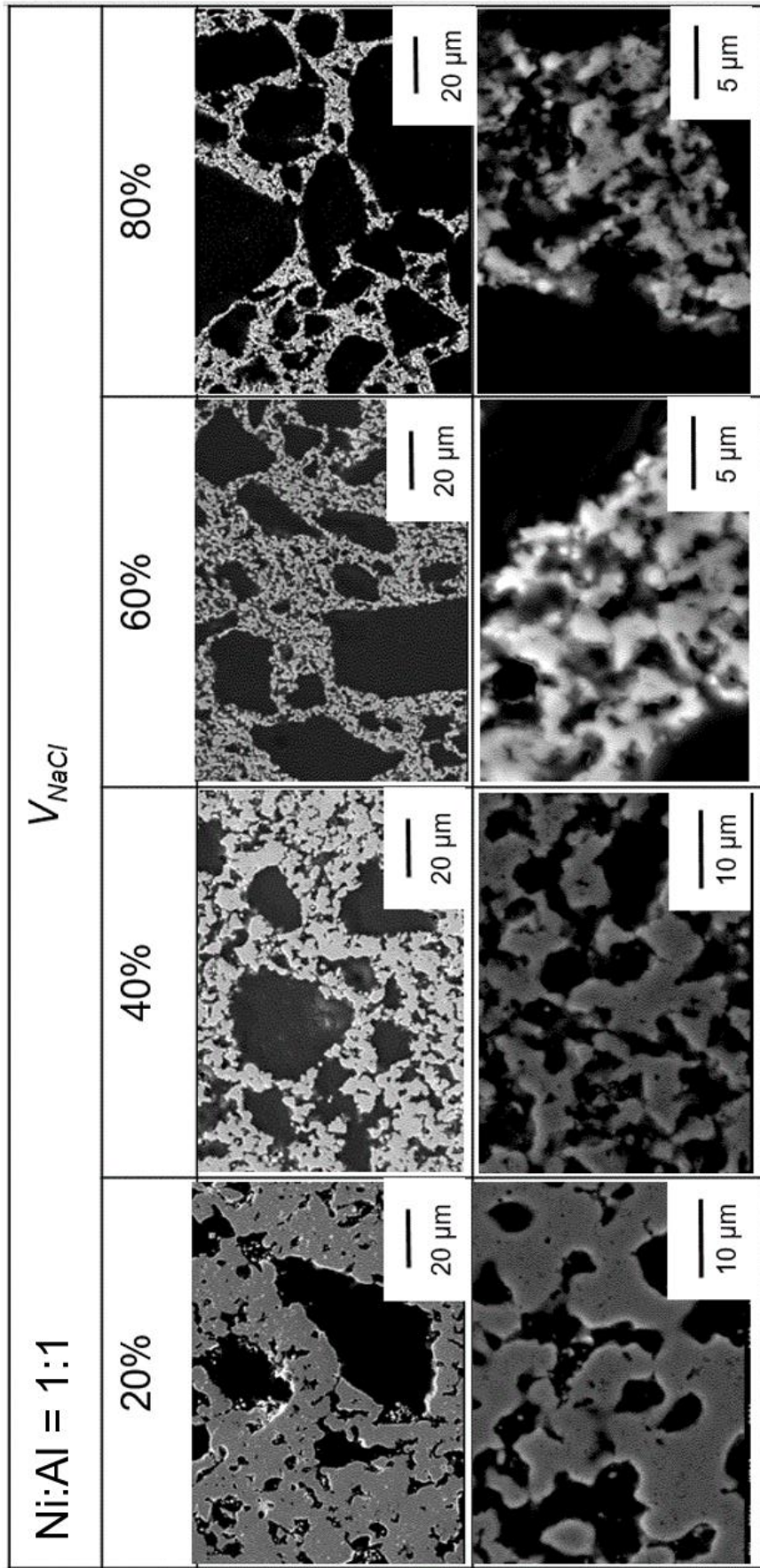


Fig. 3-2 SEM images of porous Ni-Al intermetallic compound with Ni:Al molar ratio of 1:1 in various NaCl volume fractions (20%, 40%, 60%, and 80%).

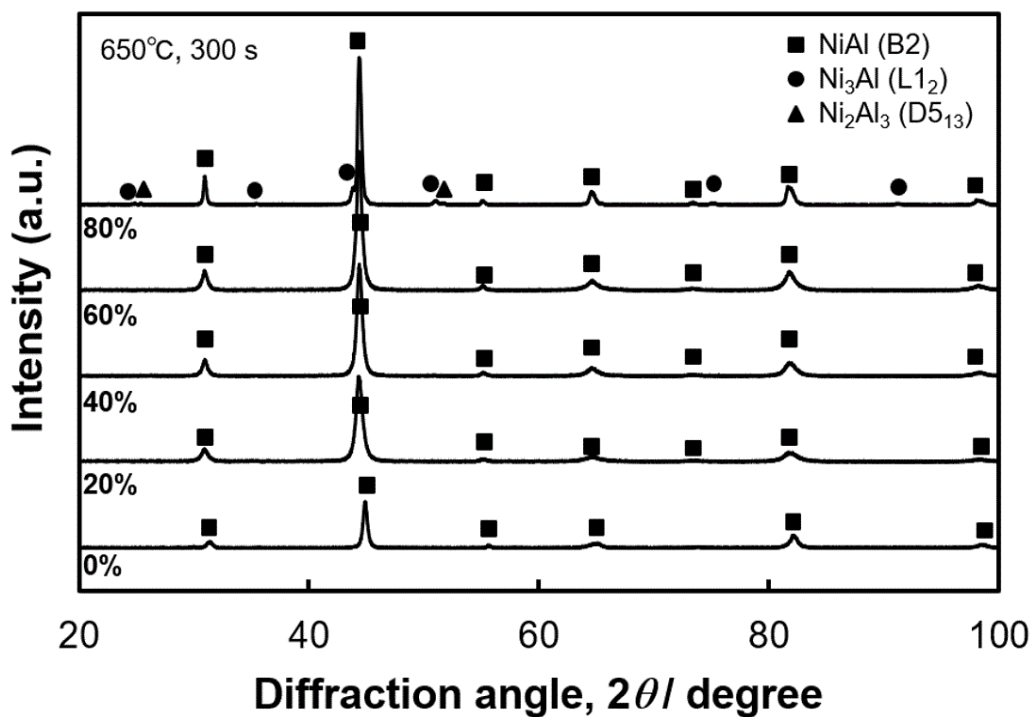


Fig. 3-3 XRD profiles of the samples sintered at 650°C for 300 s with different NaCl volume fractions.

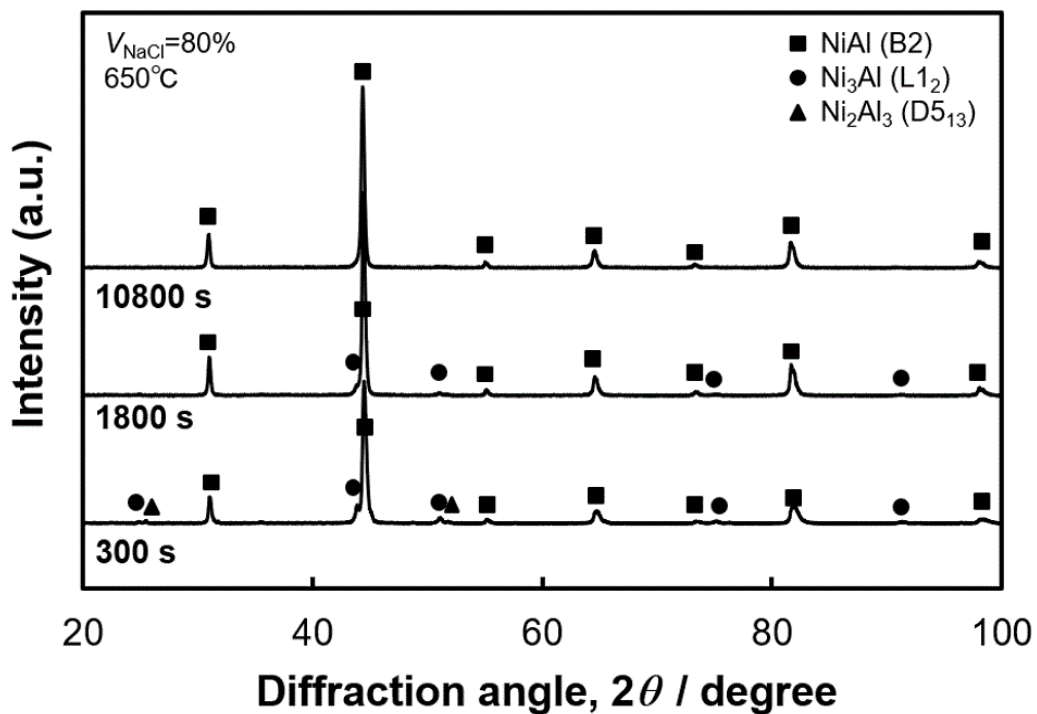


Fig. 3-4 XRD profiles of the samples sintered at 650°C for various sintering times ($V_{\text{NaCl}} = 80\%$).

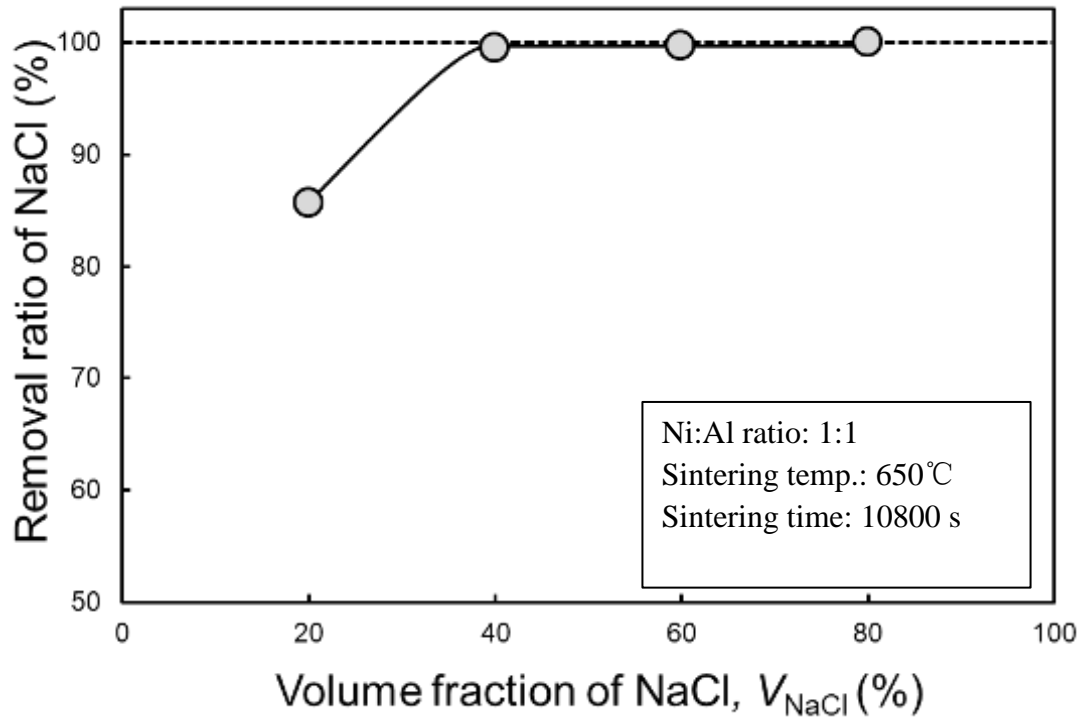


Fig. 3-5 Change in removal ratio of NaCl as a function of the volume fraction of NaCl in Ni+Al+NaCl powder mixture when Ni:Al molar ratio was 1:1.

3.3.2 The effects of Ni:Al molar ratio

3.3.2.1 The effects of sintering time

Fig. 3-6 presents the typical changes of temperature displacement of the graphite punch measured by the thermocouple and the displacement of the graphite punch during heating process in the case of Ni:Al=1:3 and Ni:Al=3:1. In this graph, positive displacement (shrinkage of sample) was defined as the direction which the graphite mold compressed towards. A small peak of temperature was presented at around 500°C where the displacement rose to form a sharp peak in the case of Ni:Al=3:1, which resemble the sintering process of Ni:Al=1:1 mentioned in previous chapter. The shrinkage of sample indicated that the combustion synthesis reaction between Al and Ni occurred at around 500°C in all the molar ratios of Ni:Al (Ni:Al=1:1, 1:3, 3:1). However, the steep rise of temperature was not obvious and shrinkage was relatively gradual in the case of Ni:Al=1:3. Figures 3-7 and 3-8 shows the morphologies of the small pores in metallic cell walls and the large pores derived from NaCl respectively with NaCl volume ranging from 20 to 80% in different cases of Ni:Al molar ratio.

Darkest contrast shows epoxy resin infiltrated into pores. Epoxy resin was perfectly infiltrated into small pores derived from combustion synthesis reaction between Ni and Al, which indicates that all the small pores were connected well with each other. When Ni:Al molar ratio was 3:1, the amount and morphologies of the small pores seemed not to change much depending on the volume fraction of NaCl. When Ni:Al molar ratio was 1:3, the amount and size small pores seems to increase with increasing NaCl. Moreover, in the case of Ni:Al=1:1, the size of small pores apparently decreased with increasing the amount of NaCl (results of last chapter). On the other hand, pores generated by space-holder NaCl particles increases apparently with increasing NaCl volume fraction in all three cases of Ni:Al molar ratio.

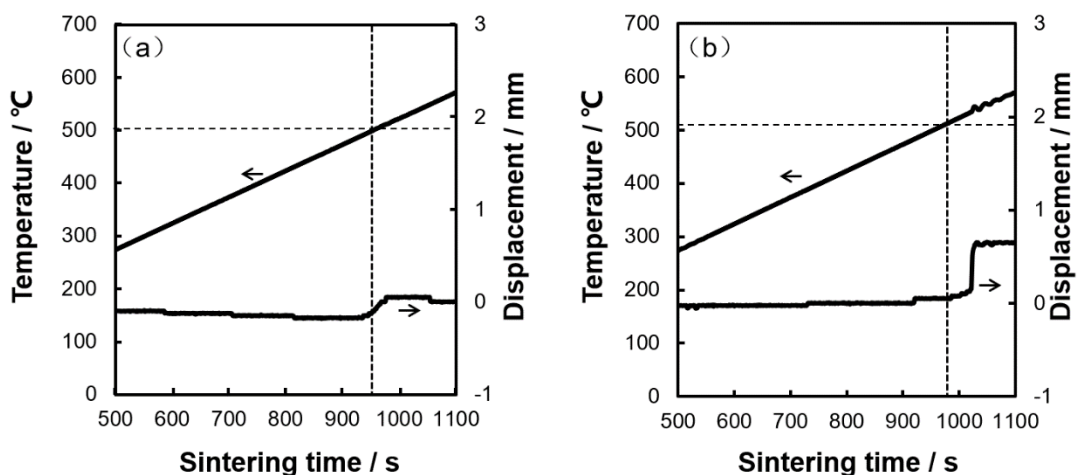


Fig. 3-6 Typical changes of temperature displacement of the graphite punch in cases of (a) Ni:Al =1:3 and (b) Ni:Al =3:1.

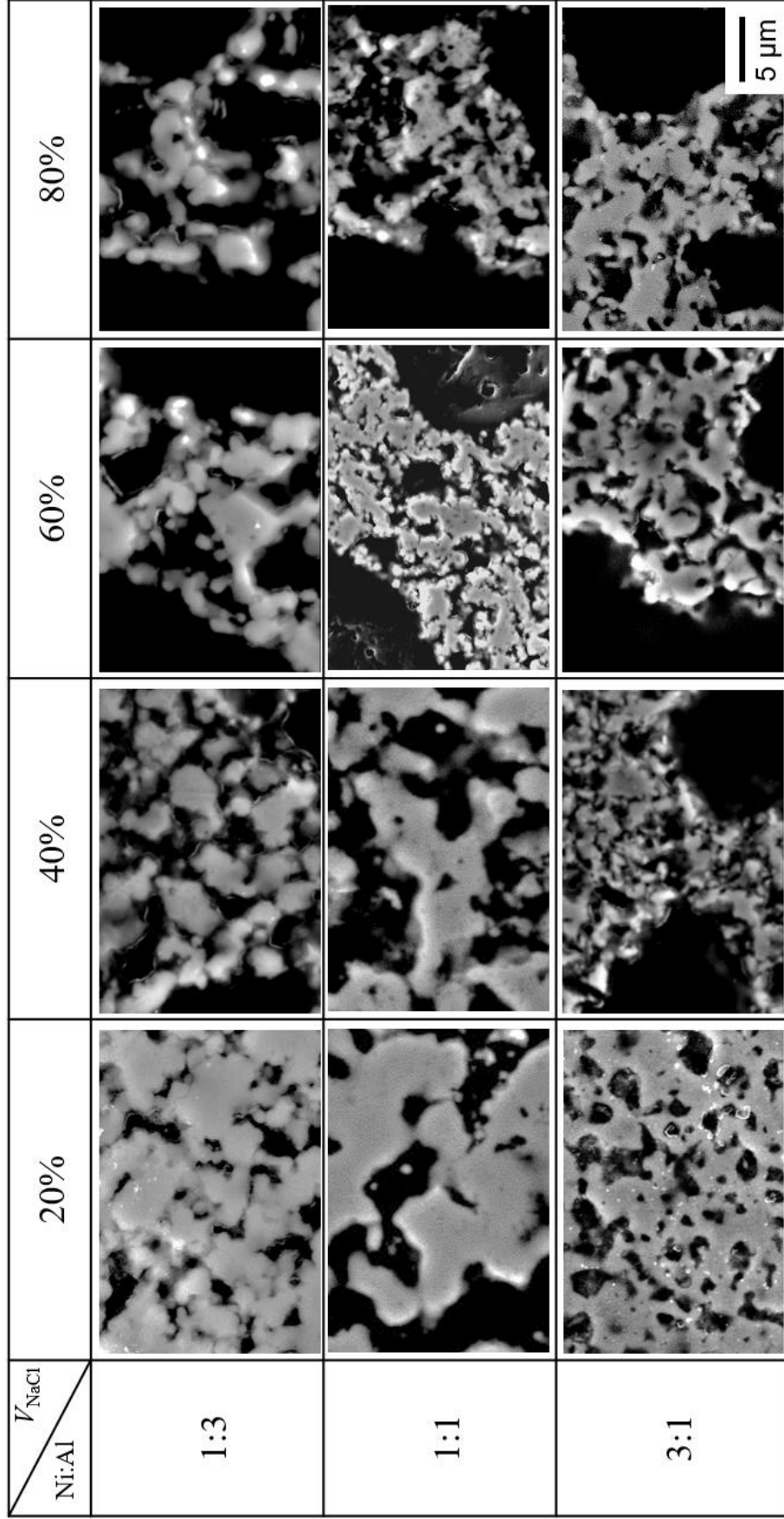


Fig. 3-7 Morphologies of the small pores in metallic cell walls with NaCl volume fraction ranging from 20 to 80% at different Ni:Al molar ratios.

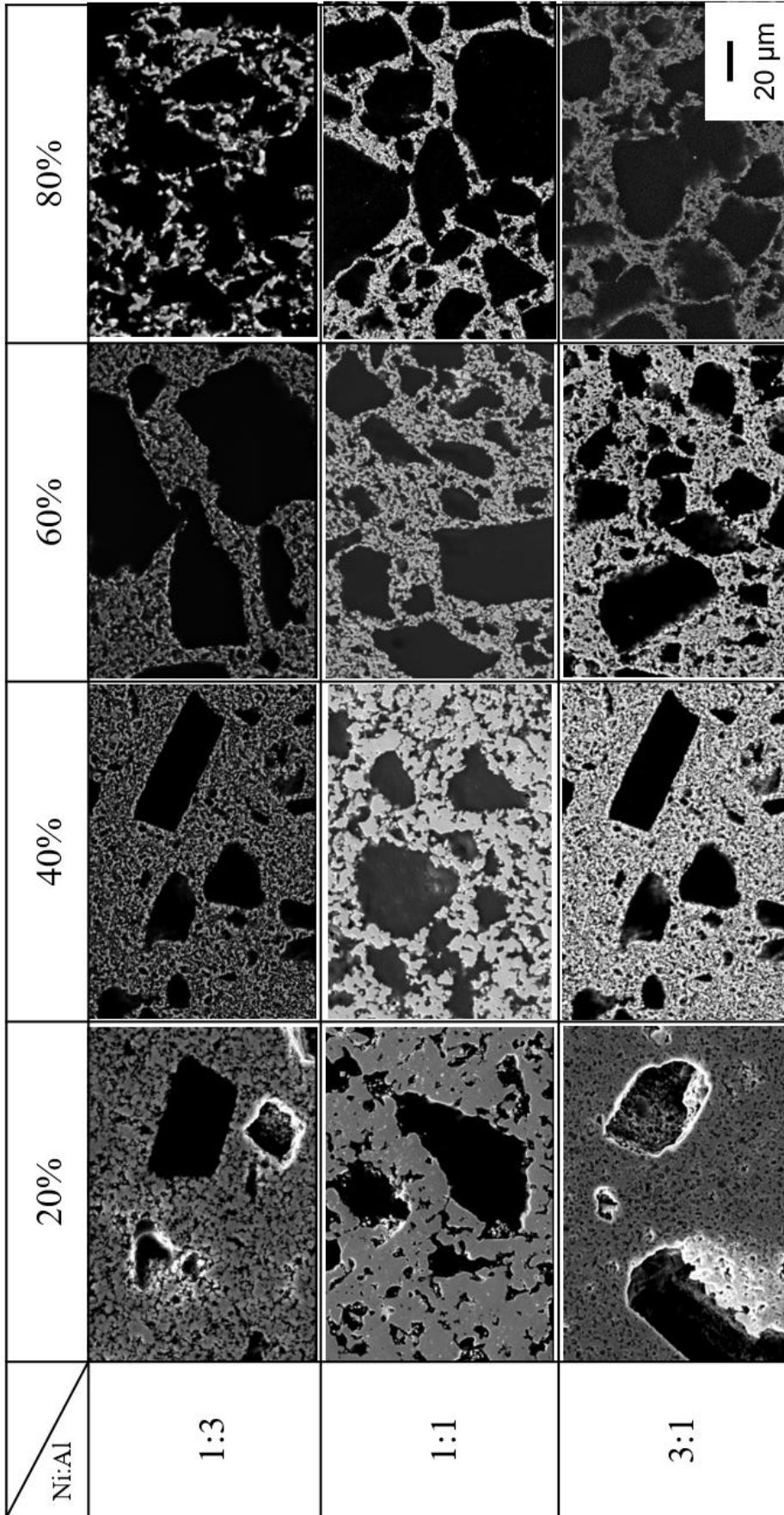


Fig. 3-8 Morphologies of the large pores derived from NaCl with NaCl volume fraction ranging from 20 to 80% at different Ni:Al molar ratios.

The constituting phases of porous Ni-Al samples in the cases of Ni:Al=1:3 and Ni:Al=3:1 were detected by X-ray diffraction (XRD). XRD profiles of porous Ni-Al samples in the cases of Ni:Al=3:1 are shown in Fig. 3-9. The diffraction peaks of Ni₃Al (L1₂), NiAl (B₂) and Ni (fcc) were detected at the sintering time of 300 s and 1800 s. However, at the sintering time of 10800 s, only the diffraction peaks of Ni₃Al (L1₂) were detected. Figure 3-10 shows the XRD profiles of porous Ni-Al samples in the cases of Ni:Al=1:3. Unlike the case of Ni:Al=3:1, single-phase porous NiAl₃ could not be obtained by extending sintering time, and the constituting phase of Ni₂Al₃ (D5₁₃) and NiAl₃ (D0₂₀) did not change with extending sintering time from 300 s to 10800 s from the XRD profiles. Figure 3-11 indicates size distribution of small pores in metallic cell walls of Ni-Al compound with different sintering time of 300 s, 1800 s and 10800 s. Porous Ni-Al compounds with sintering time of 300 s, 1800 s and 10800 s have almost the same size distribution of small pores, which indicates the same average size. In the histogram, frequency is almost in the range of <4.0 μm. Therefore, the same result with chapter 2 that sintering time has no effects on porous structure of small pores derived from combustion synthesis reaction is acquired.

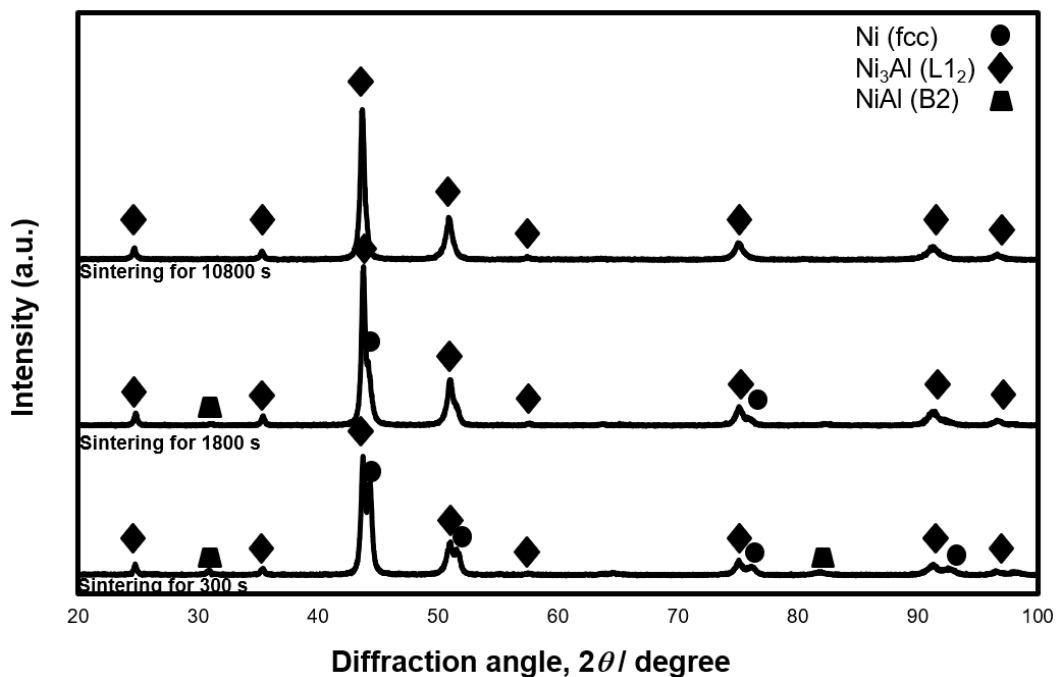


Fig. 3-9 XRD profiles of the Ni-Al samples sintered at 650°C for 300 s, 1800 s and 10800 s in the case of Ni:Al=3:1 ($V_{\text{NaCl}} = 60\%$).

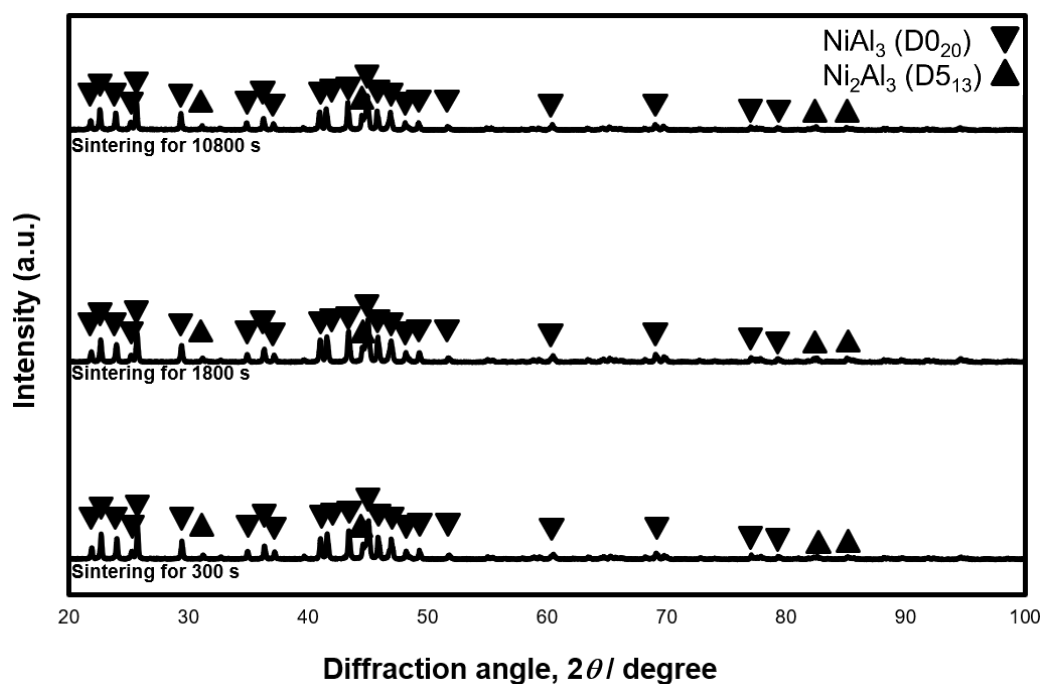


Fig. 3-10 XRD profiles of the Ni-Al samples sintered at 650°C for 300 s, 1800 s and 10800 s in the case of Ni:Al=1:3 ($V_{\text{NaCl}} = 60\%$).

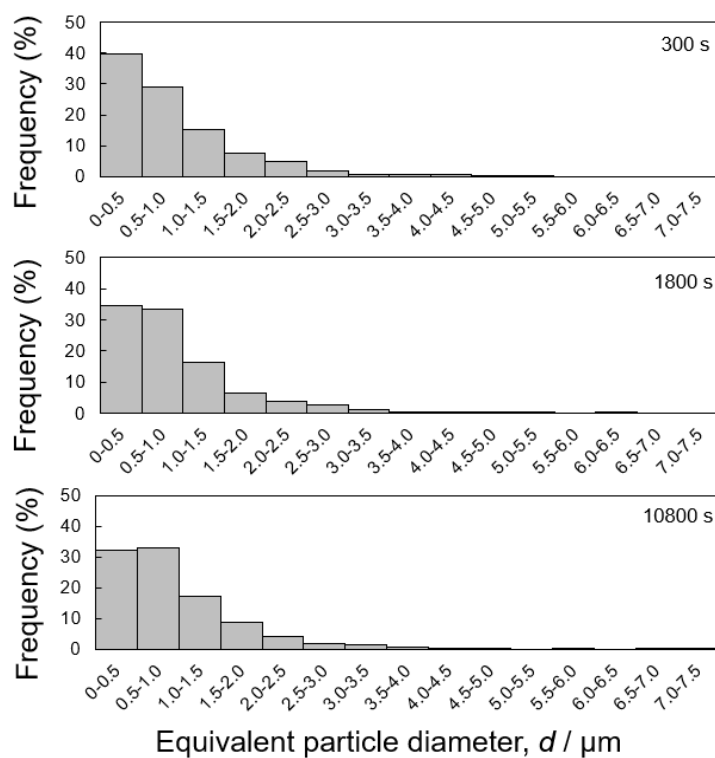


Fig. 3-11 Size distribution of small pores in cell walls with the sintering time of 300 s, 1800 s and 10800 s.

3.3.2.2 The effects of Ni:Al ratio on porous structure

Fig. 3-12 and 3-14 show the size distribution of small pores in metallic cell walls derived from the combustion synthesis reaction and large pores derived from NaCl particles of porous Ni-Al intermetallic compounds with different molar ratios of Ni:Al=3:1, 1:1, 1:3. And Average size of small pores and large pores of porous Ni-Al intermetallic compounds with different molar ratios are shown in Fig. 3-13 and 3-15. The average size and size distributions of large pores are almost the same in any porous Ni-Al compound because the large pores replicate the morphologies of NaCl space holders (30-50 μm). Porous Ni-Al intermetallic compounds with Ni:Al=1:3 and 3:1 have almost the same size distribution of small pores, which results in the almost the same average size. In the histogram of Ni:Al=1:3, frequency of $<1.0 \mu\text{m}$ is smaller and frequency of $>2.0 \mu\text{m}$ is larger than in the histogram of Ni:Al=3:1 and 1:1. As a result, average size in the sample of Ni:Al=1:3 is relatively large.

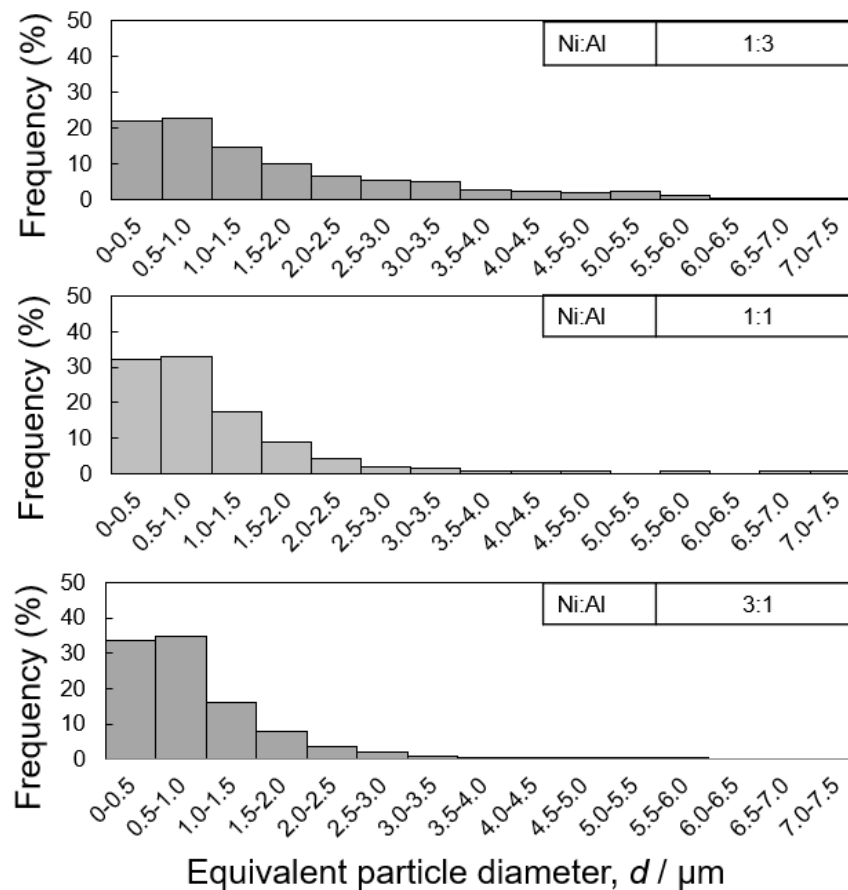


Fig. 3-12 Size distributions of small pores in cell walls with various Ni:Al molar ratios of 1:3, 1:1 and 3:1.

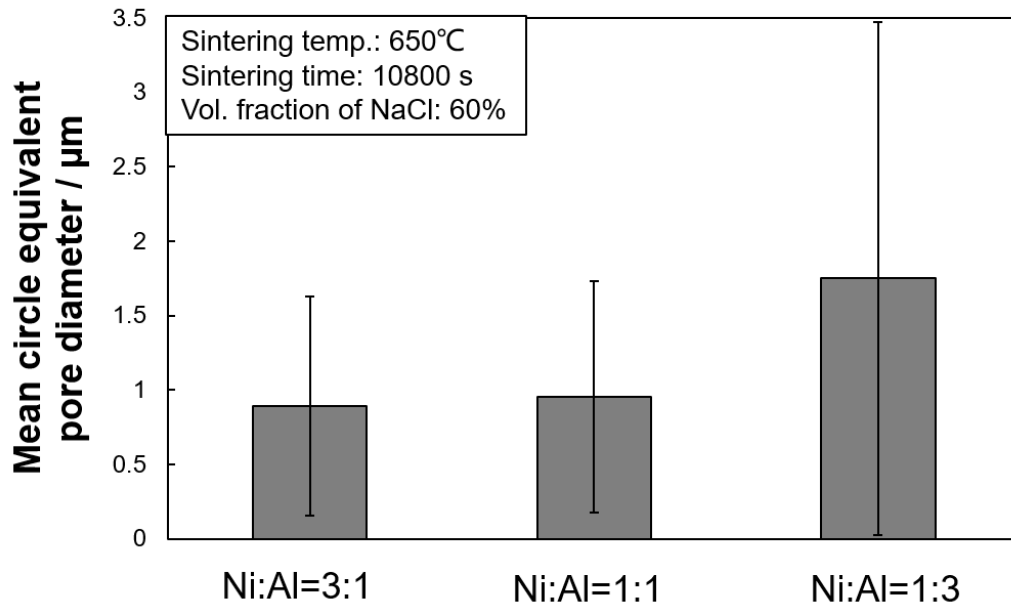


Fig. 3-13 Mean pore size of small pores in various Ni:Al molar ratios.

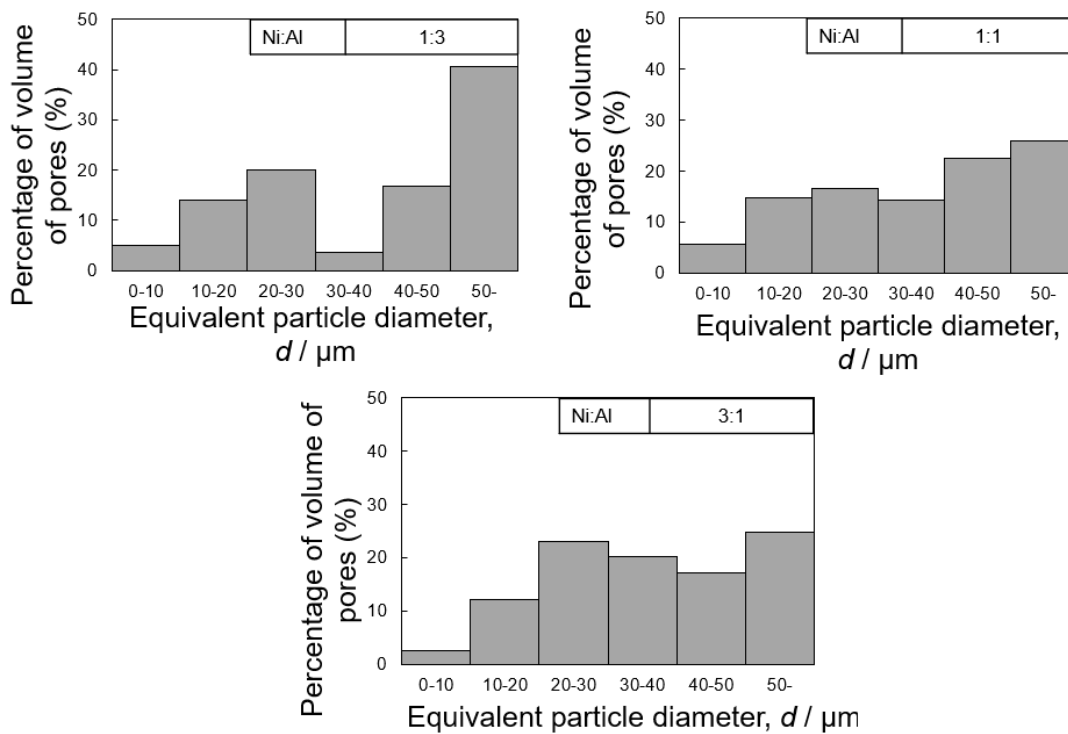


Fig. 3-14 Size distributions of large pores derived from NaCl with various Ni:Al molar ratios of 1:3, 1:1 and 3:1.

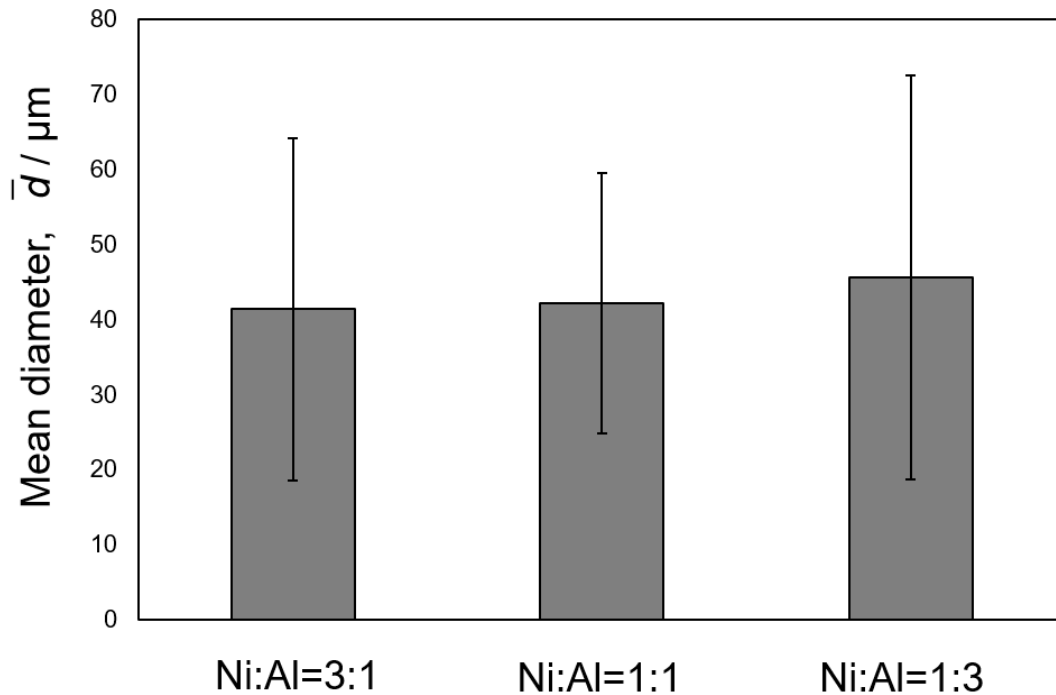


Fig. 3-15 Mean pore size of large pores derived from NaCl in various Ni:Al molar ratios.

Figures 3-16 presents the change in the porosity and size of small pores with the volume fraction of NaCl. When Ni:Al molar ratio was 3:1, both the porosity and size were almost constant and independent of the volume fraction of NaCl. In the case of Ni:Al=1:1, the porosity had a variation but no trend depending on the amount of NaCl. The pore size decreased with increasing the NaCl volume fraction. In particular, the size decreased drastically from 40% to 60%. When the Ni:Al molar ratio was 1:3, both the porosity and size increased monotonically with increasing the volume fraction of NaCl. Thus, NaCl affected not only large pores but also the small pores. It is interesting that the trend of change in porous structure like porosity and pore size with the amount of NaCl was different depending on the Ni:Al molar ratio.

Figures 3-17 and 3-18 show the porosity of large pores in overall samples and small pores in the cell wall respectively. It is noted that this porosity of small pores is not a volume fraction of small pores in the overall sample but a volume fraction of small pores in the portion excluding the pores derived from NaCl (the cell wall of the pores derived from NaCl). The porosity of large pore is almost the same in any samples. The porosity of small pores increased with increasing Al content. In particular, In the case of Ni:Al = 1:3, porosity in the cell wall is higher by 13~15% than in the case of Ni:Al = 1:1 or 3:1. Thus, Ni:Al molar ratio is important parameter to control the porous structure of porous Ni-Al intermetallic compounds.

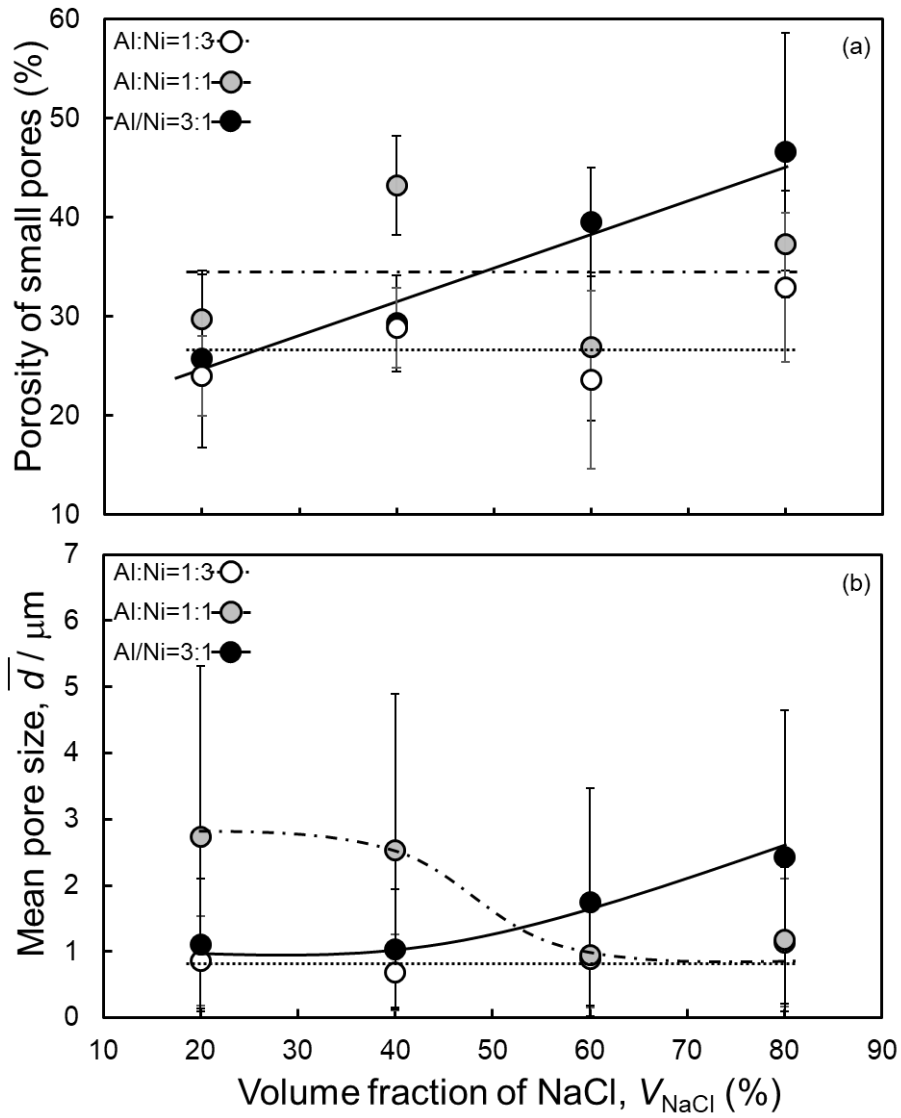


Fig. 3-16 Image analysis of mean pore size and porosities in cell walls.

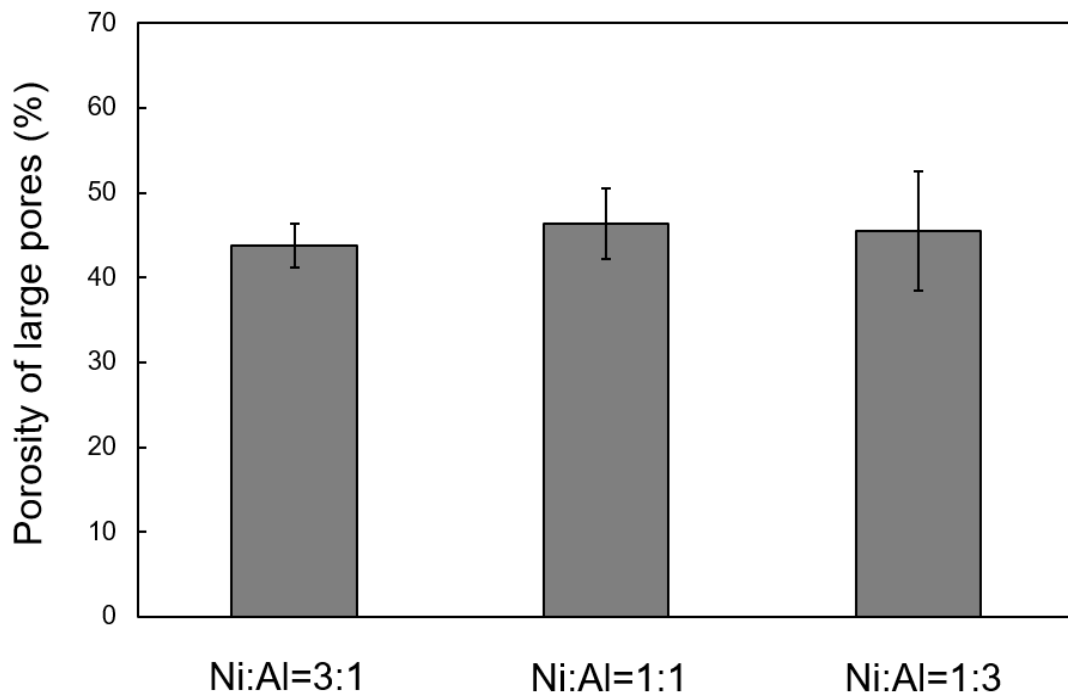


Fig. 3-17 Porosities of large pores derived from NaCl in various Ni:Al molar ratios.

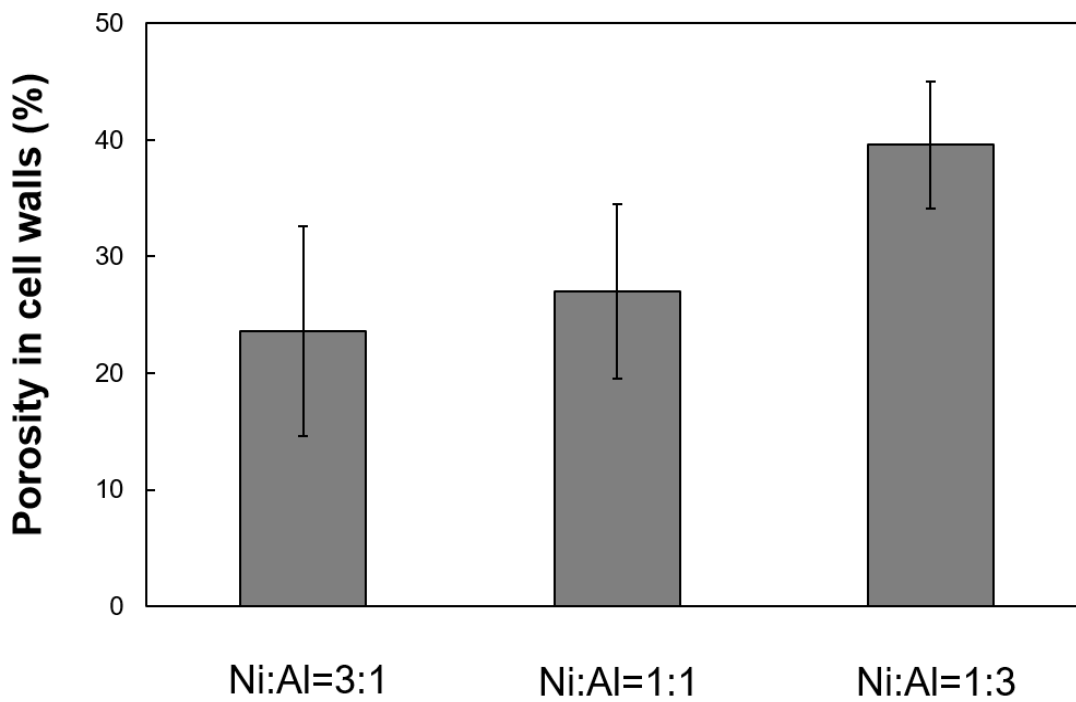


Fig. 3-18 Porosities in cell walls of small pores in various Ni:Al molar ratios.

3.4 Discussion

In this study, effects of the volume fraction of NaCl and Ni:Al molar ratio on porous structure of pores formed by combustion synthesis reaction between Ni and Al together with NaCl (space holder) have been investigated.

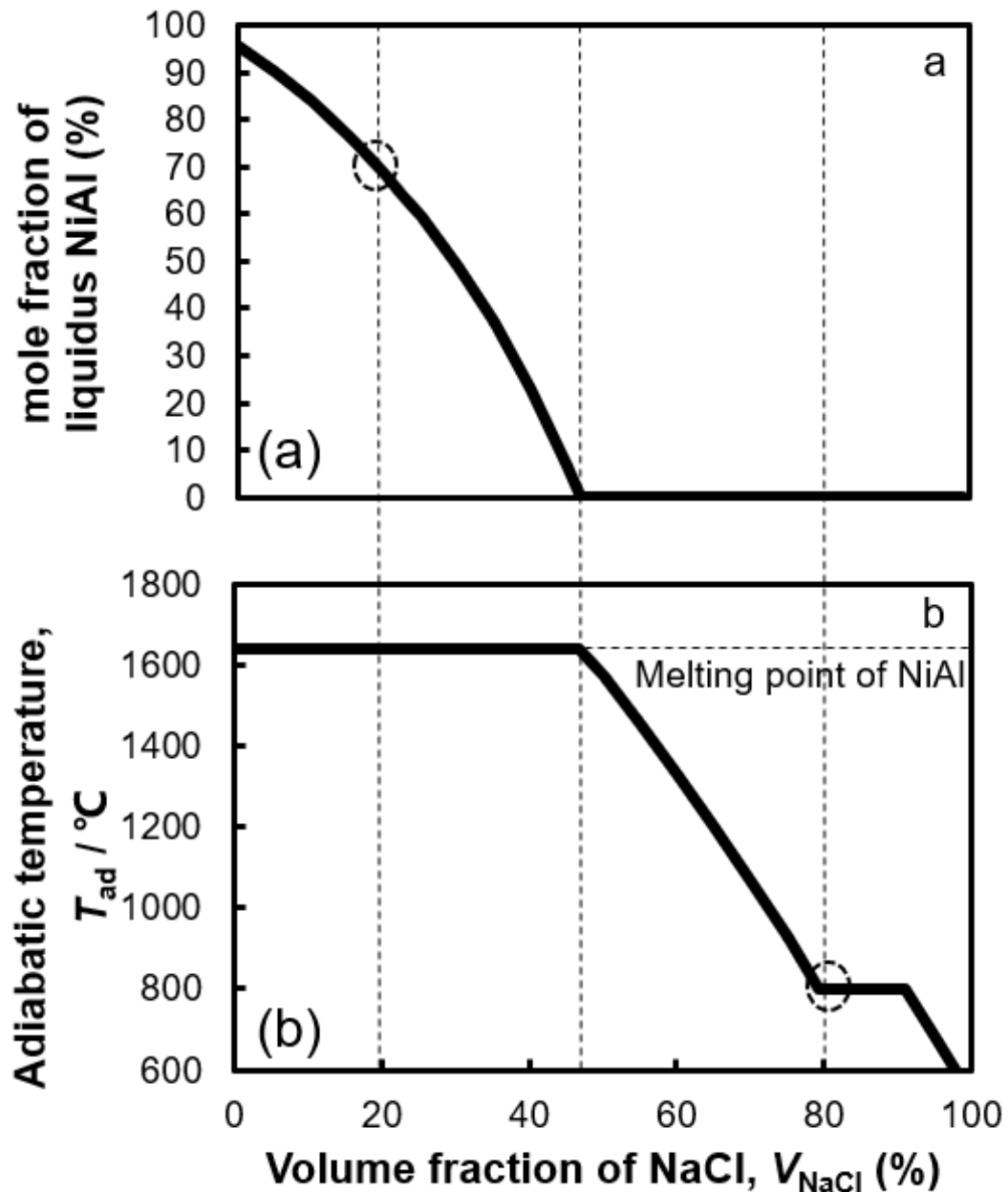


Fig. 3-19 Changes in the (a) mole fraction of liquidus NiAl and (b) adiabatic combustion temperature as a function of the volume fraction of NaCl.

First, the effect of NaCl volume fraction was investigated in the case of Ni:Al = 1:1. When volume fraction of NaCl was in the range 0–60%, the reaction was complete and the NiAl single phase was obtained by sintering at 650 °C for 300 s (Fig. 3-3). However, the reaction did not complete when the NaCl volume fraction was up to 80%. The reason for this phenomenon is related to adiabatic temperature (T_{ad}), which was discussed in chapter 2. As shown in Fig. 3-19, the T_{ad} in the case of $V_{NaCl} = 80\%$ was much lower than that for $V_{NaCl} = 0\%–60\%$ and the liquidus NiAl was 0%. As a result, the combustion synthesis reaction did not finish. Therefore, one of the significances of this research is in determining the sintering conditions (650 °C, 10,800 s) to obtain a highly porous NiAl single phase. On the other hand, as shown in Fig. 3-19 (a), the mole fraction of the liquid NiAl phase falls curvilinearly from 95.9% to 0% within the V_{NaCl} range of 0–46.7%. The reason for this trend is that the volume fraction is used instead of the molar fraction of NaCl on the horizontal axis. As presented in Fig. 3-19(b), T_{ad} decreased with increasing V_{NaCl} because the reaction heat is also absorbed by NaCl space holder. When V_{NaCl} is in the range of 0–46.7%, T_{ad} becomes constant due to the latent heat caused by the melting of NiAl. When V_{NaCl} is 20%, a part (69%) of the NiAl phase melts, but the solid phase (31%) also remains. Therefore, the pores in metallic cell walls were not crushed by the applied pressure and were connected by the flow of the Ni-Al melt to generate relatively large pores (Fig. 3-2).

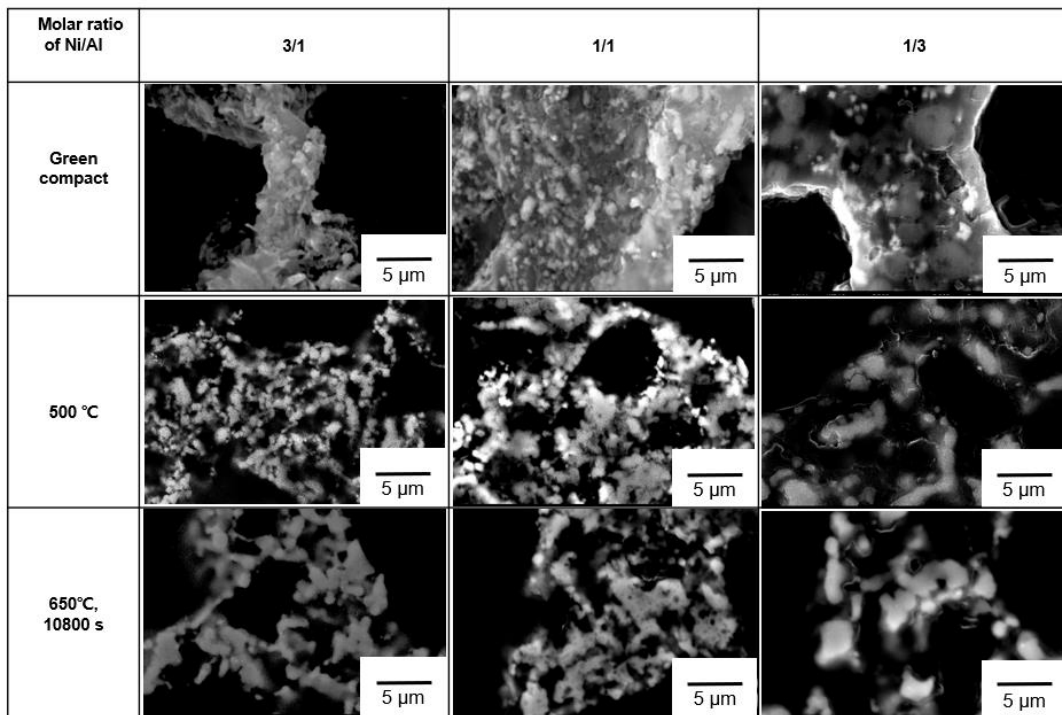


Fig. 3-20 SEM images of compacted precursors, intermediate products (sintered at around 500°C) and final products (sintered at around 650°C) in various Ni:Al molar ratios with a NaCl volume fraction of 80%.

Next, the effect of Ni:Al molar ratio on porous structure was investigated together with the effect of NaCl volume fraction on porous structure of small pores formed by combustion synthesis reaction.

All the porous Ni-Al samples possessed small pores in metallic cell walls surrounding large pores derived from NaCl space holders (Fig. 3-2, 3-7, 3-8). Space holder particles affected not only the large pores derived from space holders, but also the small pores derived from combustion synthesis reaction between Al and Ni. The size of small pores and porosity changed according to the volume fraction of NaCl. Furthermore, trends of change in the porosity and pore size with the NaCl amount were different depending on the Ni:Al molar ratio (Fig. 3-16). Also, NaCl does not react with Ni or Al. As mentioned in the previous chapter, NaCl acts as a heat absorber and affects the amount of liquidus phase, which is formed by reaction heat between Ni and Al [3-6]. As along with decreasing the volume fraction of NaCl, the formation and increment of liquid phase connect pores and increase pore size. However, in this study, pore size increased with increasing the NaCl volume fraction in the case of Ni:Al=1:3 and was almost constant in the case of Ni:Al=3:1. Hence, it is indicated that NaCl affects not only the amount of liquid phase. In this study, all the samples sintered at 650 °C for 10800 s reached almost the equilibrium condition, which was independent of the amount of NaCl space holder and Ni:Al molar ratio. According to the result of chapter 2, the porosity and pore size were almost determined at 500 °C just after the reaction occurred, and then were constant with sintering process proceeding. Figure 3-20 shows the SEM images of compacted precursors, intermediate products (sintered at around 500 °C) and final products (sintered at around 650 °C) respectively in various Ni:Al molar ratios. Small pores derived from combustion synthesis reaction didn't exist until the sintering temperature was risen up to 500 °C, which is in accordance with the result obtained in Chapter 2. Therefore, the pore size and porosity of all the samples sintered at 500 °C were investigated and the changing curves are shown in Figs. 3-21. Comparing Figs. 3-16 with Figs. 3-21, trends of change in the pore size and porosity with the NaCl volume fraction are almost accordant although the values were little different. Hence, the changing tendency presented in Figs. 3-16 depends on porous structure right after the combustion synthesis reaction occurs. As a heat absorber, NaCl space holder is able to affect the constituting phases and the extent of reaction. Therefore, the constituting phases just after the reaction occurs were investigated by the RIR (Reference Intensity Ratio) method. Table 3-1 reveals the changing rate of true volume from metallic powder to intermetallic compounds by assuming that all the reactants are converted into final products. True volume shrinks from reactants to products through combustion synthesis reaction between Ni and Al, and shrinkage rate is highest when NiAl generates. Figure 3-22, 3-23 and 3-24 show the XRD data at sintering temperature of 500 °C (just after reaction occurring) with Ni:Al molar ratio of 1:3, 1:1, and 3:1 respectively. It is noted that there are usually a plenty of fluctuations in the XRD curve when XRD test is performed with sample soaked in cured resin. However, these fluctuations in the XRD curves are not capable to influence the analysis results in our study. Various constituting phases and different intensities of the constituting

phases indicate the different volume shrinkage rate in each condition.

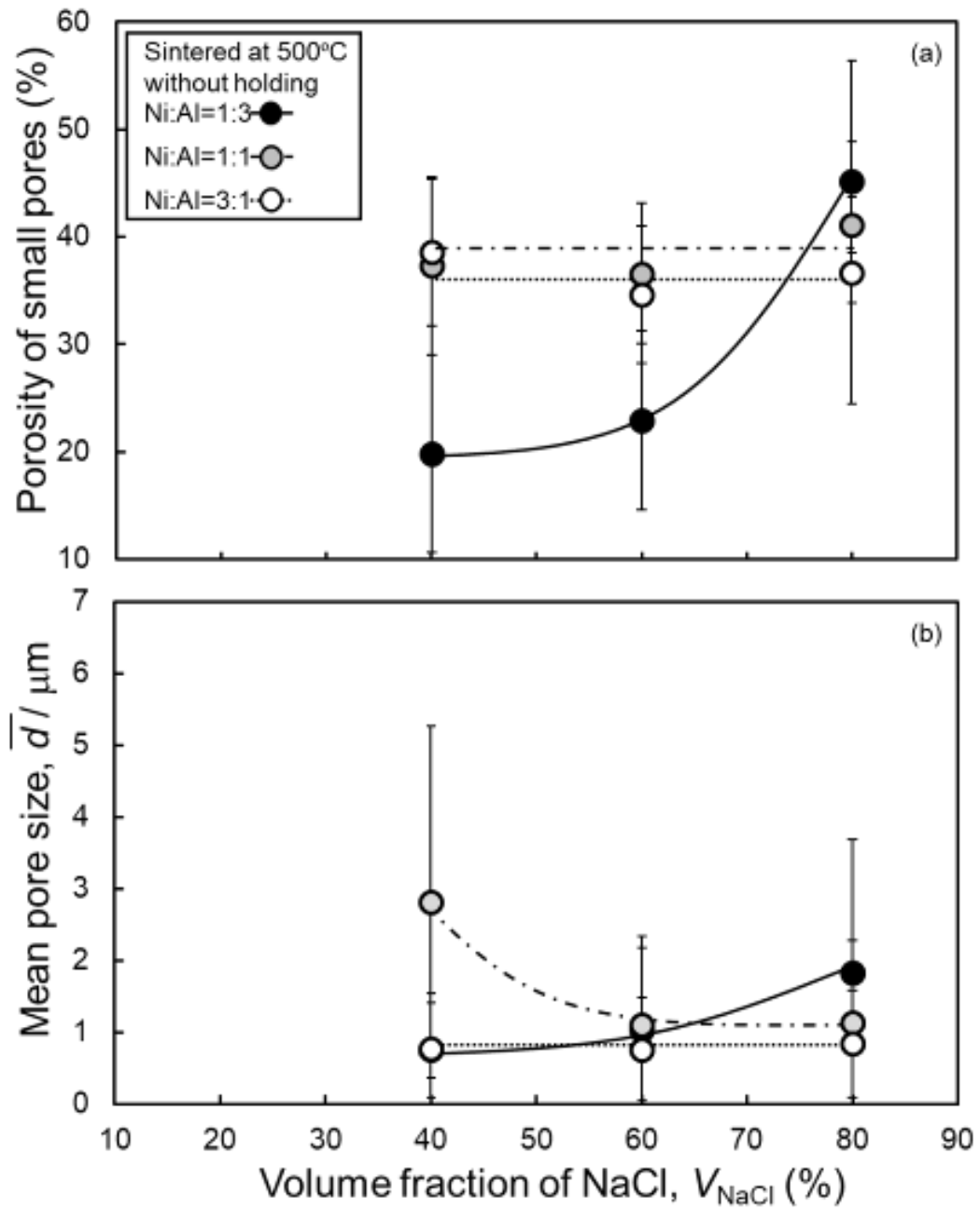


Fig. 3-21 Change in (a) porosity and (b) mean size of small pores as a function of the volume fraction of NaCl of the samples sintered at 500 °C.

Table 3-1. Changing rates of true volume from metallic powder to intermetallic compounds.

Raw materials	Compounds	changing rate of true volume, D_V (%)
Ni+Al	NiAl	-12.6
	Ni ₃ Al	-5.2
	Ni ₂ Al ₃	-4
	NiAl ₃	-3.4

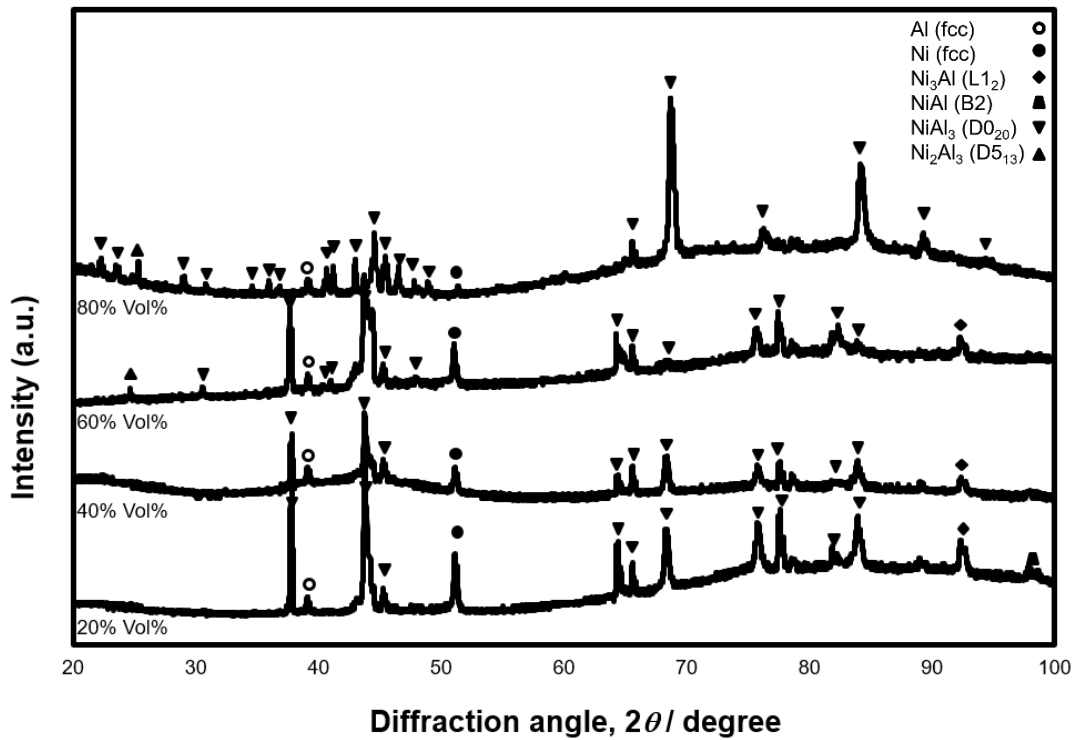


Fig. 3-22 XRD profiles of Ni:Al=1:3 at sintering temperature of 500°C

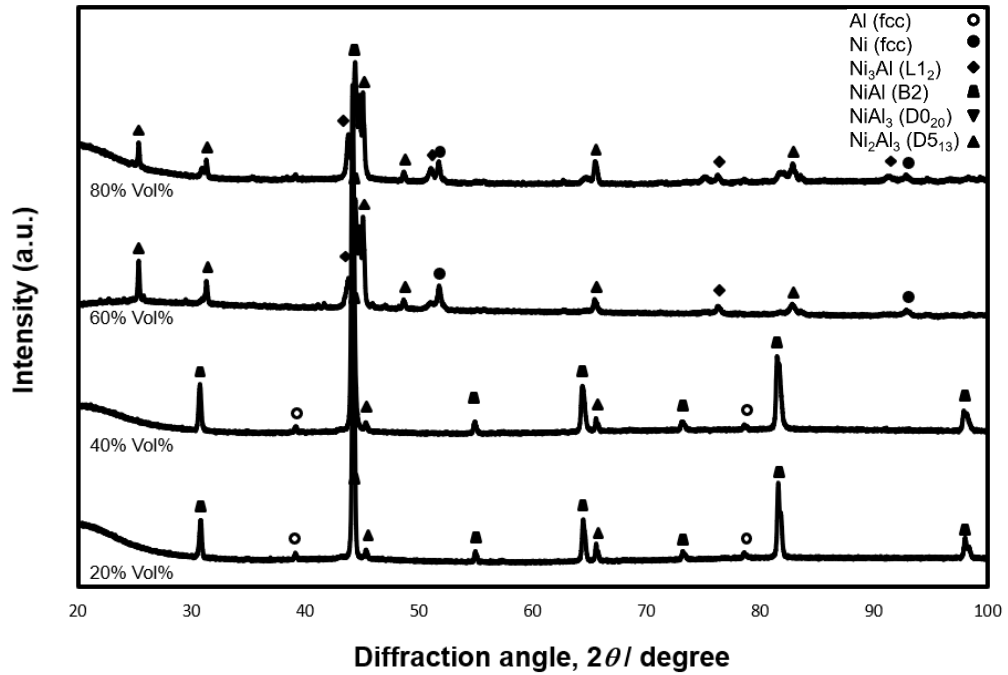


Fig. 3-23 XRD profiles of Ni:Al=1:1 at sintering temperature of 500°C

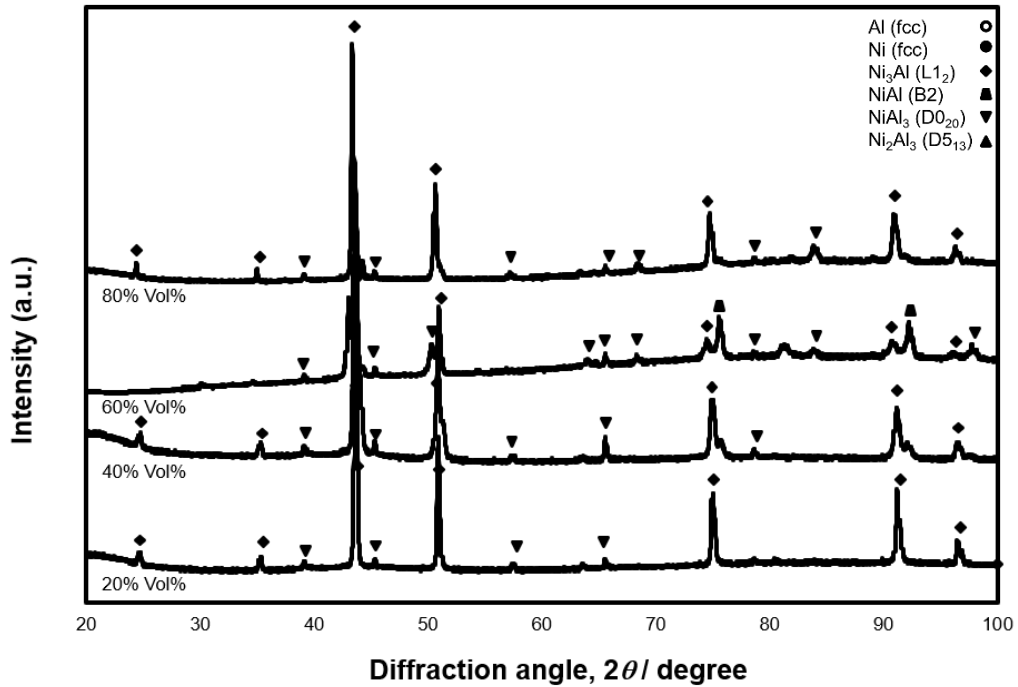


Fig. 3-24 XRD profiles of Ni:Al=3:1 at sintering temperature of 500°C.

Figs. 3-25 presents mole fractions of the constituting phases of the samples sintered at 500 °C estimated by the RIR method using XRD profiles. When Ni:Al molar ratio was 3:1, there is no trend of change in constituting phases with the NaCl volume fraction. When Ni:Al molar ratio was 1:1, the mole fraction of NiAl phase, which is the final product in this condition, decreased with increasing the volume fraction of NaCl. This result means that the NaCl space holder particles inhibited the progress of the reaction. On the contrary, when the Ni:Al molar ratio was 1:3, NiAl₃, which is the main phase in the equilibrium condition, increased with increasing the volume fraction of NaCl, meaning that NaCl space holder particles apparently promoted the progress of the reaction. Thus, trends of change in the constituting phase in each condition with the volume fraction of NaCl were different depending on Ni:Al molar ratios. Figs. 3-26 (a) shows change in average atomic volume as a function of Al concentration in Ni–Al binary system reported in the literatures [3-6, 3-7]. The broken line shows average atomic volume of Al+Ni mixture. The average atomic volume of all the Ni-Al intermetallic compounds is smaller than that of Al+Ni mixture at the same composition. The volume shrinks when Ni-Al intermetallic compounds are formed by combustion synthesis reactions between Al and Ni. Figs. 3-26 (b) shows shrinkage rate of average atomic volume in formation of Ni-Al compounds from Al+Ni mixture estimated from Figs. 3-26 (a). The volume shrinkage rate is the highest when NiAl is formed. When Al-rich Ni-Al intermetallic compounds (NiAl₃, Ni₂Al₃) are formed, the shrinkage rates are lower. It is also well known that change in the average atomic size by phase transformation generates voids, pores, or cracks, which can highly affect the porous structures. Combining Figs. 3-26 (b) with Fig. 3-21, the shrinkage rates of cell walls just after reaction occurs were estimated and shown in Fig. 3-27. The change tendency of shrinkage rate along with the volume fraction of NaCl is almost in accordance with that of pore size and porosity shown in Figs. 3-21. Hence, shrinkage of metallic wall affects the formation and growth of the small pores derived from reaction.

However, the magnitude relation of shrinkage rate is inconsistent with that of porosity and pore size shown in Figs. 3-21. For example, when the volume fraction of NaCl was 80%, porosity and pore size in the case of Ni:Al=1:3 are the largest but the shrinkage rate are not the largest. He et al. claimed that porosity and pore size of porous Ti-Al alloy sintered at a temperature of 650 °C increased with raising Al content [3-8]. By sintering at a temperature close to the melting point of Al (660 °C), the atomic diffusion rate of Al becomes faster than the atomic diffusion rate of Ti with a higher melting point than Al, resulting in the formation of Kirkendall voids at the place where Al originally existed. As a result, porosity increases with increasing Al content. It is considered that pores are easier to form as Al concentration increases as well as the case of Ni-Al binary system.

Ohmi and Hayashi reported that Kirkendall voids are observed around lining microchannels produced by powder-metallurgical process using aluminum sacrificial cores [3-9]. As the concentration of Al increases, the probability that Al particles are adjacent to each other increases, so that the pores formed by the Kirkendall effect are also easy to connect, resulting in increasing in pore size. Thus, shrinkage in formation

of nickel aluminides and the Kirkendall effect changes porosity and size of small pores formed by combustion synthesis reaction between Al and Ni. However, the reason why the mole fraction of NiAl_3 phase (equilibrium phase) increases with increasing the amount of NaCl (heat absorber) in the case of Ni:Al=1:3 shown in Figs. 3-25 (c) remains unclear, and further investigation is going to be needed.

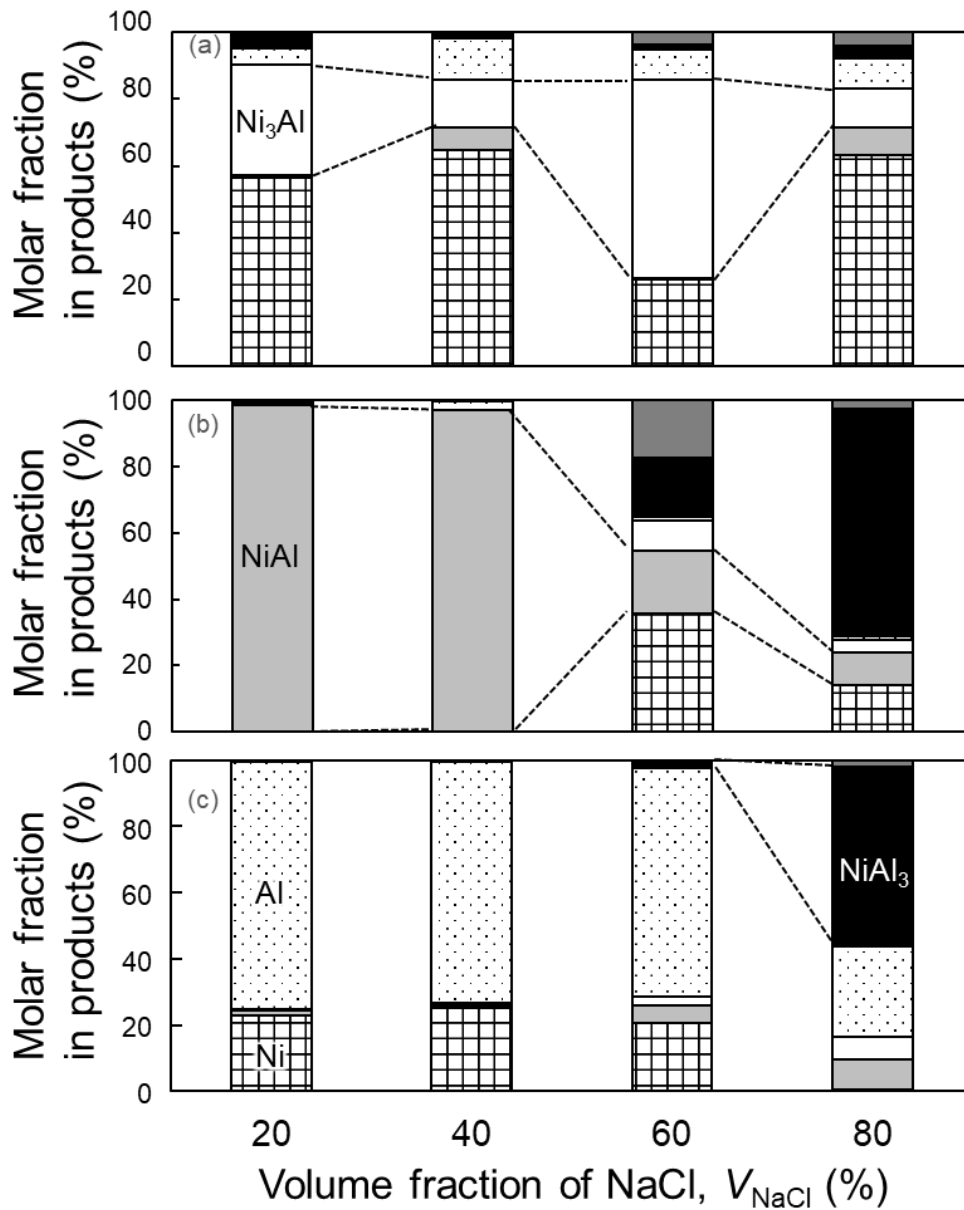


Fig. 3-25 Changes in molar fraction of constituting phases in the samples sintered at 500 °C as a function of the volume fraction of NaCl in the cases of (a) Ni:Al=3:1, (b) Ni:Al=1:1, (c) Ni:Al=1:3.

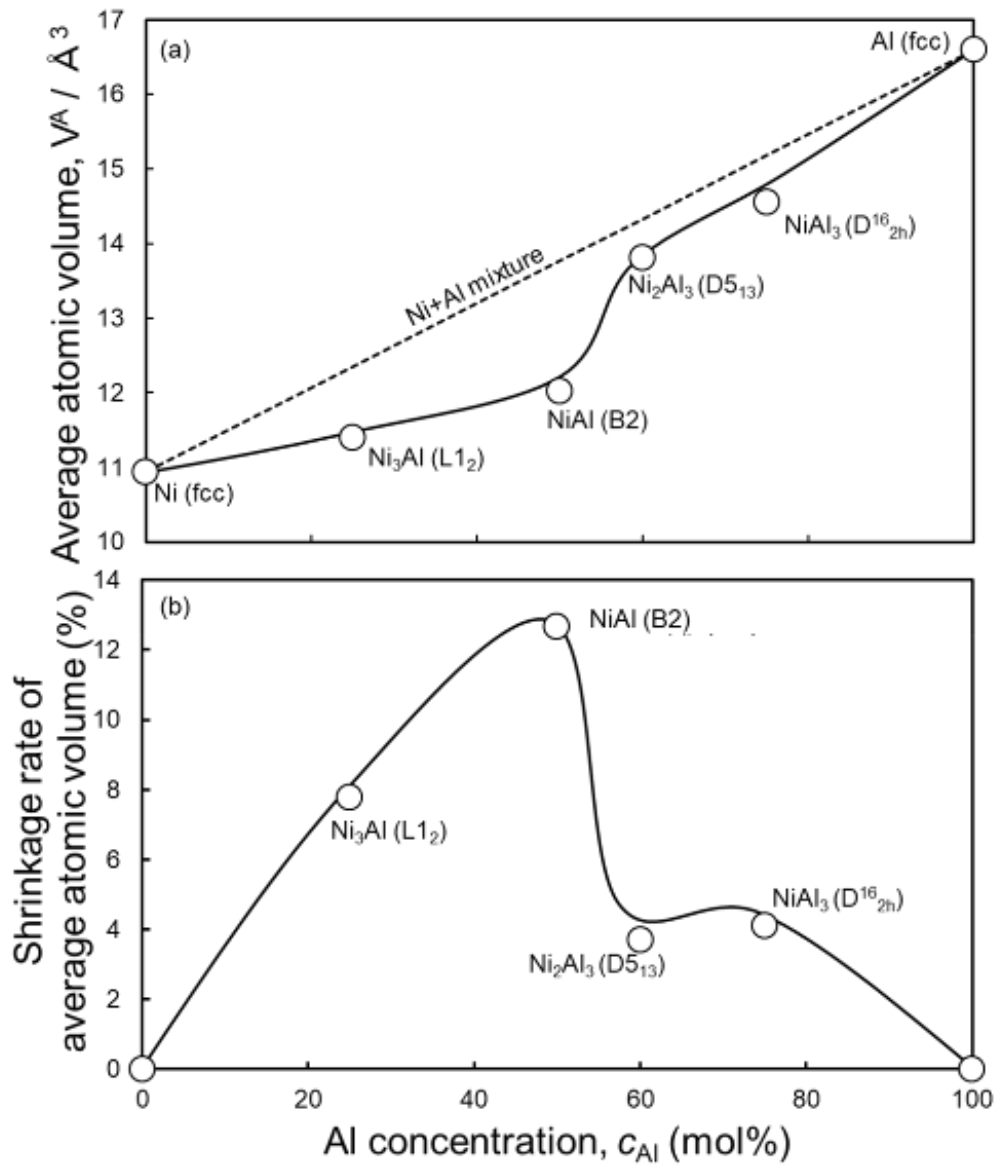


Fig. 3-26 Change in (a) average atomic volume in Ni-Al binary system reported by M.Ellner et al. [3-6], and (b) shrinkage rate of average atomic volume by formation of Ni-Al intermetallic compounds from Ni+Al mixture as a function of Al concentration.

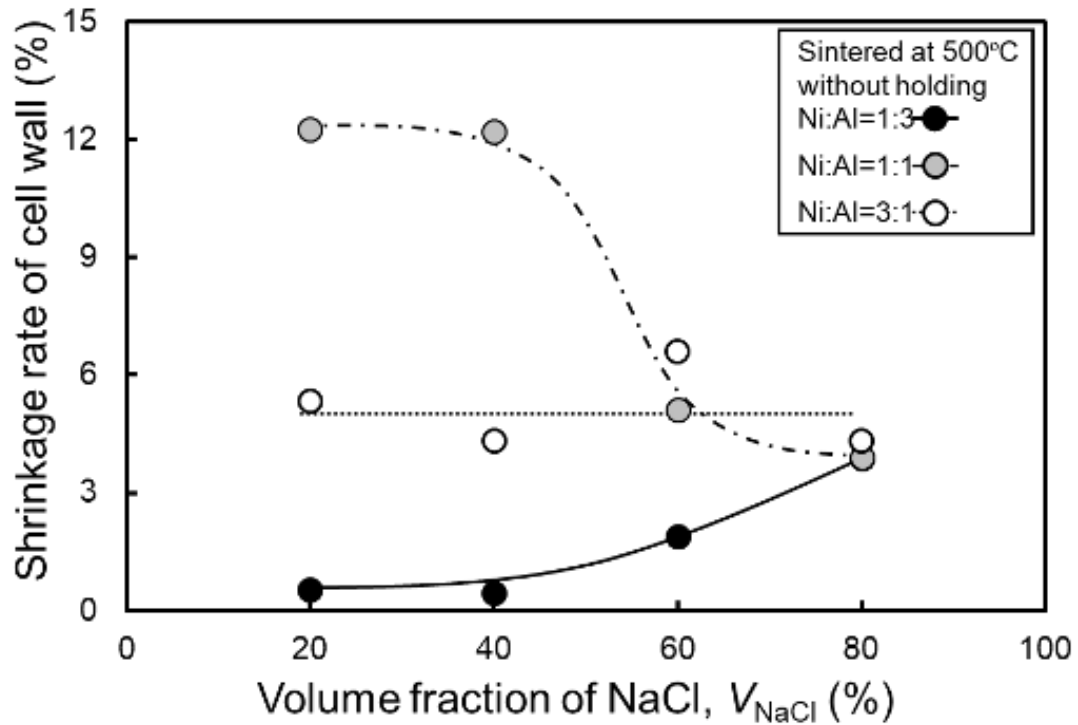


Fig. 3-27 Changes in shrinkage rate of metallic wall in the samples sintered at 500 °C due to the formation of Ni-Al intermetallic compounds from Ni+Al mixture as a function of the volume fraction of NaCl.

3.5 Summary

In this study, effects of NaCl volume fraction and Ni:Al molar ratio on porous structure of small pores in metallic cell walls derived from combustion synthesis reaction between Ni and Al were investigated. NaCl affected not only the large pores derived from NaCl, but also the small pores derived from reaction. NaCl affects the progress of reaction, constituting phases as well as the melting of product just after the reaction occurred. Shrinkage rates of average atomic volume from mixture of Ni and Al to Ni-Al intermetallic compounds vary by Al content, resulting in differences in shrinkage rate of metallic cell wall. Once the small pores are formed, they do not change much with increasing temperature. Size and porosity of small pores also increases with raising Al content due to the Kirkendall effect. In order to control the porosity and morphologies of the small pores, we need to select appropriate Al content and control the constituting phase just after the reaction occurs.

Reference

- [3-1] Chan Byon, Sung Jin Kim: Capillary performance of bi-porous sintered metal wicks, *International Journal of Heat and Mass Transfer*, 55 (2012), pp. 4096-4103.
- [3-2] Christopher M. A. Parlett, Karen Wilson, Adam F. Lee: Hierarchical porous materials: catalytic applications, *Chemical Society Reviews*, (42) 2013, pp. 3876-3893.
- [3-3] Haitao Zhao, Qi Xiao, Donghui Huang, Shiping Zhang: Influence of Pore Structure on Compressive Strength of Cement Mortar, *The Scientific World Journal*, 2014.
- [3-4] YunFeng Luo, QiJun Yu, JiangXiong Wei, Jie Hu, FangXian Li: Characteristics of Pore Structure of Free-Steamer Foamed Concrete and its Influence on the Compression Strength, *Applied Mechanics and Materials*, (357-360) 2013, pp. 1130-1137.
- [3-5] Okamoto, H.: Al-Ni (Aluminum-Nickel), *J. Ph. Equilib.* 14 (1993), pp. 257–259.
- [3-6] M. Ellner, K. Kolatschek and B. Predel, *J. Less-Common. Met.*, 170, (1991), pp. 171-184.
- [3-7] S. Miura, S. Takizawa, T. Suzuki, Y. Mishima and T. Mohri, *Acta Materialia*, 53, (2005), pp. 5175-5181.
- [3-8] Y. He, Y. Jiang, N. Xu and J. Zou, *Adv. Mater.*, 19, (2007), pp. 2102-2106.
- [3-9] T. Ohmi and N. Hayashi, *Materials Transactions*, 57, (2016), pp. 1816-1822.

Chapter 4. Investigation of mechanical properties

4.1 Introduction

Porous metals possess several unique properties such as thermal insulation, ultra-low density, sound absorption, energy absorption, fluid permeability, and so on [4-1, 2]. Among all the mechanical properties, the impact energy absorption of porous metals is the most attractive property. Besides, plenty of investigations about compressive strength and absorption energy of porous metals have been done recently [4-3, 4, 5]. The intermetallic compounds which possess high stiffness strength and high corrosion/oxidation resistance have been considered as expectant candidates in applications of energy absorption. Particularly, Naoki Takata et al. [4-6] reported the compressive properties of porous Ti-Al intermetallic compounds, which have a significantly higher energy absorption capacity and efficiency than porous Al. Also, capability of energy absorption indicates the mechanical strength and protective capability of porous metals.

The stress-strain curve of porous metals which could express the compressive properties are commonly used in evaluating mechanical properties. The characteristic of compressive deformation of porous metals is that the deformation of materials carries on with a constant compressive stress (plateau stress) in certain range (plateau region). The most important factors in this stress-strain curve are plateau region and plateau end strain (ε_{end}). Plateau region is the region with constant compressive stress which is named as plateau stress (σ_{pl}), and plateau end strain is defined as the termination boundary of the plateau region. Plateau stress is defined as the average stress of the nominal strain from 20% to 30% by JIS H7902. Plateau end strain can be expressed by follow equation:

$$\varepsilon_{end} = 1 - 1.4 \left(\frac{\rho^*}{\rho_s} \right) \quad (1)$$

Where ρ^* is the density of porous metal, and ρ_s is the density of matrix metal. The ratio of ρ^* and ρ_s is defined as relative density of porous metals, which is correlated with the porosity. Value of plateau end strain is equal to the strain of 1.3 times of plateau stress.

In addition, yield stress of porous metals is correlated with relative density as well. The relationship is as below:

$$\frac{\sigma_y^*}{\sigma_y} = C \left(\frac{\rho^*}{\rho_s} \right)^n \quad (2)$$

Where C is the coefficient of pore morphologies, n is the coefficient correlated with deformation pattern, σ_y^* is the yield stress of porous metal, and σ_y is the yield stress of

matrix metal. From equation (2) we understand that the morphologies of pores and relative density have effects on yield stress of porous metals. In the compressing process, the yield point which means the start of deformation is like a moment barrier to compressive stress. The energy absorption capacity and energy absorption efficiency are expressed by equation (3) and (4) respectively:

$$W = \int_0^{\varepsilon_{end}} \sigma(\varepsilon) d\varepsilon \quad (3)$$

$$\eta = \frac{\int_0^{\varepsilon_{end}} \sigma(\varepsilon) d\varepsilon}{1.3\sigma_{pl} \cdot \varepsilon_{end}} \quad (4)$$

Combining the equations of (3) and (4) with the stress-strain curve, we understand that high plateau end strain and flat plateau region are essential to obtain high energy absorption efficiency. Also, energy absorption efficiency is the directional evaluation of compressive properties.

Moreover, the relationship between porosity and relative density can be expressed as follow:

$$\varepsilon = 1 - \frac{\rho^*}{\rho_s} \quad (5)$$

The ε in equation (5) is porosity of porous metals. From the above equations, we know the parameter of porosity can affect the plateau end strain and yield stress, thereby, affect the compressive properties of materials indirectly. Therefore, controlling of matrix materials and pore structure can be used to achieve excellent compressive properties.

Normally, two forms of deformation exist in compression process of porous materials: plastic collapse and brittle crushing [4-7]. Porous metals which yield plastically would have a plastic collapse, when the moment on the cell wall exceeds the fully plastic moment. In the case of open-cell structure, the fully plastic moment (M_p) can be expressed as follow:

$$M_p = \frac{1}{4} \sigma_{ys} t^3 \quad (6)$$

Where the σ_{ys} is the yield stress of matrix material, and t is the cell wall thickness, and the l represents side length of open-cell face. For open-cell structure as shown in Fig. 1-8, the equation of $\rho^*/\rho_s \propto (t/l)^2$ (ρ^* is the density of porous material and ρ_s is the density of matrix material) is applicative. When the open-cell structure is applied a force F from top cell face to bottom cell face vertically, the plateau stress σ_{pl}^* of this porous metal can be expressed as below:

$$\frac{\sigma_{pl}^*}{\sigma_s} = C_1 \left(\frac{\rho^*}{\rho_s} \right)^{3/2} \quad (7)$$

Where σ_s is the yield strength of matrix material, and C_1 is a factor depends on cell-wall structure which is reported that $C_1=0.3$, when $\rho^*/\rho_s \leq 0.3$ [4-7]. In the case of brittle porous materials such as ceramics or several porous intermetallic compounds, brittle crushing happens when a moment on the open-cell wall exceeds:

$$M_p = \frac{1}{4} \sigma_f t^3 \quad (8)$$

Where the σ_f is bending strength of matrix material. Same way as above, we can obtain the crushing strength (σ_f^*) of the brittle porous material:

$$\frac{\sigma_f^*}{\sigma_f} = C_2 \left(\frac{\rho^*}{\rho_s} \right)^{3/2} \quad (9)$$

Because the brittleness, the precise data and result are difficult to obtain, and also compression tests on brittle porous materials are rare. Therefore, the reports about the value of factor C_2 are uncertain.

Porous metals absorb shock energy by deforming largely under almost constant stress (plateau stress) during plastic deformation (plateau region). Hence, it is also required that porous metals have high yield strength, high plateau end strain, and flat plateau region. On the other hand, intermetallic compounds like TiAl, NiAl, and Ni₃Al have high stiffness strength, high melting points, high oxidation and corrosion resistance at high temperature, which indicate a number of applications in various harsh environments. Porous intermetallic compounds which have all the above properties, are expected as high-strength and stable functional materials in various applications mentioned before. Therefore, the compressive properties and the effects on compressive property of porous Ni-Al intermetallic compounds are investigated for inspecting the capability on applications in the future.

In this research, we have developed a powder metallurgical process to synthesize innovative hierarchical porous Ni-Al intermetallic compounds by combination of combustion synthesis reaction with spacer method [4-8]. The porous Ni-Al intermetallic compounds which possess alluring prospects in applying in a number of fields, still need to be investigated on the mechanical property. In this study, investigations of compressive properties of porous Ni-Al compounds were performed.

4.2 Experimental method

Porous Ni-Al intermetallic compounds for compressive test were fabricated by the

process introduced in chapter 2, and then compressive tests were carried out. The flow chart of this experimental process is shown in Fig. 4-1. First, the volume fractions of NaCl (V_{NaCl}) in raw mixture were prepared in 60%. Then, the Ni and Al powders were blended in an atomic ratio of 3:1, 1:1 and 1:3 for further investigating the effects of Ni:Al molar ratio on porous structure of small pores derived by reaction. It is noted that fabrication conditions such as sintering temperature which result in single-phase and multiple-phase porous Ni-Al products respectively were adjusted for investigating the effects of constituting phases of matrix materials. After sintering, the samples were cooled in furnace to ambient temperature. Then, the specimens were soaked in pure water for 24 h to remove the NaCl space holder for the formation of large pores, which were replicated from space-holder NaCl. After removing the NaCl particles, the compressive tests were carried out. In order to evaluate the compressive property of porous Ni-Al intermetallic compounds, a cylindrical sample of a diameter of 20 mm and height of 20 mm with an overall porosity of approximately 70% (large porosity of 60% and small porosity of 10%) was fabricated. Subsequently, the cellular structure was evaluated by the calculation method and sectional image analysis. In addition, for contrast, porous Al with a porosity of 70% was also fabricated by the spacer method with the same size and porosity. The compressive tests of porous Ni-Al samples and porous Al were carried out at an initial strain rate of $3.3 \times 10^{-3} \text{ s}^{-1}$ and $4.4 \times 10^{-3} \text{ s}^{-1}$ respectively. The applied load was divided by the sectional area to estimate the nominal stress, and the measured displacement was divided by the height of the samples to estimate the nominal strain.

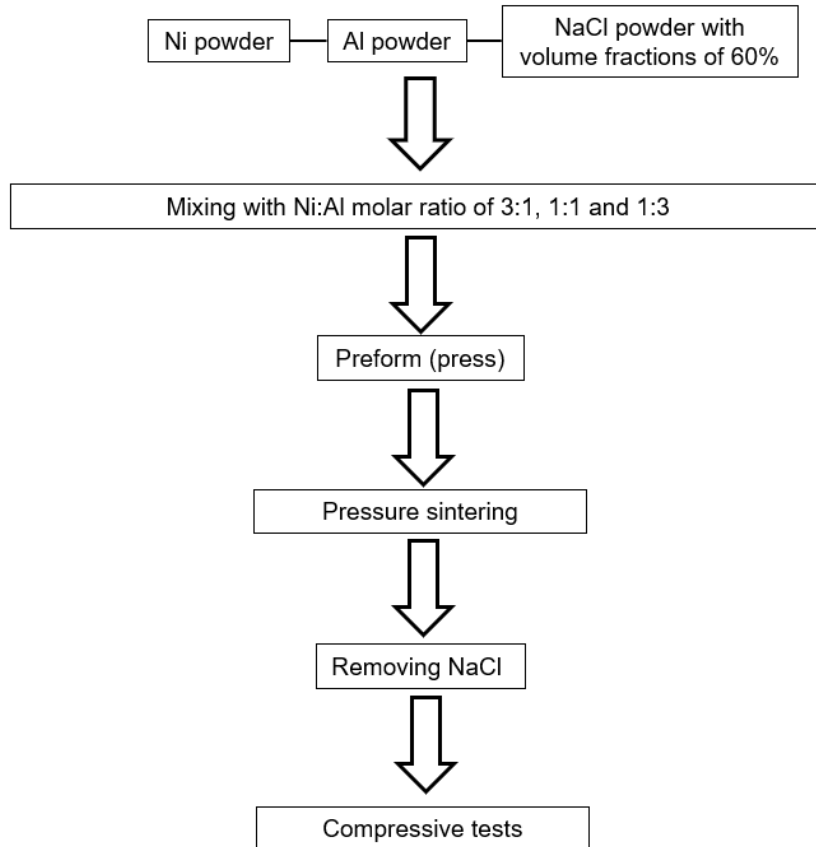


Fig. 4-1 Process of fabricating porous Ni-Al intermetallic compounds.

4.3 Results

4.31 Comparison with porous Al

Figure 4-2 presents the nominal stress-strain curve of porous Ni-Al intermetallic compounds and Fig. 4-3 shows the compressive deformation behavior at strains indicated in Fig. 4-2. Total porosity (sum total of small pore and large pore) of these samples was approximately 70%. For comparison, two stress-strain curves (almost overlapped) of porous Al with porosity of approximately 70% is also presented. When the porous Al was compressed, flow stress in the plateau region increased slightly with increasing strain because of the strain hardening of Al. The plateau end strain, which is defined as the strain when the flow stress reaches 1.3 times the plateau stress [4-9], was approximately 36%. On the other hand, porous Ni₃Al showed higher strength (initial maximum compressive stress was approximately 30 MPa). After initial maximum compressive stress, nominal stress decreased because of crack initiation (Fig. 4-3 (a-b)). Although the stress slightly increased, the stress decreases due to the initiation or propagation of cracks, resulting in relatively flat plateau region and plateau end strain larger than 60% respectively. The other porous Ni-Al intermetallic compounds (NiAl, NiAl₃) exhibited similar compressive deformation behavior. The results of porous NiAl correspond well with compressive properties of porous NiAl using carbamide particles as a spacer reported by Wu et al [4-10]. Figure 4-2 reveals that the plateau stress of Ni₃Al is the highest in the porous Ni-Al intermetallic compounds. Two stress-strain curves of porous NiAl are shown in the figure. The initial maximum stress and plateau end strain are exhibited good reproducibility, but plateau stresses of two specimens are a little different due to brittle fracture.

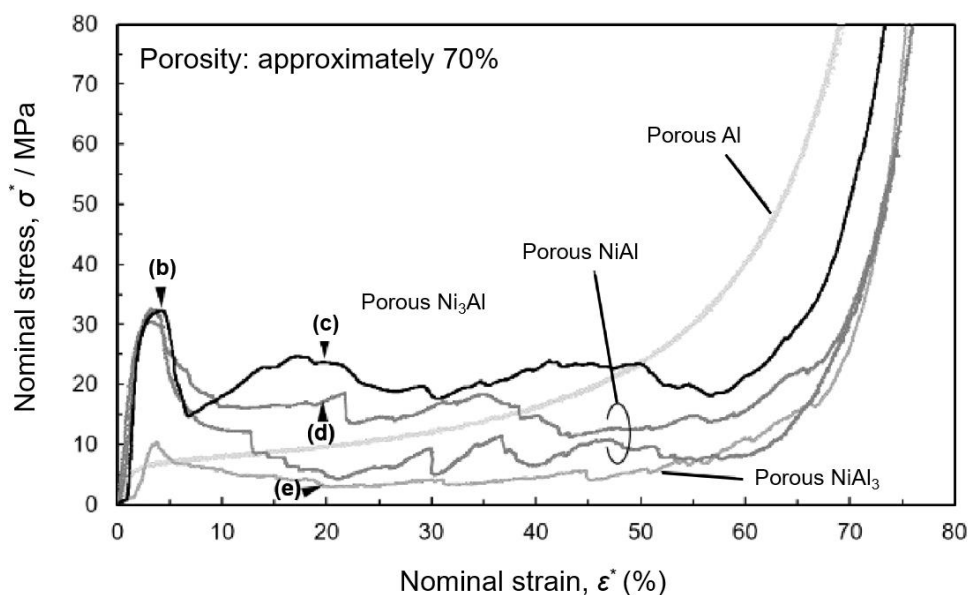


Fig. 4-2 Nominal stress-strain curves of Nickel Aluminides and Al with porosity of approximately 70%.

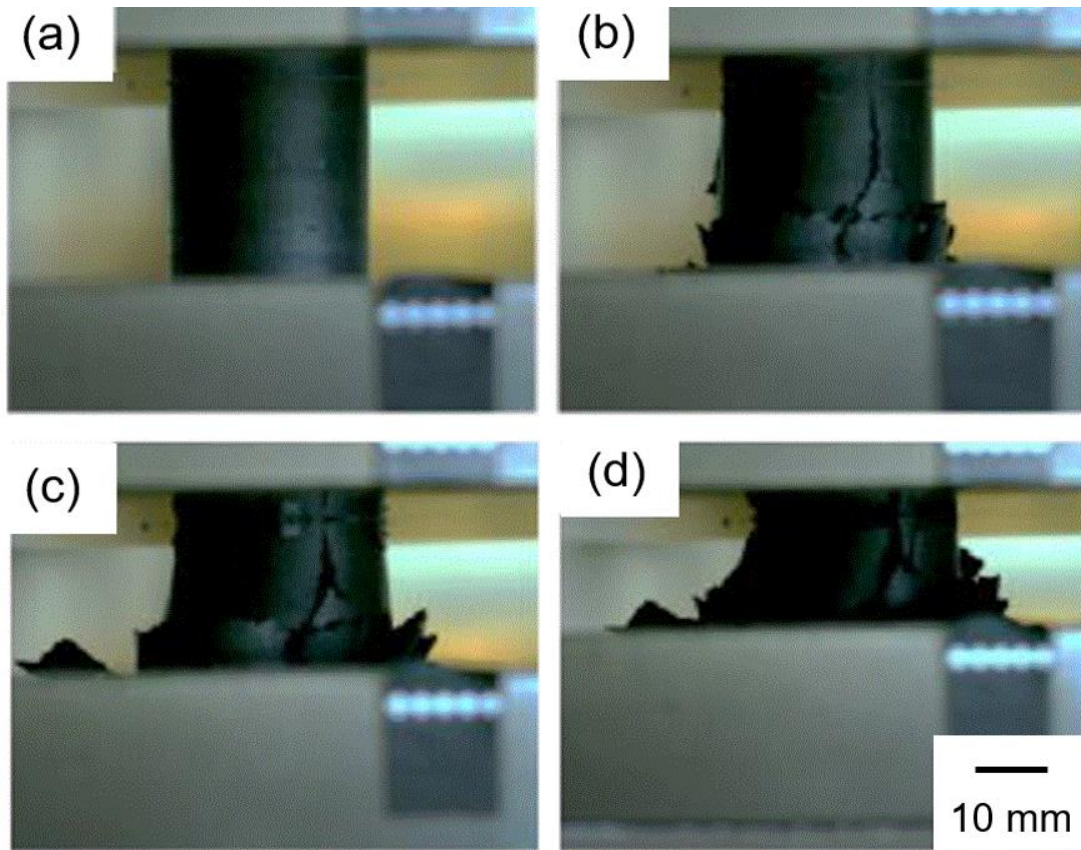


Fig. 4-3 Compressive behavior of porous Ni-Al intermetallic compound in different compressive stages.

4.32 Comparison between single-phase and multiple-phase products

Figure 4-4 shows the nominal stress-strain curves of NiAl_3 with porosity of approximately 70%. The curve in red color represents the porous product with single-phase matrix material (NiAl_3), and the curves in ash black (three curves) represent the porous products with multiple-phase matrix materials (dominant phase is NiAl_3). It is noted that absolute single-phase NiAl_3 is impossible to be synthesized due to the narrow region of NiAl_3 in equilibrium phase diagram of Ni-Al binary system. Therefore, the single-phase products told in the case of Ni:Al = 1:3 is an approximation of single-phase NiAl_3 . In the case of single-phase NiAl_3 , relatively good plateau region including initial yield stress (10.3 MPa), plateau stress (3.36 MPa) and plateau end strain (40%) was presented. However, in the case of multiple-phase products (dominant phase is NiAl_3), there were almost no plateau regions could be obtained due to the lower strength and higher brittleness.

The nominal stress-strain curves of NiAl with porosity of approximately 70% are shown in Fig. 4-5. The curves in red colors represent the porous Ni-Al intermetallic

compounds with single-phase matrix material (NiAl), and the curve in black represents the porous Ni-Al intermetallic compound with multiple-phase matrix materials (dominant phase is NiAl). Both single-phase and multiple-phase specimens show obvious plateau regions. In particular, single-phase specimens show higher yield stress (approximately 30 MPa), higher plateau stress (approximately 15 MPa) and plateau end strain (approximately 60%) than those of multiple-phase specimen (yield stress \approx 13 MPa, higher plateau stress \approx 4 MPa, plateau end strain \approx 40%). It is indicated a better compressive property when the matrix material is single-phase NiAl.

Likewise Fig. 4-6 presents the nominal stress-strain curves of Ni₃Al with porosity of approximately 70%. The curve drawn in red represents the product with single-phase matrix material (Ni₃Al), and the curves drawn in ash black colors (three curves) represent the products with multiple-phase matrix materials (dominant phase is Ni₃Al). Also, comparing with the case of multiple-phase matrix material, higher plateau stress (approximately 20 MPa) and plateau end strain (approximately 63%) is shown in the case of single-phase matrix material.

Therefore, higher initial yield stress and better compressive properties including higher plateau end strain and ideal plateau region are acquired by converting matrix material into single phase in this study.

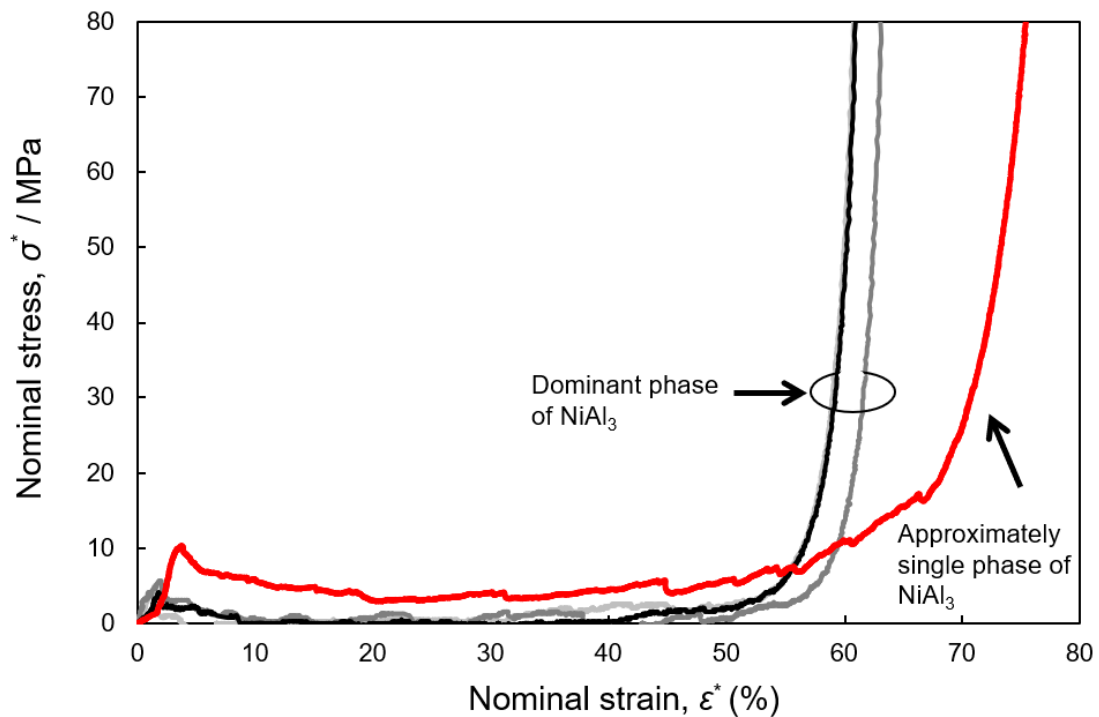


Fig. 4-4 Nominal stress-strain curves of NiAl₃ with porosity of approximately 70%.

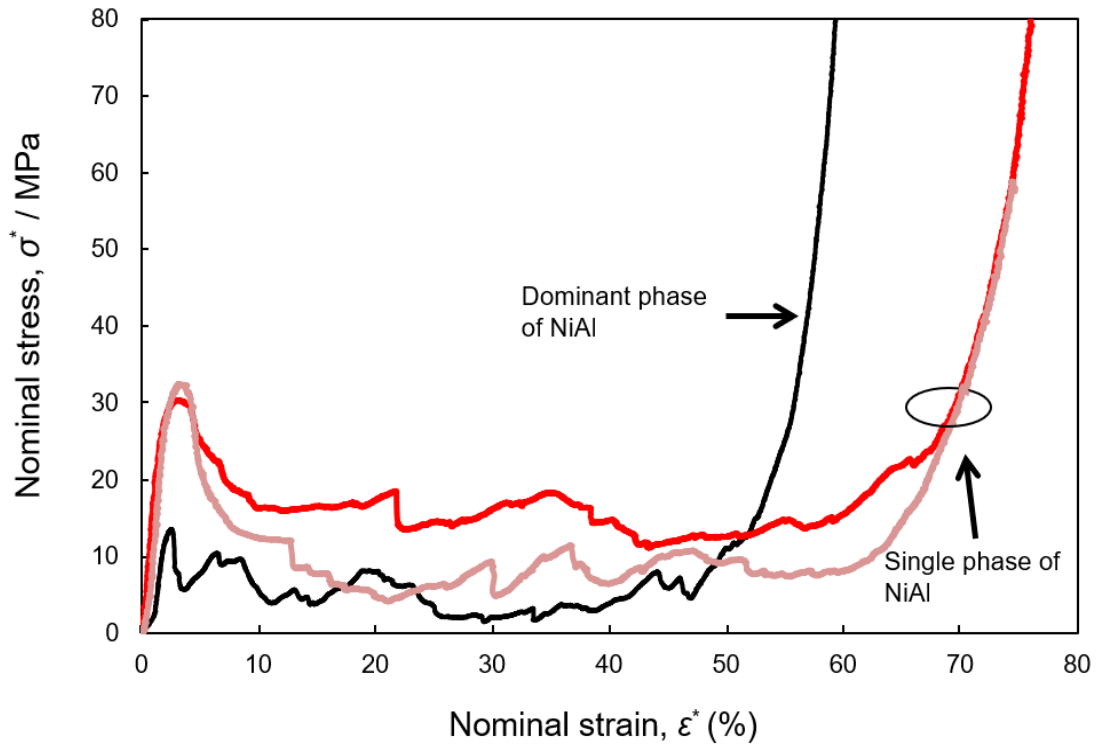


Fig. 4-5 Nominal stress-strain curves of NiAl with porosity of approximately 70%.

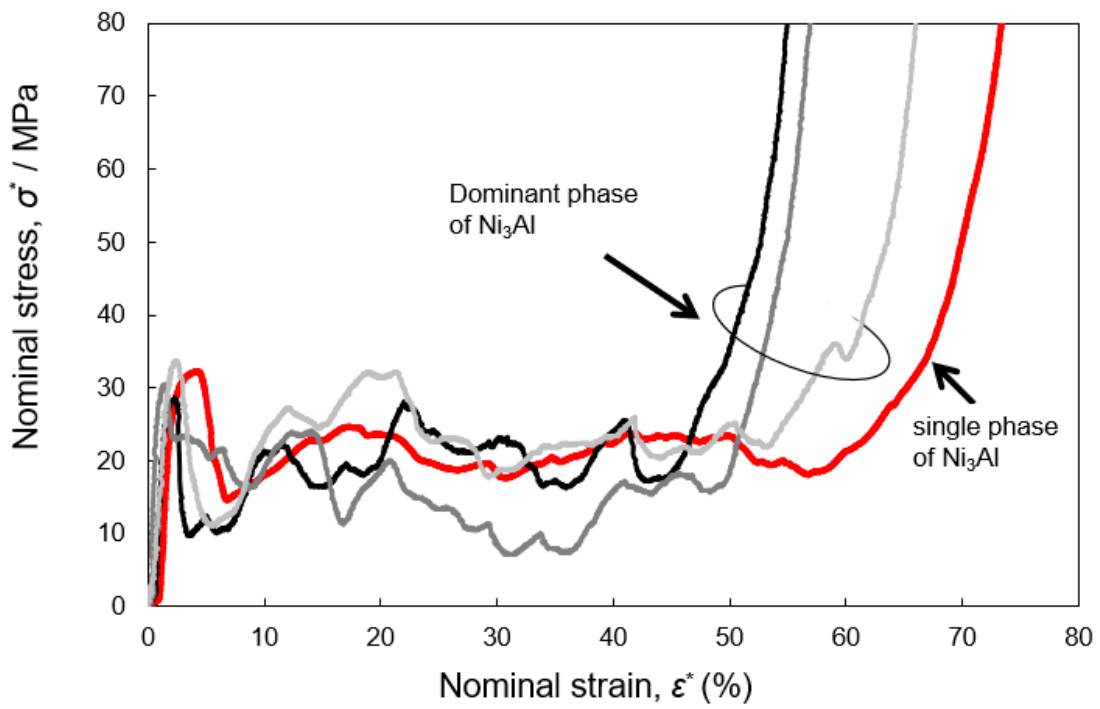


Fig. 4-6 Nominal stress-strain curves of Ni₃Al with porosity of approximately 70%.

4.4 Discussion

4.41 Comparison with porous Al

Comparing with porous Al, Porous Ni-Al intermetallic compounds fabricated in this research exhibited higher plateau end strain, and relatively flatter plateau region (Fig. 4-2). When porous Al (a porous material composed of ductile metal) is compressed, it is inevitable that the plateau region shows a slope. This is because strain hardening of Al is generated by bending deformation of the metallic cell wall. On the other hand, in the porous Ni-Al intermetallic compounds (a porous material composed of brittle metal without plastic deformation), the deformation progresses while repeating local fracture, resulting in a relatively flatter plateau region than that of porous Al. In order to fabricate a porous material as a high-performance shock absorbing material, a brittleness of intermetallic compounds can be effectively utilized. Takata et al. reported that porous Ti_3Al fabricated through a reactive process with NaCl space holder exhibited high plateau stress (approximately 100 MPa) and high plateau end strain (over 50%) [4-6]. On the other hand, the porous Ni-Al intermetallic compounds which are composed of intermetallic compounds exhibited unstable plateau region and plateau stress due to their brittleness (Fig. 4-2). Therefore, combining brittle materials with ductile materials could be applied to obtain stable and flat plateau region in the future.

4.42 Comparison between single-phase and multiple-phase products

Obviously higher initial yield stress was shown up in the case of Ni:Al = 1:3 and Ni:Al = 1:1 when constituting phase was single. Besides, distinctly higher plateau end strains were also presented in both three cases when constituting phase was single phase. It is indicated a superior mechanical strength of single-phase matrix materials compared to that of multiple-phase matrix materials. As known, comparing with single-phase materials, phase interfaces (interfaces between different phases) largely exist in multiple-phase materials. Therefore, high interfacial energy (γ) of phase interfaces is brought in the multiple-phase material, which is much larger than that in single-phase material. The free energy of system (G) could be expressed by follow equation:

$$G = G_0 + A\gamma \quad (10)$$

Where G_0 is the free energy of system by assuming that all the parts inside this system have no interfaces and possess properties of agglomerate, A is the area of interfaces of

this system [4-11]. On the other hand, free energy of system highly affects the stability of this system by affecting the strain energy, which is presented as the mechanical strength of materials at the macro level. Also, interfacial energy of phase interfaces decreases the strain energy, resulting in lower mechanical strength of materials. Moreover, brittleness of multiple-phase materials increases obviously while the grains of one phase randomly disperse into the grain boundaries of other phases. Multiple-phase structure influences the mechanical properties of materials by increasing total interface energy inside the materials, resulting in higher brittleness or lower strength. Therefore, promoting the degree of single-phase transformation by controlling fabricating process could enhance the mechanical properties of porous Ni-Al intermetallic compounds in this research.

4.5 Summary

The fabricated porous Ni-Al intermetallic compounds exhibited higher plateau end strain, relatively flatter plateau region and higher initial yield stress than those of porous Al. Porous Ni-Al intermetallic compounds show a superior mechanical strength, and also can be effectively utilized in various applications including shock absorbers.

Moreover, comparing to porous Ni-Al intermetallic compounds with multiple-phase matrix, the porous Ni-Al intermetallic compounds with single-phase matrix exhibited higher initial yield strength and longer plateau end strain. It is suggesting that higher mechanical strength and stability for applications could be acquired when the matrix materials are single-phase structure. Therefore, higher mechanical strength and stability for applications could be realized by increasing the degree of single-phase transformation in final products.

Reference

- [4-1] John. Banhart: Manufacture, characterisation and application of cellular metals and metal foams, *Progress in Materials Science*, 46 (2001), pp. 559-632.
- [4-2] Francisco Garc á-Moreno: Commercial Applications of Metal Foams: Their Properties and Production, *Materials* 9(2) (2016), 85.
- [4-3] Michael F. Ashby, Tony Evans, NA Fleck, J.W. Hutchinson, H.N.G. Wadley, L. J. Gibson: *Metal Foams: A Design Guide*, Elsevier Science, 2000.
- [4-4] E. Koza, M. Leonowicz, S. Wojciechowski, F. Simancik: Compressive strength of aluminium foams, *Materials Letters*, 58 (2004), pp. 132-135.
- [4-5] N.Michailidis, F.Stergioudi, A.Tsouknidas: Deformation and energy absorption properties of powder-metallurgy produced Al foams, *Materials Science and Engineering: A*, 528 (2011), pp. 7222-7227.
- [4-6] Naoki Takata, Keisuke Uematsu, Makoto Kobashi: Compressive properties of porous Ti–Al alloys fabricated by reaction synthesis using a space holder powder, *Materials Science and Engineering: A*, 697 (2017), pp. 66-70.
- [4-7] S.K.Maiti, L.J.Gibson, M.F.Ashby: Deformation and energy absorption diagrams for cellular solids, *Acta Metallurgica*, 32 (1984), pp. 1963-1975.
- [4-8] Yunmao Shu, Asuka Suzuki, Naoki Takata, Makoto Kobashi, *Journal of Materials Processing Tech.* 264 (2019), pp. 182–189.
- [4-9] International Organization for Standardization: *Metallic materials-Ductility testing- Compression test for porous and cellular metals*, ISO 13314 (2011).
- [4-10] J. Wu, H. Cui, L.L. Cao, Z.Z. Gu, *Trans. Nonferrous Met. Soc. China*, 21 (2011), pp. 1750-1754.
- [4-11] David A.Porter, Kenneth E Easterling, Mohamed Sherif: *Phase Transformations in Metals and Alloys Third Edition*, CRC Press Taylor & Francis Group, 1992.

Chapter.5 Investigation of fluid permeability

5.1 Introduction

As introduced in first chapter, the motivation of this study is to improve the flow permeability of porous metals, so that applications of porous metals on catalytic, heat management, environment protection and fuel cells can be realized or optimized.

Table 5-1 Permeabilities of common porous materials in nature [5.1]

Name	Permeability K / m^2
Leather	$9.5 \times 10^{-14} \sim 1.2 \times 10^{-13}$
Limestone	$2.0 \times 10^{-15} \sim 4.5 \times 10^{-14}$
Soil	$2.9 \times 10^{-13} \sim 1.4 \times 10^{-11}$
Sandstone	$5.0 \times 10^{-16} \sim 3.0 \times 10^{-12}$
Cement	$10^{-13} \sim 2.3 \times 10^{-11}$
Hair	$8.3 \times 10^{-10} \sim 1.2 \times 10^{-9}$
Cork board	$2.4 \times 10^{-11} \sim 5.1 \times 10^{-11}$

According to the Darcy Law which was proposed through the specific experiment by Darcy in 1865, and the equation of this law could be expressed as follow:

$$q_v = \frac{K}{\eta} A \frac{\Delta p}{H} \quad (1)$$

Where A (m^2) is the cross-sectional area of porous material, H (m) is the thickness which the liquid flows through, q_v (m^3/s) is the volume rate of flowing through Newtonian fluid, η ($Pa \cdot s$) is the dynamic viscosity of work liquid, Δp (Pa) is the pressure drop from inflow to outflow of work liquid, and K is the specific permeability. The above-mentioned permeability (K) depends not on the properties of work liquid but the porous structure of materials. Permeabilities of common porous materials in nature were measured through experiments, and shown in Table 5-1 [5-1].

According to the categories of porous materials, various mathematical models were established for predicting the permeability of porous materials [5-2]. Among the mathematical models, the Carman-Kozeny model is the most famous one and appropriate for the porous materials composed of fibers or powders. The Carman-Kozeny equation is shown below [5-1]:

$$K = \frac{d_p^2 \phi^3}{180(1-\phi)^2} \quad (2)$$

Where d_p is the effective mean diameter of particles constituting the cell walls of porous material, and ϕ is the porosity of porous material. It is noted that effective mean diameter of particle size has a positive correlation with the effective mean diameter of pores inside porous materials. It could be inferred from Carman-Kozeny equation that permeability of porous material is positively correlated with the mean diameter of pores. However, in practical terms, the interconnection of pores affects permeability of porous material obviously. This is because the interconnection of pores inside materials provides the channels for transporting flow, which is considered as the root of flow permeability. Besides, the interconnection of pores also determines the effective pore size or quantity of effective pores which are contributing to flow transmission, and thereby determines the flow permeability.

Therefore, we focused on increasing the degree of interconnection of pores, so that flow permeability could be enhanced fundamentally. In this study, we utilized combustion synthesis reaction between Ni and Al to generate small pores in cell walls of pores derived from NaCl, resulting in improvement of interconnection of pores derived from NaCl and thereby increasing the flow permeability of porous metals. And the effect of porosity of small pores in metallic cell walls derived from combustion synthesis reaction between Ni and Al on permeability was also investigated.

5.2 Experimental method

Porous Ni-Al intermetallic compounds for permeability test were fabricated by the developed method in this study using the same raw powders (Ni:1 μ m, Al: 2 μ m, NaCl: 30~50 μ m, 60 Vol%). The porous Ni-Al samples with Ni:Al molar ratios of 1:1 and 3:1 were prepared in order to obtain different porosity in metallic cell walls, so that the effects of porosity of small pores derived from combustion synthesis reaction between Ni and Al on permeability could be also investigated simultaneously. The whole process is shown in Fig. 5-1.

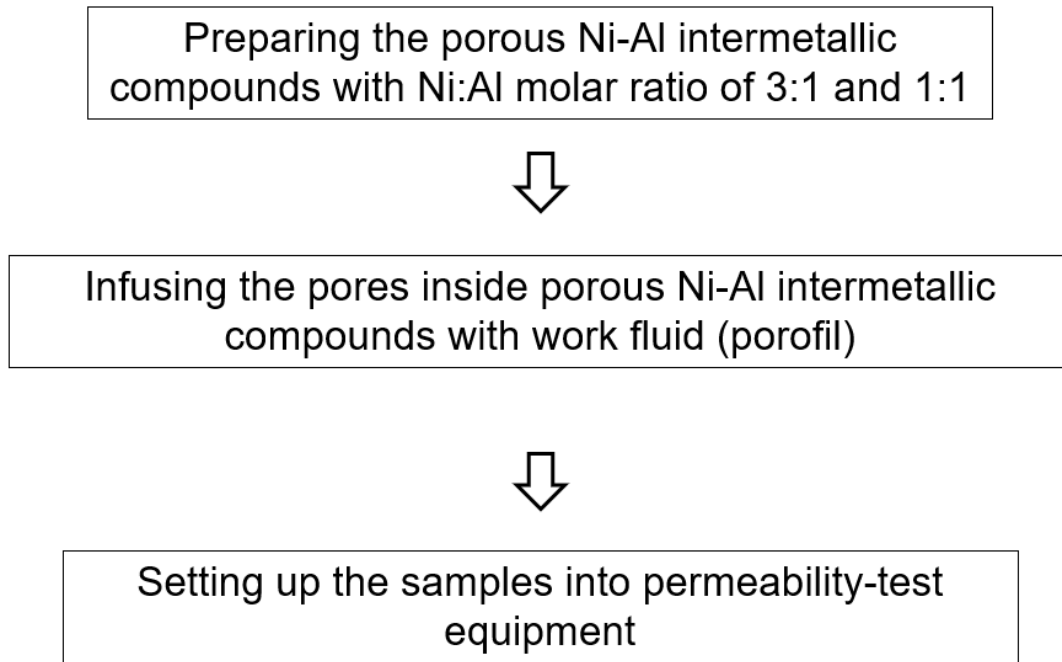


Fig.5-1 Process of permeability test

First, powder mixture of Ni, Al and NaCl was prepared. The Ni:Al molar ratios in powder mixture were 1:1 and 3:1 respectively in order to obtain different porous structure. Next, porous Ni-Al intermetallic compounds were fabricated by sintering process and space-holder removal (Fig. 5-2). Subsequently, the fabricated porous samples were set up into a vacuum device (Fig. 5-3 (b)) for the work liquid (called Porofil and shown in Fig. 5-3 (a)) inflowing and filling up the pores inside the samples. It is noted that Porofil is a sort of liquid which has a high wettability and contact angle is nearly 0° . After infusing porous Ni-Al samples with Poofil, permeability test was carried out by utilizing the Capillary force/ permeability testing device (Fig. 5-3 (c)). Inside the permeability-test instrument, nitrogen gas was injected into the porous Ni-Al intermetallic sample which was filled with the Porofil liquid, and then the nitrogen flow pushed out the filled porofil from porous Ni-Al sample, followed by forming a nitrogen gas flow through the entire sample (wet-type test). The gas flow running through the porous Ni-Al sample was measured in this capillary force/ permeability testing device (Fig. 5-3 (c)). Also, nitrogen gas flow of porous Ni-Al sample without Porofil inside was measured using the capillary force/ permeability testing device (dry-type test). Hence, the curve which shows N_2 gas flow as a function of N_2 gas pressure could be obtained by utilizing the capillary force/ permeability testing device. It is noted that Porofil is held by the capillary force (P) of the pores inside the materials, and the capillary force (P) is expressed by follow equation:

$$P = \frac{2\gamma \cos \theta}{r} \cdot S \quad (3)$$

Where r is the radius of pores, γ is the surface tension of Porofil, θ is the contact angle between Porofil and material, and S is the shape factor of pores. As mentioned before, Porofil is a kind of liquid which has an extremely high wettability so that the contact angle (θ) is approximately 0° . Moreover, the surface tension of Porofil is 1.6 N/m, and the shape factor (S) of pores in our case is approximately 1. Therefore, the equation (3) could be converted into the equation as bellow:

$$d \approx \frac{6.4}{P} \quad (4)$$

Where d is the diameter of pores. Hence, the curve showing the gas flow as a function of pore size could be acquired instead of the gas flow as a function of pressure. Also, both cumulative frequency (CF_n) and differential frequency (DF_n) could be calculated from the gas flow of wet-type test and dry-type test to replace the gas flow in the former curve. Cumulative frequency (CF_n) is obtained by follow equation:

$$CF_n = \frac{Q_n(\text{Wet})}{Q_n(\text{Dry})} \cdot 100 \quad (5)$$

Where $Q_n(\text{Wet})$ and $Q_n(\text{Dry})$ are the N_2 gas flow of wet-type test and dry-type test respectively. Also, differential frequency (DF_n) could be calculated by follow equation:

$$DF_n = \frac{CF_{n+1} - CF_{n-1}}{2} \quad (6)$$

As a result, not only flow permeability but also the pore size distribution of the pores which are contributing to the flow permeability could be measured. Moreover, the permeability of porous Ni-Al samples could be estimated by the follow equation which are converted from equation (1):

$$K = \eta \cdot \frac{Q(\text{Dry})}{\Delta P} \cdot \frac{H}{A} \quad (7)$$

Where $Q(\text{Dry})$ is the volume rate of flow in the case of dry test as shown in Fig. 5-4 and 5-5. It is noted that $Q(\text{Dry})/\Delta P$ is equal to the slope of approximate straight line of the dry-type plot presented in Fig. 5-4 and 5-5, and the dynamic viscosity (η) of 1.79×10^{-5} Pa \cdot s was utilized for estimating the permeability.



Fig. 5-2 Appearances of the representative sintered samples for permeability test.

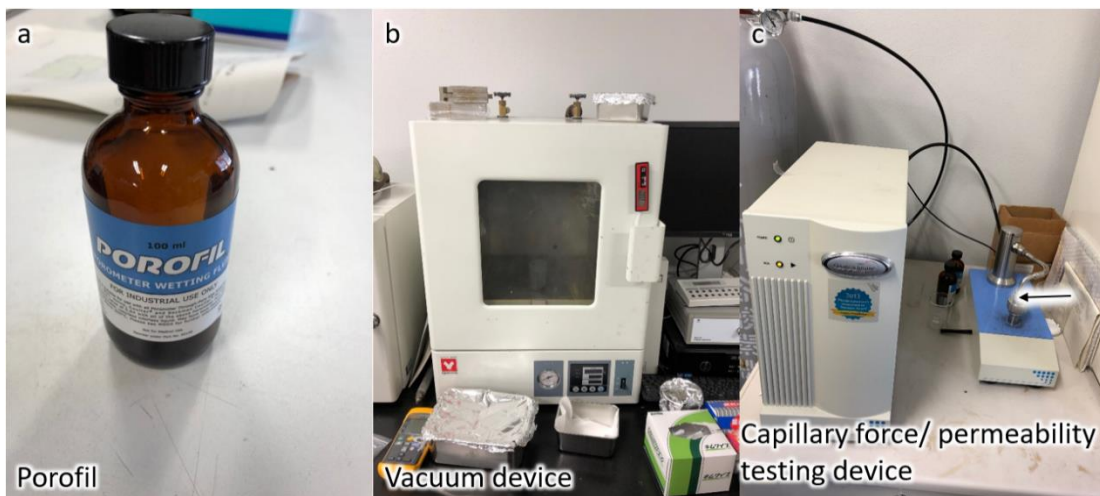


Fig. 5-3 Appearances of the Porofil (a), vacuum device (b) and capillary force/ permeability testing device.

5.3 Results

5.3.1 Size distribution of pores contributing to permeability

The relationship between pressure and gas flow of Ni:Al = 3:1 and Ni:Al = 1:1 are shown in Fig. 5-4 and Fig. 5-5 respectively. In the dry-type test, the gas flow increases almost linearly with increasing the pressure of N₂ due to the constant channels for transferring gas flow. However, the pressure-flow curve in case of wet-type test is different from that in case of dry-type test. In the case of wet-type test, the gas flow did not increase and remain 0 m³•s⁻¹ with increasing gas pressure until the pressure reached a certain point, followed by the almost linear increasing of gas flow with increasing the pressure of N₂ in the case of wet-type test. In initial stage of wet-type test, the Porofil filling up the pores existed and occupied the porous channel for passing into gas flow until the gas pressure rose above the value of capillary force, which resulted in the initial invariability of gas flow with increasing the gas pressure. From Fig. 5-4 and 5-5, it could be seen that the gas flow of wet-type test is lower than that of dry-type test before the Porofil is drained out of porous Ni-Al samples. After draining the Porofil, the gas flows of dry-type test and wet-type test tend to be consistent due to the totally same porous channels. In Fig. 5-4 and 5-5, the equation (4) could be utilized to convert the horizontal axis from pressure (P) into pore size (d), and equation (5) and (6) could be utilized to convert the vertical axis from gas flow (Q) into cumulative frequency (CF_n) and differential frequency (DF_n) respectively. Therefore, Fig. 5-6 and 5-7 are obtained from the conversion of Fig. 5-4 and 5-5. It is noted that the pore size (d) on horizontal axis represents the size of pores which are contributing to the flow permeability only. In other words, cumulative frequency (CF_n) indicates the distribution range of pores and differential frequency (DF_n) indicates the specific size distribution in the range indirectly. In the case of Ni:Al=3:1, the pores contributing to the flow permeability are mostly distributed in the range of 0.38~2.7 μm, and the mean size of pores contributing to the flow permeability is approximately 1.7 μm. On the other hand, the pores contributing to the flow permeability are mostly distributed in the range of 0.2~1.6 μm, and the mean size of pores contributing to the flow permeability is approximately 1.2 μm in the case of Ni:Al=1:1. Moreover, the relative density are 0.26 and 0.32 respectively in the case of Ni:Al=3:1 and Ni:Al=1:1.

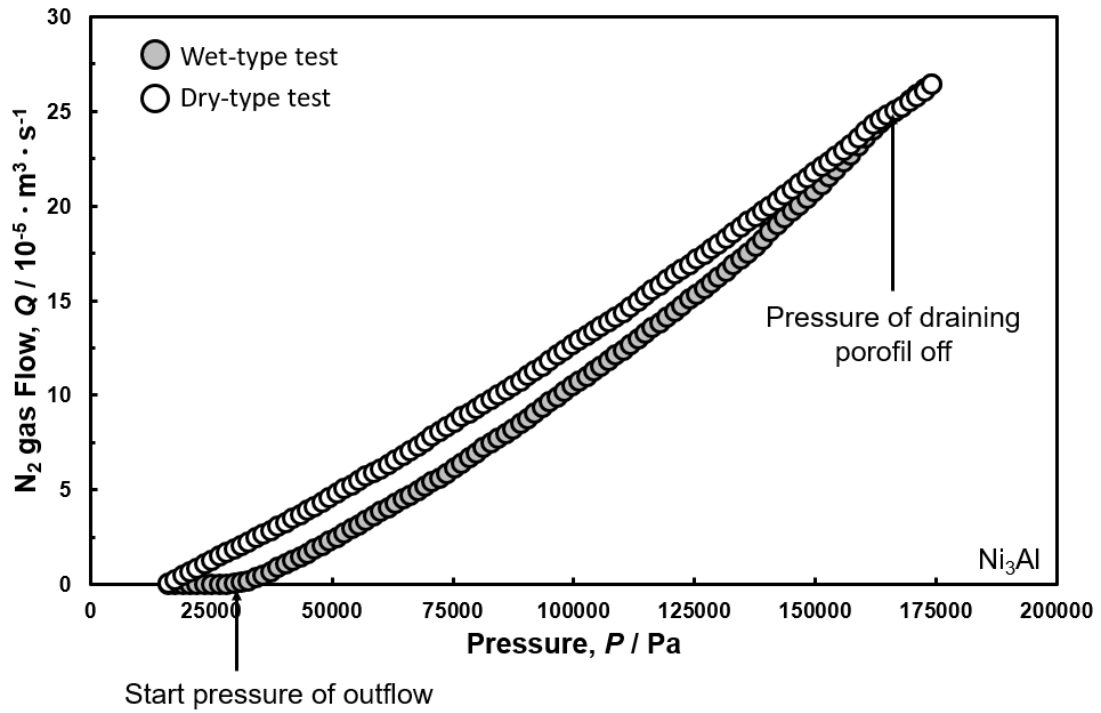


Fig. 5-4 Relationship between pressure and gas flow of N_2 (case of Ni_3Al).

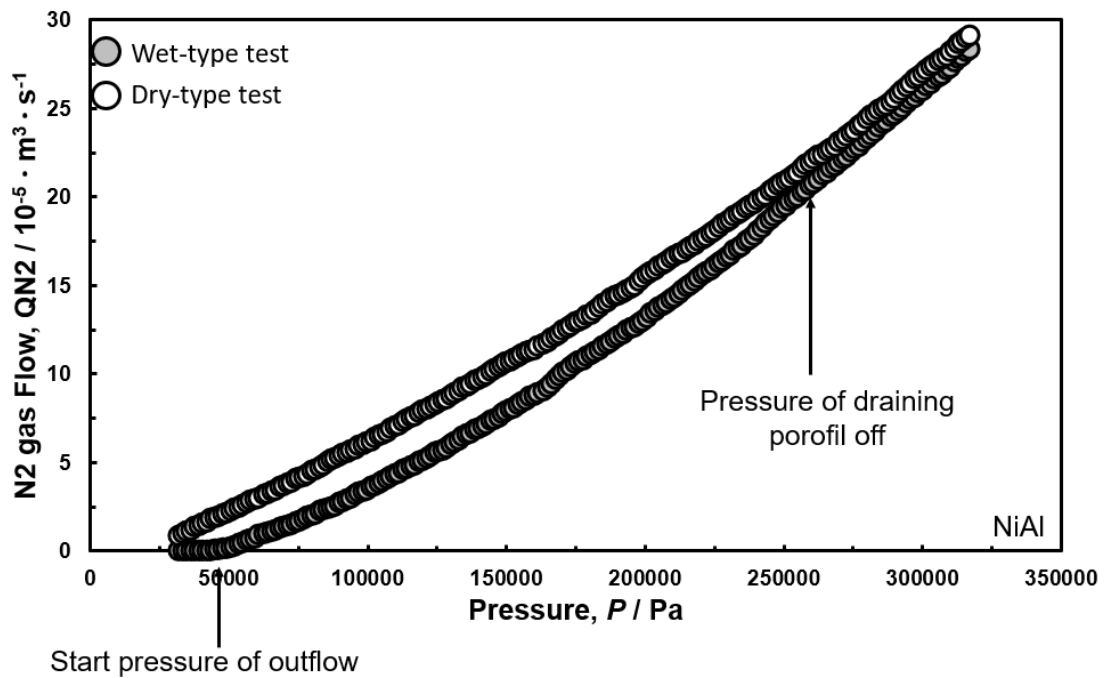


Fig. 5-5 Relationship between pressure and gas flow of N_2 (case of $NiAl$).

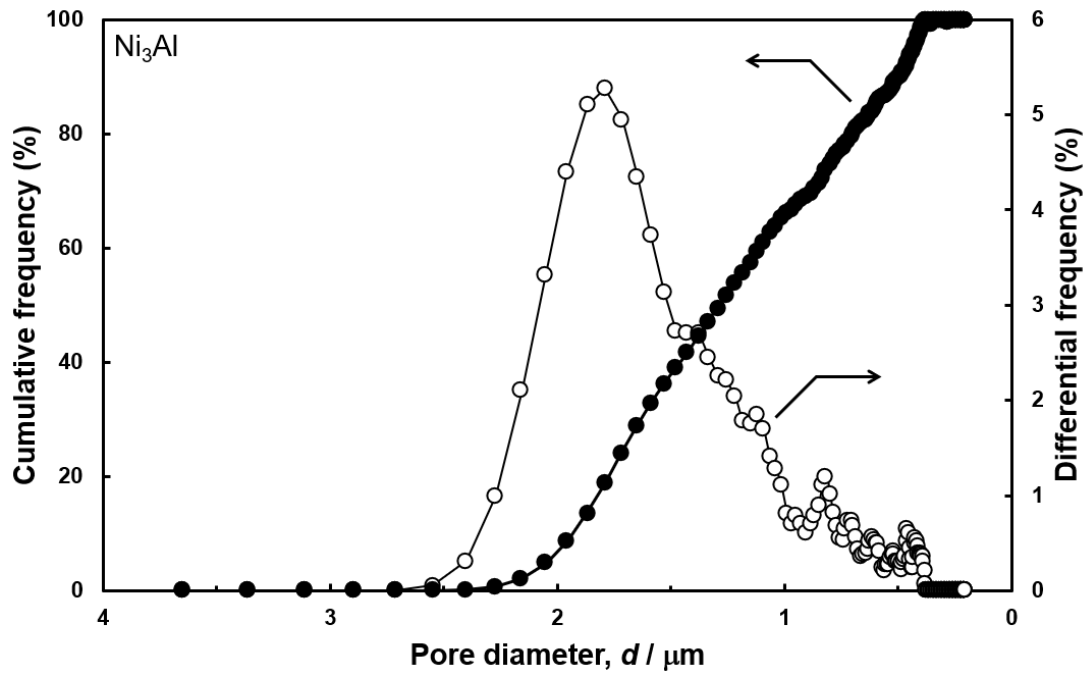


Fig. 5-6 Pore size distribution and relationship between pore size and flow permeability (the case of Ni_3Al).

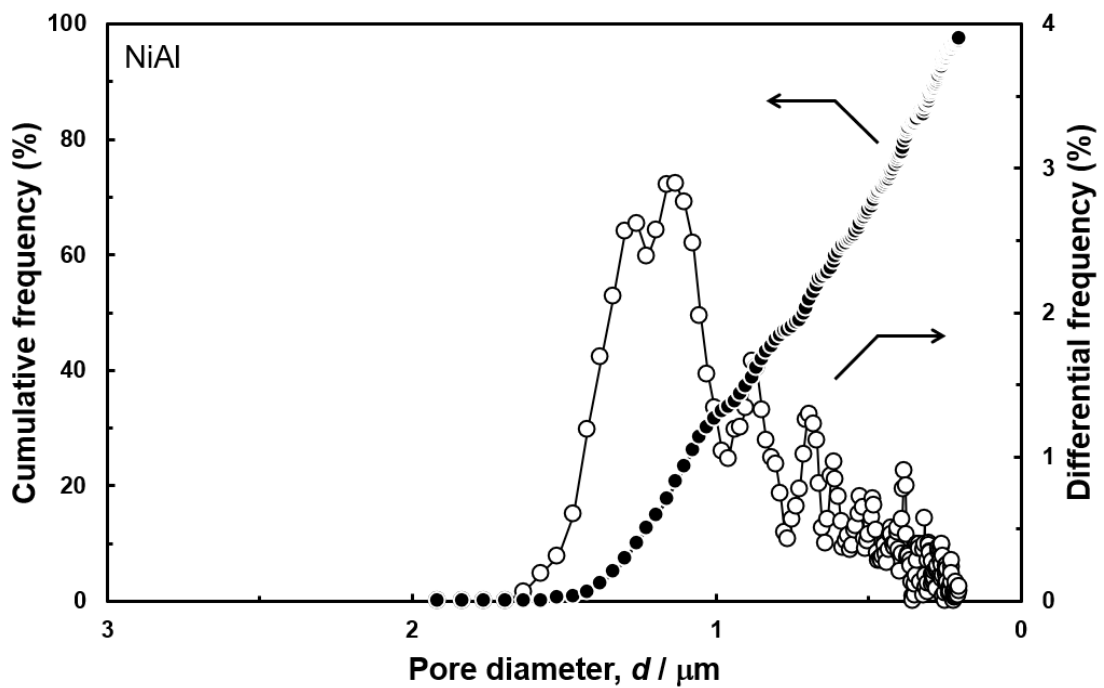


Fig. 5-7 Pore size distribution and relationship between pore size and flow permeability (the case of $NiAl$).

5.3.2 Optimization on permeability

The parameters of porous NiAl and porous Ni₃Al used for measuring in this study are shown in Table 5-2. The permeability of porous Ni-Al samples in this study is estimated from Fig. 5-4 and 5-5 by using equation (1) (Darcy equation). As known, the permeability is correlated to the conditions of porous materials like porous structures or matrix materials, but not dependent on the variety of fluids. Therefore, the permeability of gas flow is capable to be considered as the normal fluid permeability in the porous Ni-Al samples. The difference in overall porosity between the porous NiAl and porous Ni₃Al is considered as the difference in small-pore porosity in cell walls because the volume fraction and size of added NaCl are the same. Similarly, the mean pore sizes of large pores are considered as approximately equal in porous NiAl and porous Ni₃Al ($\approx 40\mu\text{m}$), and this value is also utilized for estimating the normalized permeability which is estimated through the pore equivalent diameter squared.

Table 5-2 Parameters of porous Ni-Al intermetallic compounds.

	Mean Pore size of large pores, d (μm)	Porosity, ϕ (%)	Permeability, K (m^2)	Normalized permeability, K / d^2
NiAl	42.2 (≈ 40)	69	1.53784E-13	9.61151E-05
Ni ₃ Al	41.4 (≈ 40)	74	3.08028E-13	1.92518E-04

Three sets of data on flow permeability are presented in Fig. 5-8. The first set is the data of the porous Ni-Al samples which were fabricated in this study. The second set is the data of porous Al fabricated by common space holder method and the third set is the data of general open-cell foams which are not fabricated by space holder method. The latter two sets of data on permeability are referenced from the previous studies [5-3, 4]. The normalized permeability which is estimated through the pore equivalent diameter squared is utilized in vertical axis of Fig. 5-8.

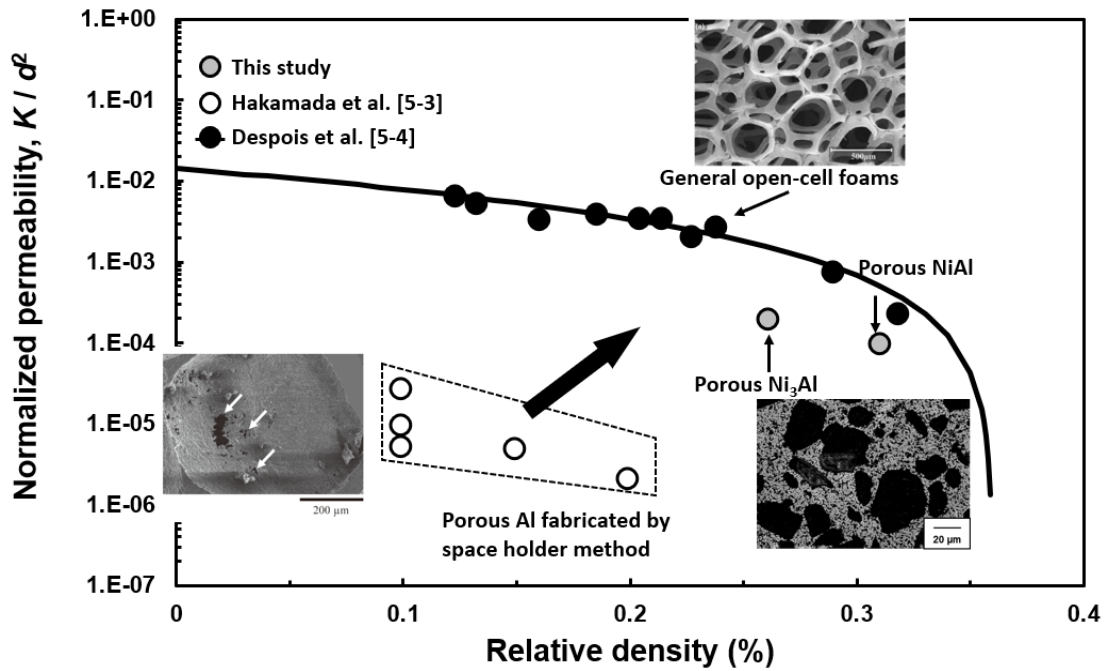


Fig. 5-8 Relationships between relative density and permeability.

The permeability of porous Al which are prepared by common space holder method is approximately two orders of magnitude lower than that of general open-cell foams which are not fabricated by space holder method. However, the permeability of porous materials which are fabricated by space holder method is significantly enhanced with an order of magnitude by combining with combustion synthesis reaction in this study. Therefore, combining combustion synthesis reaction with space holder method was experimentally confirmed highly effective on improving the fluid permeability of porous metals which are fabricated by space holder method in this study.

5.4 Discussion

5.4.1 Size distribution of pores contributing to permeability

According to the results of size distribution shown in Fig. 5-6 and 5-7 (approximately in the range of 3µm and below), we could tell that the size of pores

which are correlated with flow penetration directly is much smaller than that of space holder (NaCl: 30~50 μm). This is considered as the result of inadequate contact between NaCl particles. Figure 5-9 presents the schematic diagram of the trim pore size which is contributing to the flow penetration. It is illustrating that the contact area between NaCl particles is much smaller than the sectional area of NaCl particles.

The contact area between NaCl particles inside porous Ni-Al sample is mainly dependent on the volume fraction of NaCl. On the other hand, the contact between solids like NaCl particles commonly takes up very small area considering the contact angle. The contact area between two NaCl particles decides the size of pores which is virtually playing roles in flow penetration. As known, the pores playing roles in flow penetration are considered as the pores which are contributing to fluid permeability in this research. Therefore, the contact area is considered as the section of pores which is contributing to fluid permeability in this permeability test, resulting in a much smaller result on size distribution.

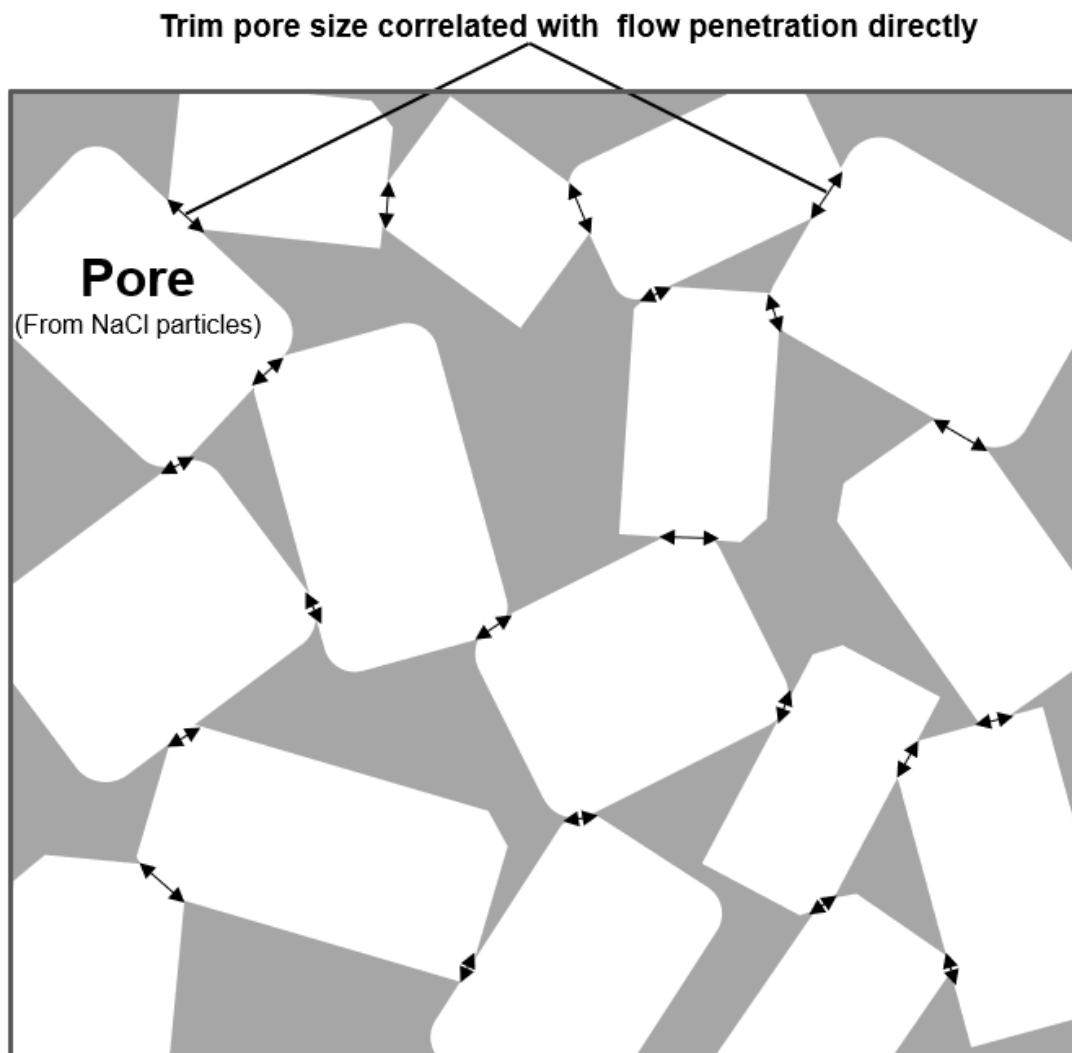


Fig. 5-9 Schematic diagram of the trim pore sizes which are contributing to the flow penetration.

5.4.2 Optimization on permeability

As mentioned in last section, it is known that the contact between the pores derived from NaCl is inadequate when the volume fraction of NaCl is not high enough. Hence, the flow paths of fluid are not plenty for achieving a high fluid permeability in the case of onefold space holder method. In order to increase flow paths inside porous metals thereby enhancing the fluid permeability, increasing the contact area between space-holder particles has become our basic strategy.

In this study, fluid permeability of porous metals which are fabricated by onefold space holder method is enhanced substantially by bringing bi-modal porous structure in our study. Figure 5-10 presents the schematic diagram of ideal flow pass in the case of combining space holder method with combustion synthesis reaction. The large-scale pores generated by NaCl (space holder) particles indeed play a major role in fluid flow, and the small-scale pores generated by Ni-Al combustion synthesis reaction also play a role of enhancing this flow pass through better contact or connection between large-scale pores.

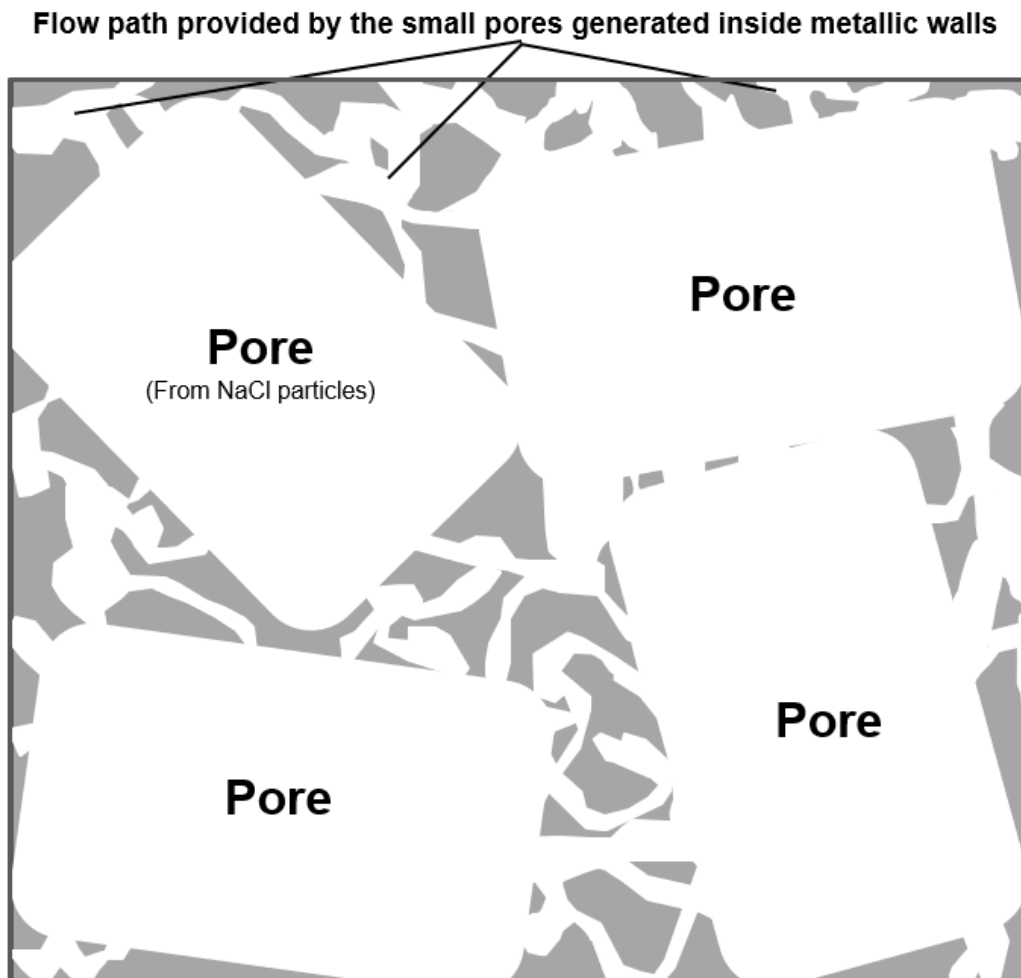


Fig. 5-10 Schematic diagram of ideal flow pass in the case of combining space holder method with combustion synthesis reaction.

5.5 Summary

Through the results of size distribution of pores which contribute to fluid permeability, the poor contact and poor connection between pores generated by NaCl are revealed. And the poor contact and connection between pores were considered as the reason of low fluid permeability derived from space holder method. Therefore, combustion synthesis reaction was utilized for raising the contact area and connection path between pores derived from space holder. In this study, the porous Ni-Al samples fabricated by combining space holder method and combustion synthesis reaction possess approximately an order of magnitude higher fluid permeability than the porous metals fabricated by onefold space holder method. Also, the fluid permeability increases with increasing the porosity of pores in metallic cell walls. In a word, this significant improvement on fluid permeability indicates more extensive applications or more effective uses of porous metals as functional porous materials.

Reference

[5-1] Donald A. Nield, Adrian Bejan: Convection in Porous Media [M], 2nd edition, Springer, 2006.

[5-2] F.A.L. Dullien: Porous media: Fluid transport and pore structure [M], 2nd edition, Academic Press, 1992.

[5-3] M. Hakamada, M. Mabuchi: Fabrication by spacer method and evaluation of porous metals, Journal of The Japan Institute of Light Metals, Vol. 62, No.8 (2012), pp. 313-321.

[5-4] J. F. Despois, A. Marmottant, L. Salvo and A. Mortensen: Influence of the infiltration pressure on the structure and properties of replicated aluminium foams, Mater. Sci. Eng. A, 462 (2007) , pp. 68-75.

Chapter 6. Summary

The motivation of this research is derived from the reflections on the hot issues today such as energy problem and environmental problem. As aforementioned in Chapter 1, the applications of porous metals highly relate to the fields of catalytic & filter (e.g. porous framework), thermal management (e.g. porous wick of Loop Heat Pipe) and electrochemistry (e.g. porous anode), which are tightly knitted with the energy and environment issues. Hence, the research on porous metals is expected on promoting the developments of the above fields. However, there were still various issues to be resolved. For example, the improvement on fluid permeability which is significantly impacting the functional properties has become the hot issues, and also a number of technologies on manufacturing were reported. Particularly, the space-holder method has attracted intense attention recent years due to the controllable porous structure, simple procedure and low cost. The porous metals fabricated by space-holder method were not presenting a satisfactory fluid permeability yet. In other word, there was still not a manufacturing technology that could fabricate controllable porous structure with ideal fluid permeability. Therefore, the goal of this research became clear that developing a manufacturing technology of porous metals with both controllable porous structure and good fluid permeability. In this research, space holder method was utilized due to the good porous structural controllability. On the basis of space holder method, combustion synthesis reaction was brought for generating more contact channels between pores fabricated by space-holder method to achieve the highly controllable porous structure as well as high fluid permeability.

In chapter 1, the backup and purpose were mainly introduced. The fluid permeability which are significantly impacting the functional properties have become the hot topics, and also a number of manufacturing technologies such as sintering method, slurry method and investment cast method are reported. However, the space holder method has attracted intense attention recent years due to the highly controllable porous structure, simple procedure and low cost. Furthermore, the porous metals fabricated by the space holder method have not presented a satisfactory fluid permeability yet. In other word, there was still no manufacturing technology that could fabricate highly controllable porous structure with ideal fluid permeability. Therefore, the goal of this research is clear that developing a manufacturing technology of porous metals with both highly controllable porous structure and high fluid permeability. In this research, space-holder method was utilized due to the excellent porous structural controllability. On the basis of space holder method, combustion synthesis reaction was brought for generating small pores between the large pores fabricated by space-holder method to achieve the high fluid permeability simultaneously.

In chapter 2, the combination of space-holder method and combustion synthesis reaction between Ni and Al was carried out, and porous Ni-Al intermetallic

compounds with hierarchical porous structure were successfully fabricated. This hierarchical porous structure was composed of small-scale pores derived from combustion synthesis reaction (between Ni and Al) and large-scale pores derived from space holders (NaCl particles) method. Small-scale pores derived from combustion synthesis reaction in metallic cell walls could not be formed without adding NaCl (space holder). This is because the melt caused by high reaction temperature which is positively related to the adiabatic temperature of combustion synthesis reaction exists during the process. It is suggesting that the NaCl particles are used not only for generating the large-scale pores but also for absorbing heat from combustion synthesis reaction between Ni and Al to avoid melt during reaction, thereby forming small-scale pores in metallic walls. Hence, the necessity of combining space-holder method with combustion synthesis reaction for generating this hierarchical porous structure was also proved in this chapter.

In chapter 3, the effects of NaCl addition and Ni:Al molar ratio on porous structure were investigated, then the strategy of controlling porous structure was acquired. The porous structure of large pores derived from NaCl is simple to control by adjusting the use of NaCl, and then controlling the porous structure of small pores derived from combustion synthesis reaction became the crucial subject in this research. As aforementioned in Chapter 2, NaCl not only affects the large pores derived from NaCl, but also affects the small pores derived from combustion synthesis reaction. The constituting phases and melting of intermediate product just after the reaction occurred are affected by NaCl and the molar ratio of Ni:Al in raw mixture. This is because shrinkage rates of average atomic volume from the mixture of nickel and aluminum to the intermediate Ni-Al intermetallic compounds vary with varying Al content and NaCl addition in raw mixture. As known, different shrinkage rates of metallic cell wall in intermediate Ni-Al intermetallic compounds results in different structures of small pores surrounded by metallic cell walls. In addition, size and porosity of small pores also increase with raising Al content due to the Kirkendall effect. In order to control the porosity and morphologies of the pores in cell walls, it is necessary to select appropriate Al content in raw mixture and control the constituting phase just after the reaction occurs.

The mechanical property of porous Ni-Al intermetallic compounds was investigated in chapter 4. The results showed us a significant enhancement on mechanical property through combining space-holder method with combustion synthesis reaction. Comparing to porous Al, the mechanical strength of porous Ni-Al intermetallic is increased as well as the corrosion and oxidation resistance at high temperature. Comparing to multiple-phase matrix, the porous Ni-Al intermetallic compounds with single-phase matrix exhibited higher initial yield strength and longer plateau end strain. This is because multiple-phase structure influences the mechanical properties of materials by increasing total interface energy inside the materials, resulting in higher brittleness and lower strength of materials. It is suggesting that higher mechanical strength and stability for applications could be acquired when the matrix materials are single-phase substance. On the basis of reliable strength, other improvements of porous Ni-Al intermetallic compounds on functional properties are

considered to be more meaningful on applications as well.

In chapter 5, the fluid permeability was investigated. In terms of fluid permeability, the poor contact and poor connection between pores result in the low fluid permeability of porous metals fabricated by space holder method. In this research, we improved the contact and connection between pores generated by space holders, thereby improving the fluid permeability significantly. The small pores derived from Ni-Al combustion synthesis reaction were formed in the metallic cell walls, and then contributed to enhancing the contact and connection between the large pores generated by space holders. As a result, the fabricated porous Ni-Al intermetallic compounds possess approximately an order of magnitude higher fluid permeability than the porous metals fabricated by traditional onefold space holder method. And we also revealed that the fluid permeability increases with increasing the porosity of small pores in metallic cell walls. Hence, manufacturing technology that could fabricate highly controllable porous structure with excellent fluid permeability and reliable strength is developed through combination of space-holder method and combustion synthesis reaction. Porous metals could be expected to play decisive roles in some fields such as energy and environment in the near future, so the study on specific applications is imperative to continue.

Taken together, manufacturing technology of fabricating porous Ni-Al intermetallic compounds is developed through the combination of space-holder method and combustion synthesis reaction. This manufacturing technology shows us a possibility to fabricate porous metals which have controllable porous structure, higher fluid permeability and better mechanical properties. Comparing to traditional metallic materials, intermetallic compounds commonly exhibit higher corrosion resistance, higher thermal stability and higher mechanical strength. Moreover, porous metals with bi-scale pores (hierarchical porous structure) are showing a higher fluid permeability than that of porous metals with mono-scale pores. Through this manufacturing technology, the follow strategy of fabricating porous metals with higher permeability and strength was acquired: 1) In the term of matrix metal, intermetallic compounds with single-phase structure are superior; 2) in the term of porous structure, hierarchical structure with bi-scale pores is preferred. Since the fabricated porous Ni-Al intermetallic compounds are expected to play decisive roles in a number of fields such as energy and environment, the study on specific applications is imperative to continue in the future.

Acknowledgements

This research benefited from many people who have spared no effort to support and help me. Without these help and support, this research would be ten times more tortuous than it is today. So not only on behalf of me but also on behalf of this research, I would like to express my most heartfelt thanks to these people introduced below.

First, I want to thank my three instructors of Kobashi & Takata Laboratory. As my main instructor, Dr. Makoto Kobashi gave me a lot of guidance in the research direction and school life. Besides, He also created many ideal research conditions for me and helped me eliminate many difficulties outside the research. As my deputy instructor, Dr. Naoki Takata gave me a lot of valuable and pertinent advices on my research, and provided me with the conditions for using all the necessary equipment. As the assistant professor, Dr. Asuka Suzuki directed almost every detail of this research personally, and indeed he took this study to the next level. Also, I would like to thank my deputy reviewers, Dr. Hosei Nagano and Dr. Toshiyuki Koyama. They took time out of busy schedule to check my thesis and gave me a lot of crucial comments, which helped me to make my thesis better. For every student like me in Nagoya University, they are not only great researchers but also great educators that we long to be in the future.

Then I want to thank the others in Kobashi & Takata Laboratory. Mrs. Nomura Kazuko, Kim Seung-Gwang (Korea), Kodaira Hirohisa, Okano Taiki, , Liu Mulin (China), Hayano Kunishisa, Nishida Ryoya and others gave me a lot of help in my hour of need. I also want to sincerely thank the commonweal foundation of Otsuka Toshimi Scholarship Foundation that funded me during my school years. Thanks to this funding, I got rid of financial difficulties and could focus on my research.

Finally, I want to express my most sincere thanks to my family. Thank them for the full support and understanding.

Published Thesis

1. Yunmao Shu, Asuka Suzuki, Naoki Takata, Makoto Kobashi: Fabrication of porous NiAl intermetallic compounds with a hierarchical open-cell structure by combustion synthesis reaction and space holder method, *Journal of Materials Processing Technology*, Vol. 264 (2019), pp. 182-189.
2. Yunmao Shu, Asuka Suzuki, Naoki Takata, Makoto Kobashi: Microstructure and Mechanical property of Porous Nickel aluminides Fabricated by Reactive synthesis with Space Holder Powder, *Journal of MRS Advances*, Vol. 4, No. 25-26 (2019), pp. 1515-1521.
3. Yunmao Shu, Asuka Suzuki, Naoki Takata, Makoto Kobashi: Effect of powder blending ratio on porous structure formed by combustion synthesis reaction between Ni and Al together with space holder, *Journal of Functionally Graded Materials*, Vol. 33 (2019), pp. 38-43.